NASA CONTRACTOR REPORT

NASA CR-207

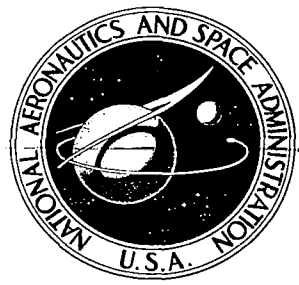


N A S A - C R

# EVALUATIONS OF FILAMENT-REINFORCED COMPOSITES FOR AEROSPACE STRUCTURAL APPLICATIONS

*by Norris F. Dow and B. Walter Rosen*

Prepared under Contract No. NASw-817 *by*
GENERAL ELECTRIC COMPANY
Philadelphia, Pa.
*for*

NATIONAL AERONAUTICS AND SPACE ADMINISTRATION • WASHINGTON, D. C. • APRIL 1965

NASA CR-207

# EVALUATIONS OF FILAMENT-REINFORCED COMPOSITES FOR AEROSPACE STRUCTURAL APPLICATIONS

By Norris F. Dow and B. Walter Rosen



Prepared under Contract No. NASw-817 by
GENERAL ELECTRIC COMPANY
Philadelphia, Pa.

for

NATIONAL AERONAUTICS AND SPACE ADMINISTRATION

For sale by the Office of Technical Services, Department of Commerce,
Washington, D.C. 20230 -- Price $5.00

ABSTRACT

Studies of the influence of constituent properties upon the performance of structural composites for aerospace applications are described. Previous elastic constant and tensile strength evaluations are extended to broaden their range of applicability. An analysis of compressive strength is presented. These analyses are then used in a structural efficiency study of sandwich cylindrical shells subjected to axial load conditions appropriate to the launch vehicle problem. Promising areas for future development of composite materials are indicated.

## FOREWORD

This document is the annual report on the program entitled, "Study of the Relationship of Properties of Composite Materials to Properties of Their Constituents" for the period, September 27, 1963, to September 26, 1964. The program was performed for the National Aeronautics and Space Administration under Contract NASw-817 and was monitored by Mr. N. Mayer of this agency.

The authors wish to acknowledge the contributions of Prof. Z. Hashin, of the University of Pennsylvania, consultant, and P. Juneau, to this report. Prof. Hashin performed the analyses of transverse strength and of elastic moduli for arbitrary phase geometry. Mr. Juneau conducted the experimental program described in Appendix 5 with the assistance of R. S. O'Brien. The contributions of T. Coffin, R. K. Cole, and O. Winter are also acknowledged.

TABLE OF CONTENTS

## INTRODUCTION

To help direct composite materials developments into areas yielding greatest performance improvements, knowledge in depth is needed of mechanics of composites as elements of aerospace structures and of properties attainable with proper combinations of constituents. Recent results of continuing studies in both of these areas and their initial application to provide guidelines for developments are reported herein.

First evaluations of elastic constants and ultimate tensile strengths of composites were reported in ref. 1. The elastic constant analyses are enhanced herein by consideration of auxiliary phase geometry, and comparisons are made with experimental data. Strength studies are expanded. The ultimate tensile strength analysis is carried to a point where it is perhaps ready for general application, and a first cut is made at the problems of compressive strength and strength transverse to the fibers. Thus, the tools are developed for an initial survey of the performance potentials of various materials for composites for aerospace structures.

For this initial survey the shell of the rocket boost vehicle is chosen as the structure and the efficiencies of a wide variety of combinations of filamentary and binder materials as composites for this application are evaluated. The evaluation procedure involves some extension of the Stein-Mayers (ref. 2) analysis of the buckling of anisotropic shells to provide a basis for the calculation of shell weights at given values of the appropriate structural index for this application (as in the efficiency analysis procedure of ref. 3). A major

intermediate output from this study is the compilation of elastic constants for the wide variety of constituent combinations surveyed, -used as inputs for the shell efficiency investigation, and tabulated herein for possible use in other such analyses. The end results of the survey are recommendations for composite types and configurations for most profitable further research and development effort.

Inasmuch as one of the more emphatic of the recommendations has to do with the need for improved binder properties for composites compared to those now available in plastic resins like epoxy, some effort was expended in carrying forward the work initiated in ref. 1 toward a three-phase (filled binder) composite. Results of this work, while not spectacularly successful, are included as perhaps helpful to future workers in this area.

## ELASTIC MODULI

The previous contract studies of the elastic moduli of transversely isotropic fibrous composites (Ref. 1 and 4) resulted in expressions and bounds for these moduli for certain types of geometry. The most important results were obtained for a special geometry which is described by a fiber-reinforced material which consists entirely of parallel composite cylinders. Each composite cylinder consists of a fiber core, which may be hollow, and of a concentric binder cylindrical shell. The cross section sizes diminish from finite to infinitesimal sizes and thus the remaining binder volume, not included in cylinders, may be made arbitrarily small. These results were also applied, subject to a geometric approximation, to the case of randomly distributed equal diameter fibers.

By a variational bounding method based on the classical principles of minimum potential energy and minimum complementary energy, expressions for four effective elastic moduli were obtained. These moduli are $K_{23}^{*}$ -the plane strain bulk modulus referred to the transverse 23 plane (normal to the fibers), $G_{1}^{*}$ -the shear modulus governing shear in a plane normal to the transverse plane (parallel to the fibers) $E_{1}^{*}$ -the Young's modulus for uniaxial stress in fiber direction and $\nu_{1}^{*}$ -the Poisson's ratio for the same case. The fifth elastic modulus $G_{23}^{*}$ -shear modulus in the transverse plane could only be bounded from below and above.

The results for these elastic constants, as well as the related expressions for constant diameter fibers in an hexagonal array, were programmed for a high speed digital computer. Typical results obtained from this program have been presented previously. Unfortunately, the results presented were not free of errors. First the equation for the transverse plane strain bulk modulus, $K_{23}^{*}$, contained an error in the Poisson ratio terms. Thus, eq. 3.24 of ref. 1 should have been presented as follows:

$$K^{*}_{23(r)} = \bar{K}_b \frac{\phi(1-\alpha^2)\left[1+(1-2\nu_b)V_t\right] + \left(1+\frac{\alpha^2}{1-2\nu_f}\right)(1-2\nu_b)V_b}{\phi(1-\alpha^2)V_b + \left(1+\frac{\alpha^2}{1-2\nu_f}\right)\left[V_t+(1-2\nu_b)\right]} \qquad (1)$$

The numerical effects of this change appear to be negligibly small for all cases considered and in fact for $\nu = 0.25$, the error is exactly zero.

Also a programming error existed in the computer program for the case of hollow fibers ($\alpha \neq 0$). For this case the results for $G_{23}^{*}$ were grossly in error and the affected curves (figs. 3 and 4 of ref. 1) are presented here in their correct form as figs. 1 and 2. Fig. 1 shows the results for transverse Poisson's ratio. It now appears that materials of extremely high Poisson's ratio can be obtained through the use of hollow glass fibers. Experimental confirmation is lacking for this phenomenon. In fact experimental data for all but the longitudinal Young's modulus are extremely scarce. A collection of data for the transverse Young's modulus was presented in ref. 5. The equations of the present study were used to calculate these values from the constituent moduli and volume fractions.

The results are shown in fig. 3 and the agreement is most encouraging. A similar comparison is made in fig. 4 for the shear modulus in the fiber plane, $G_{12}^{*}$. Here the agreement is not as good.

The above mentioned results appear to be valuable as approximate expressions and they have been used herein in extensive parametric structural efficiency studies. There are, however, certain remaining unanswered questions associated with the elastic constants of fibrous composites. Principal among these is the effect of non-uniform fiber spacing. One method of assessing the possible magnitude of effects associated with this uncertain transverse geometry is to determine bounds on the elastic constants for arbitrary transverse geometry. This will also provide information for consideration of non-circular fibers.

An alternate approach is to apply statistical techniques to the problem of specifying transverse geometry. This may be done in terms of joint probability functions. To give an example, let it be assumed that the fibers have full cross sections (no voids). Consider two arbitrary points $\underline{x}^{(1)}$ and $\underline{x}^{(2)}$ in a transverse plane. The distance between the points is given by

$$\underline{r} = \underline{x}^{(2)} - \underline{x}^{(1)} \tag{2}$$

One may now define four two point probabilities. For example, $g^{11}$ is the probability that both points are in phase one (say binder) $g^{12}$ is the probability that the first point is in phase one (binder) and the second in phase two (fibers). Analogously one has the joint probabilities $g^{21}$ and $g^{22}$. Let these

probabilities be denoted shortly by $g^{mn}$. The assumption of statistical homogeneity of the material implies

$$g^{mn} = g^{mn}(\underline{r}) \tag{3}$$

that is to say the actual position of the two points in the material is of no consequence. The further assumption of statistical transverse isotropy implies that for $\underline{r}$ in the transverse plane:

$$g^{mn} = g^{mn}(r) \tag{4}$$

where r is the magnitude of $\underline{r}$. Eq. (4) means that the actual direction of $\underline{r}$ in the transverse plane is of no consequence. For $\underline{r}$ not in the transverse plane, the joint probability functions remain functions of $\underline{r}$.

In the same way one may define three point, four point ... and N point joint probabilities. As more and more joint probabilities are known the statistical geometry becomes more and more specified. In general the joint probabilities must be determined by experiment.

It is interesting to note the meaning of one point probabilities. These are the probabilities that a point thrown at random into the material is either

in one or the other phase. It is easy to realize that the one point probabilities are just the volume fractions of the phases.

## Arbitrary Phase Geometry

The general definition of the effective elastic moduli $C^*_{ijkl}$ is

$$\bar{\sigma}_{ij} = C_{ijkl}\,\bar{\varepsilon}_{kl} \tag{5}$$

where the range of subscripts is 1, 2, 3, a repeated subscript denotes summation and overbars denote average values over large volume elements. Eq. (5) is meaningful only for boundary displacements or loadings which produce uniform states of stress and strain in homogeneous media, (ref. 1 and 4). In the present case of statistical transverse isotropy there are five independent effective elastic moduli, for example the one listed above.

In general the effective elastic moduli are functions of the phase moduli and the phase geometry. For random geometry they are thus functions of all the N point joint probability functions of all orders. It is at present not known how to establish this functional relationship in general. The present analysis is concerned with a simpler yet very important question: Given only phase moduli and phase volume fractions, (i.e. one point averages), to what extent are the effective elastic moduli defined by such information? Such information will henceforth be referred to as simplest information. The present method of investigation is again a variational bounding method which

is, however, based on new variational principlesin the classical theory of elasticity (Ref. 6). The bounding method is also based on statistical analysis.

The details of the analysis, which is quite lengthy, will be reserved for the open literature. Here only the final results will be stated. With the notation employed in Refs. 1 and 4 and for a material consisting of full elastic fibers and an elastic binder the bounds are:

$$K_{23}^{*(-)} = k_b + \frac{v_f}{\frac{1}{k_f - k_b} + \frac{v_b}{k_b + G_b}}$$

$$K_{23}^{*(+)} = K_f + \frac{v_b}{\frac{1}{k_b - K_f} + \frac{v_f}{K_f + G_f}} \qquad (6)$$

$$G_{23}^{*(-)} = G_b + \frac{V_f}{\frac{1}{G_f - G_b} + \frac{V_b (K_b + 2G_b)}{2G_b (K_b + G_b)}}$$

$$G_{23}^{*(+)} = G_f + \frac{V_b}{\frac{1}{G_b - G_f} + \frac{V_f (K_f + 2G_f)}{2G_f (K_f + G_f)}} \qquad (7)$$

$$G_1^{*(-)} = G_b + \frac{V_f}{\frac{1}{G_f - G_b} + \frac{V_b}{2G_b}}$$

$$G_1^{*(+)} = G_f + \frac{V_b}{\frac{1}{G_b - G_f} + \frac{V_f}{2G_f}} \qquad (8)$$

R. Hill has obtained bounds for $E_1^*$ and $\nu_1^*$ of transversely isotropic fiber reinforced materials in terms of volume fractions and phase moduli only by different methods, (private communication, to be published). His bounds show that from a practical point of view the law of mixtures is in general a good approximation. Similar conclusions have been reached in Refs. 1 and 4. Thus good approximations for $E_1^*$ and $\nu_1^*$ are:

$$E_1^* \approx v_b E_b + v_f E_f \tag{9}$$

$$\nu_1^* \approx v_b \nu_b + v_f \nu_f \tag{10}$$

It has been shown that the bounds (6), (7) and also Hill's bounds are best possible in terms of phase moduli and phase volume fractions. By this is meant: If the only information available is the simplest information then these bounds give the best information one may possibly obtain about the effective elastic moduli. Obviously, in order to improve the bounds one has to use additional information such as two point and higher order joint probabilities. It is as yet not known how to use such information. It is not yet known whether the bounds (8) are also best possible in terms of the simplest information, however, the method of derivation suggests that it is possible that they are.

The nature of the bounds described above is of considerable practical significance. A designer of a fiber reinforced material certainly knows the elastic moduli of the constituents from experiments and also has control over the volume fractions. He has, however, no control over the higher order statistical details of the geometry. Therefore, the usual method of manufacture of such materials must invariably lead to scatter in the effective elastic moduli. The worst possible amount of scatter is defined by the bounds given above. Unfortunately, the distance between the bounds is quite large. This is to be expected as the arbitrary phase geometry includes the extremes of each material being either matrix or inclusion. The arbitrary phase

geometry bounds are compared to the previous random array bounds for the transverse shear modulus in Fig. 5. It is seen that, for all but small ratios of constituent moduli, the arbitrary geometry bounds are extremely far apart. An interesting and unexpected result is that the lower bound for arbitrary transverse geometry is higher than the lower bound obtained in refs. 1 and 4 for circular fibers in a random array. This arbitrary geometry lower bound has therefore been substituted into the existing elastic constants computer program used in the efficiency studies herein, resulting in a reduction in the distance between the previous bounds on transverse Young's modulus.

## STRENGTH OF FIBROUS COMPOSITES

The strength of fibrous composites has previously been studied as part of this program for tensile loads applied in the fiber direction. This work has been extended, as described in the following section, to illustrate how constituents of various characterizations can be accommodated by the analysis. An initial analytical treatment of failure under a compressive load parallel to the filaments has been undertaken. Also a study of composite strength under loads transverse to the fiber direction has been made for the condition of a perfectly plastic matrix material. These studies are described in the following sections.

Tensile Strength Parallel to Fibers

Various models have been proposed for the tensile failure of a fibrous composite loaded in a direction parallel to the set of uniaxial reinforcing fibers. There continues to be substantial disagreement as to the actual mechanics of failure within such a composite. The model treated in the present analysis (see Ref. 1 and 7 ) is shown in Fig. 6 and consists of a set of parallel fibers which are assumed to be strong and stiff with respect to the matrix material in which they are imbedded. The fibers treated are high strength brittle fibers whose strength is dependent upon the degree of surface imperfection. When such a composite is subjected to a tensile load a fiber fracture will occur at one of the serious flaws or imperfections. When such a fiber breaks, the stress in the vicinity of the broken fiber is perturbed substantially so that the axial stress in the fiber vanishes at the fiber break and gradually builds back up to its undisturbed stress value due to shear stresses being transferred across the fiber matrix interface. The general stress pattern in the fiber is shown in the figure and has been discussed in the previous work (Ref. 1 and 7 ). When such a break occurs several possibilities for the future behavior of the composite exist. First the high interface shear stresses could produce interface failure which could propagate along the length of the fiber reducing the fiber effectiveness over a substantial fiber length. In order to achieve the potential of the fiber strength it is necessary to study and determine the fabrication conditions which will yield an interface sufficiently strong to withstand this interface

shear failure. This can be done either through the use of a high strength bond or of a ductile matrix which permits redistribution of the shear stresses. In the latter case the length of fiber which is affected by the break will increase as it will take a longer distance to retransmit the stresses back into the fiber at the low stress level of a ductile matrix. With a strong bond, the interface conditions can be overcome as a potential source of failure, and a second possibility is that the initial crack will propagate across the composite resulting in failure. This is influenced by the fracture toughness of the matrix and again since it is clear that with brittle fibers one can always expect a fracture to occur at a relatively low stress level, it is important that the fracture toughness of the matrix material be sufficient to prevent the propagation of this crack across the composite. If these two potential modes of failure are arrested it will then be possible to continue to increase the applied tensile load and to obtain breaks at other points of imperfection along the fibers. Increasing the load will produce a statistical accumulation of fiber fractures until a sufficient number of ineffective fiber lengths in the vicinity of one cross-section interact to provide a weak surface. At the point of incipient fracture all of the failure modes described may very well interact to produce the final fracture.

This statistical model of failure has been discussed in some detail in the previous work (Ref. 7 ). The present study is concerned with an extension of certain aspects of this problem to clarify the relationship

between predicted results and experimental data, and to emphasize the potential for application of this analysis. A brief review of the method will be presented first.

The model which is used to evaluate the influence of constituent properties upon the tensile strength considers that in the vicinity of an individual break a portion of each fiber may be considered ineffective. The composite may then be considered to be composed of layers of dimension equal to the ineffective length. Any fiber which fractures within this layer will be unable to transmit a load across the layer. The applied load at that cross section would then be uniformly distributed among the unbroken fibers in each layer. The effect of stress concentrations which would introduce a non-uniform redistribution of these loads is not considered initially. A segment of a fiber within one of these layers may be considered as a link in the chain which constitutes an individual fiber. Each layer of the composite is then a bundle of such links and the composite itself a series of such bundles. Treatment of a fiber as a chain of links is appropriate to the hypothesis that fracture is due to local imperfections. The links may be considered to have a statistical strength distribution which is equivalent to the statistical flaw distribution along the fibers. The realism of such a model is demonstrated by the length dependence of fiber strength. That is, longer chains have a high probability of having a weaker link than shorter chains, and this is supported by experimental data for brittle fibers which demonstrate that mean fiber strength is a monotoni-

cally decreasing function of fiber length. For this model it is first necessary to define a link dimension by consideration of the perturbed stress field in the vicinity of a broken fiber. It is then necessary to define the statistical strength distribution of the individual links which can be obtained indirectly from the experimental data for the fiber-strength-length relationship. These results can then be used in the statistical study of a series of bundles and utilized to define the distribution function for the strength of the fibrous composite. This has been treated in Ref. 7 . The example used in the previous work uses the case of individual fiber strengths characterized by a distribution of the Weibull type:

$$g(\sigma) = L\alpha\beta\sigma^{\beta-1} exp(-L\alpha\sigma^{\beta}) \tag{11}$$

where $g(\sigma)$ is the distribution function for fibers of length, L, and and $\alpha$ & $\beta$ are the two parameters characterizing the function. For such fibers, the statistical mode, $\sigma_t^*$ , of the composite tensile strength is found to be:

$$\sigma_t^* = V_f (\alpha\delta\beta e)^{-1/\beta} \tag{12}$$

One of the reasons for the existence of many tensile failure models is that for gross behavior, there are many similarities in the predictions which are obtained from widely differing models. Consider first the influence of fiber volume fraction upon strength. In equation (12) the ineffective length is a function of fiber volume fraction, $V_f$ . This function is given in Ref. 7 as:

$$\frac{\delta}{d_f} = \frac{1}{2}\left[\frac{(1 - V_f^{1/2})}{V_f^{1/2}}\left(\frac{E_f}{G_b}\right)\right]^{1/2} \cosh^{-1}\left[\frac{1 + (1-\phi)^2}{2(1-\phi)}\right] \tag{13}$$

where $\phi$ is the fraction of the undisturbed stress value at which the fiber is considered to be effective. Thus for given constituents:

$$\frac{\delta}{d_f} = C_1 \left(\frac{1 - V_f^{1/2}}{V_f^{1/2}}\right)^{1/2} \tag{14}$$

and from eq. (12)

$$\sigma_t^* = \sigma_{ref} V_f \left(\frac{1 - V_f^{1/2}}{V_f^{1/2}}\right)^{-\frac{1}{2\beta}} \tag{15}$$

where $\sigma_{ref}$ is a reference stress level which is a function of fiber and matrix properties.

This equation is plotted in Fig. 7 (for $\beta = 7.7$, which is a typical value for commercial E-glass filaments) where it is compared with the rule of mixtures value, namely:

$$\sigma_t = \sigma_{ref} V_f \tag{16}$$

The tensile strength of the matrix has been neglected since it is usually of little import in this sense except at low fiber volume fractions. The curve of eq. (15) does not go to unity at a fiber volume fraction of unity because the maximum packing density of fibers is a hexagonal array for uniform diameter fibers with $v_f = 0.904$. The proximity of the two curves indicates the

hazard of inferring from agreement with experimental data that the analysis which generated one or the other curve is a correct model of the failure process.

The next problem is the question of selecting a reference fiber strength with which to make comparisons between composite performance and expected composite performance. In treating fibers which are characterized statistically, the hazard of using a mean value should be quite apparent from the previous observations of the variation in fiber strength. Thus the strength value does not have a meaning unless there is a length value associated with it. Consider fibers characterized by eq. (11) and composed of n links of length $\delta$, where $L = n\delta$, which links are characterized by:

$$f(\sigma) = \alpha\delta\beta\sigma^{\beta-1}\exp(-\alpha\delta\sigma^{\beta}) \tag{17}$$

The $k^{th}$ moment of such a distribution function is defined by:

$$M_k = \int_{\sigma}^{\infty} \sigma^k f(\sigma)\, d\sigma \tag{18}$$

The mean, $\bar{\sigma}$, and standard deviation, $s$, are defined in terms of this moment function as follows:

$$\bar{\sigma} = M_1 \tag{19}$$

$$s = \left[M_2 - M_1^2\right]^{1/2} \tag{20}$$

Substitution of (17) and (18) into (19) and (20) yields:

$$\bar{\sigma} = (\alpha\delta)^{-1/\beta}\,\Gamma\left(1 + \frac{1}{\beta}\right) \tag{21}$$

$$s = (\alpha \delta)^{-1/\beta} \left[ \Gamma\left(1 + \frac{2}{\beta}\right) - \Gamma^2\left(1 + \frac{1}{\beta}\right) \right]^{1/2} \qquad (22)$$

Similarly, for fibers of length, L, eqs. (11), (18) and (19) yield the mean strength of such individual fibers, $\bar{\sigma}_L$, as:

$$\bar{\sigma}_L = (\alpha L)^{-1/\beta} \Gamma\left(1 + \frac{1}{\beta}\right) \qquad (23)$$

It is now possible to answer the question: what is the relationship between the composite strength (the statistical mode) and the mean strength of individual fibers of length, L? The answer is:

$$\frac{\sigma_t^*}{\bar{\sigma}_L} = \left(\frac{\delta}{L}\right)^{-1/\beta} \frac{(\beta e)^{-1/\beta}}{\Gamma\left(1 + \frac{1}{\beta}\right)} \qquad (24)$$

It is of interest to plot this strength ratio as a function of the fiber coefficient of variation which is obtained from eqs. (19) and (20) as:

$$\frac{s}{\bar{\sigma}} = \frac{\left[ \Gamma\left(1 + \frac{2}{\beta}\right) - \Gamma^2\left(1 + \frac{1}{\beta}\right) \right]^{1/2}}{\Gamma\left(1 + \frac{1}{\beta}\right)} \qquad (25)$$

Note that for the Weibull distribution, this ratio is independent of fiber gage length. Simultaneous solution of eqs. (24) and (25) for selected values of $L/\delta$ is achieved by varying $\beta$. The results are plotted in Fig. 8 where composite strength is plotted as a function of the fiber coefficient of variation, that is, the standard deviation divided by the mean value at that same length.

Thus it is seen that in dealing with composites of length equal to one ineffective length, that is the basic bundle of fiber links of the model previously described, the mode of the bundle strength is slightly lower than the mean strength of individual fibers and departs from this value as the variation increases. The other curves show that as the length ratio increases, as is the case for reasonable specimens where the fiber length is large compared to the ineffective length, one would expect from this analysis that composite strength would be somewhat larger than the mean strength of fibers of the same length. And since these numbers are close to one, for coefficients of variation as large as 15%, it is easy to interpret the composite performance as having been equal to some fraction of the fiber performance. In general, the composite strength indicated here would not be achieved because the damage to the fibers during the fabrication process changes the population characterization. Curves of this type then have an important use in assessing how far the composite deviates from its potential strength value because of additional damage introduced after the time of the measurement of the fiber strength. To emphasize the point, note that if one tests fibers of a given length and then tests a composite and compares the two strength values, these results indicate that, in general, the numbers are expected to be close together for fibers which do not have extreme variations. However, the fact that they are close together does not indicate that there is any understanding of the mode of failure. Thus, one may consider the experimental data to support the theory that failure is governed by the rule of mixtures or that

failure is governed by this statistical fracture theory. Both yield similar results for this gross effect, yet the different models suggest different methods of increasing the composite strength. The importance of obtaining a correct model for the mechanics of fracture lies in the potential for achieving improved composites.

The validity of the present model was investigated by a new experimental technique described in Ref. 7 . This experimental program was directed toward making possible the observation of the failure mechanism during the actual loading process of the composite. The experimental model is shown in Fig. 9 and consisted of a single layer of glass fibers imbedded in an epoxy matrix and loaded in tension parallel to the fibers. In the present extension of the study, fibers of a diameter which is large compared to commercial fibers were used. These were 3 1/2 mil E-glass fibers furnished through the courtesy of Narmco. The fiber spacing was relatively close and the thickness of the specimen was only slightly larger than the diameter of the fiber. The overall specimen gage section dimensions were a 1/2" width, a 1" length and a thickness of about four thousandths of an inch. The fiber volume fraction was in the vicinity of 50%. The specimen was observed photoelastically during the test process in a fashion such that the unloaded specimen appears black. The major contributor to the photoelastic effect is the glass fibers and as they are loaded the fibers will brighten. Thus, when the fiber is at high load and appears bright a broken fiber will

result in a zero stress region which is dark.

The fibers used in these specimens were tested individually at three different gage lengths and the results are plotted in Fig. 10 in the form of average strength as a function of gage length. To indicate the effect of the matrix properties upon the composite, two test series were conducted utilizing epoxies which were very nearly identical except that one specimen had a flexibilizer added to it. This resulted in a decrease of the elastic modulus and an increase in the total strain to failure as shown in Fig. 11. The matrix materials used are those labeled 1 and 4 in Fig. 11. The test results are presented in Table 1 . The effect of matrix properties on the character of the results is shown in Fig. 12. Fig. 12a is a typical picture at 99% of ultimate load of 3 1/2 mil E-glass fibers in an epoxy having a modulus of .48 million. The fiber ineffective lengths are on the order of 10 diameters and distribution of fiber breaks is random. Fig. 12b shows the similar specimen using a matrix material of modulus 0.28 million psi again taken at 99% of the maximum load. Here it is seen that (1) the ineffective lengths are substantially larger, being on the order of 30 diameters and (2) that the number of breaks are smaller and (3) the effect of stress concentrations is larger. Since the ineffective lengths are larger, it takes fewer of them to produce a weak cross section and hence failure of the composite. The role of the matrix in confining the detrimental effect of perturbations of the stress field which result from a fiber break are clearly evident. Thus it is seen that although a ductile matrix is desirable from the point of

view of alleviating the stresses and preventing interface failure, and also for having a higher fracture toughness, a strong and stiff matrix would have a greater effect on confining the perturbations to the stress field thus producing a beneficial effect for the statistical failure model. Experiments using constituents which trade off these various factors are sorely lacking, and the proper evaluation of the relative merits of various failure models will require more experimental work. It is hoped that the experiments that have been described here can be extended to aid in this work.

Since the test data of Fig. 10 yielded a straight line and since the Weibull distribution of eq. (11) would also produce such a straight line, as is apparent from eq. (23) , the fiber test data can be used directly in the analytical model to predict composite strengths. This has been done and the results are presented in Fig. 13 based on the fiber diameter of 3 1/2 mils for the experimental fibers used. The curve is linear on this logarithmic plot where the ineffective length ratios one to ten are appropriate to elastic matrix materials and the range 10 to 100 is the appropriate range for the inelastic results. The two test points previously described (average values from Table 1 ) are shown on this plot and it is seen that the two appear to have the trend of the analytical result but the strength levels are substantially below those shown. Several reasons exist for this; one important one being the fact that the fiber strength values of Fig. 10 cannot be extrapolated to very short fibers since data (e.g. Ref. 8 ) show that the curve flattens out at very short lengths. Since the ineffective length, for a practical composite,

is a very short fiber length, one must reconsider what amounts to an extrapolation of the straight line of Fig. 10 down into the short fiber range. To do this consider some simple fiber populations; for example, the rectangular distribution shown in Fig. 14a. Given this simple rectangular distribution function for the links in a fiber chain the cumulative distribution function is readily obtained as shown in Fig. 14b. The chain representing a fiber containing n links would have a distribution function of the general shape shown in Fig. 14c and its associated cumulative distribution function as shown in Fig. 14d. However, it appears from data, for glass fibers for example, that the general characteristics of the distribution function indicates that the bulk of the fibers fail within a finite band at high stress level and occasional fibers fail at small stress levels so that an idealized link distribution function would look more like that shown in Fig. 15a. Here the bulk of the fibers are shown as in the simple rectangular distribution function proceeding with a small portion of the population isolated at a lower stress level. The effect on the cumulative distribution function for the fiber lengths is trivial. It departs from zero over the lower range as opposed to running along the axis to the stress $\sigma_3$ but the value p can be quite a small value. However, if one now looks at the effect of this small additional low stress group on the strength of a chain it is seen that there exists a distribution function which has two peaks, where the maximum value of the two peaks are as shown, and also the cumulative distribution function rather drastically modified. The analysis defining these results is presented in

Appendix 1.

For p arbitrarily small there is some large n value which will sufficiently diminish the right hand peak of Fig. 15 with respect to the left hand peak so that a long enough chain will soon have its strength dominated by the low stress level group of the population. Fig. 16 shows the number of elements n required to make these two peaks equal to one another as a function of, p, the fraction of the population in the low strength region. The number of elements required is a function of the ratio of the width of upper rectangular band, $\sigma_4 - \sigma_3$ , to the width of the lower rectangular band, $\sigma_2 - \sigma_1$ . Results are shown for three different values of this ratio. It can be seen that even for fractions of the population in the low strength region as low as 1% only several hundred elements are required before the lower peak equals the upper peak. The influence of the distribution of fibers between the two different regions is shown more clearly in Fig. 17 in which the average fiber strength is plotted as a function of the fiber length where the distribution function for the individual elements is as shown in the lower left portion. Here the upper band is twice the width of the lower band and only 1% of the link elements are considered to be in the lower band. The result for the mean strength curve very closely simulates the experimentally observed bilinear distribution of strength versus length. It is considered significant that distributions of this form can reproduce the experimental data. Evidently the prospects are encouraging for using such a distribution directly in the failure model that has previously been described.

The original example for the computation of composite strength was based on the use of a single straight line, such as the latter portion of this curve of Fig. 17. It is clear that this can lead to an overestimate of the composite strength. Having demonstrated the ease with which the experimental fiber strength data can be simulated, it now remains to select an appropriate compound distribution function and use it in the previously derived statistical analysis. For example a Weibull distribution can be utilized in the following form:

$$f(\sigma) = p\alpha_1\delta\beta_1\sigma^{\beta_1-1}\exp(-\alpha_1\delta\sigma^{\beta_1}) + (1-p)\alpha_2\delta\beta_2\sigma^{\beta_2-1}\exp(-\alpha_2\delta\sigma^{\beta_2}) \qquad (26)$$

and the associated cumulative distribution function:

$$F(\sigma) = 1 - p\exp(-\alpha_1\delta\sigma^{\beta_1}) - (1-p)\exp(-\alpha_2\delta\sigma^{\beta_2}) \qquad (27)$$

It is seen that for p equals either zero or one, the result reduces to a simple Weibull distribution and for any p value this compound distribution can be used in the preceding equations in exactly the same fashion as the simple one was with only the sacrifice of algebraic simplicity.

## Conclusions Regarding Tensile Failure

The tensile model indicates that randomly distributed fiber fractures occur well below the ultimate composite strength. The statistical strength characterization of the fibers determines the frequency of these fiber breaks. The strength of the composite is determined by this and by the efficiency with which the matrix limits the effect of the perturbation of the local stress field produced by a fiber break. The need for statistical characterization of fibers and for consideration of matrix deformations is strongly indicated. A new experimental technique for the evaluation of the tensile failure process has been presented and the results support the analytical model.

The analysis does not include all possible detrimental effects and hence it is perhaps best to view the results as indications of the potential for advanced structural composites. These potentials are the major conclusions of the present study. Simply stated, the conclusion is that high strength fibers used in an appropriate matrix can yield composites having tensile strengths usually attained only in very short lengths of very small diameter filaments.

Compressive Strength Parallel to Fibers

The problem considered is the compressive strength of a fibrous composite formed by the set of parallel fibers imbedded in an otherwise homogeneous matrix. The composite is considered to be subjected to compressive load parallel to the fiber direction. It has been suggested by Dow (Ref. 9) that the mode of failure for such a composite is the small wavelength buckling of the fibers in a fashion analogous to the buckling of a column on an elastic foundation. One of the motivations for such a composite failure model is indicated in fig. 18. Photoelastic stress patterns are shown for three individual glass fibers imbedded in an epoxy matrix which has been cured at a temperature of about 250°F. As is well known, the shrinkage of the epoxy from its cure temperature down to room temperature results in the frequently observed elastic instability of the glass fiber. E-glass fibers of five, three and one half, and one half mil diameter in three separate blocks of epoxy are shown. It is clear from the repeated stress pattern that a buckling failure has occured. All three blocks consist of the same epoxy subjected to the same cure conditions. The only apparent difference between specimens is the difference in amplitude and wavelength of buckling. The shrinkage of the epoxy resin provides a convenient means for applying a compressive strain to this glass fiber and observing the resultant instability. The analytical model of a column on an elastic foundation indicates that the buckling wavelength of a circular column would be directly proportional to the fiber diameter (see ref. 10). The three fibers shown here are all in

identical epoxy matrices and hence the foundation modulus, although unknown, can be considered to be the same in all cases. Thus, it would be expected that the buckling wavelength would be linearly dependent upon the fiber diameter. Fig. 19 shows the measured experimental results. Here the buckle wavelength is plotted against the fiber diameter on logarithmic paper so that a linear relationship between the two appears as a 45° line on this graph. The three test points shown in fig. 18 are plotted along with a best fit 45° line. The agreement between this analytical curve and the test data indicates at least qualitatively that there is some justification for considering the elastic instability mode as the failure mode for the glass fibers.

The problem of quantitatively evaluating this instability failure for multiple fibers imbedded in the homogeneous matrix is not as straight forward. The analytical model considered in the present analysis is shown in fig. 20. A series of parallel fibers are treated as a two dimensional problem, so that the model consists of plates of thickness h separated by a matrix of dimension 2c. Each fiber is subjected to a compressive load, P , the fiber length is given by the dimension, L. Now, two possibilities are considered for the failure mode here. First, the fibers may buckle in opposite directions in adjacent fibers as shown on the left portion of fig. 20 and the so-called extension mode occurs. This mode receives its name from the fact that the major deformation of the matrix material is an extension in the direction perpendicular to the fibers. The model considers that the fibers are stiff relative to the matrix and that shear deformations in the fiber can be neglected relative to those in the matrix.

The second possibility is shown on the right portion of the figure where adjacent fibers buckle in the same wavelength and in phase with one another, so that the deformation of the matrix material between adjacent fibers is primarily a shear deformation. Hence, the shear mode label for this potential mode. The energy method for evaluation of the buckling stress for these modes has been utilized, where the procedure is to consider the composite stressed to the buckling load and then to compare the strain energy in this compressed but straight deformation pattern to a deformation pattern following an assumed buckling shape under the same load. Thus, a change in the strain energy of the composite consisting of the strain energy change in the fiber, $\Delta V_f$, and the strain energy change in the binder, $\Delta V_b$, can be compared to the change in the potential energy associated with the shortening of the distance between the applied loads at the end of the fibers, $\Delta T$. The condition for instability is given by equating the strain energy change to the work done by the external loads during buckling. Details of the analysis are presented in Appendix 2.

The results for the compressive strength, $\sigma_c$, for the extension mode is given by:

$$\sigma_c = 2V_f \left[ \frac{V_f E_b E_f}{3(1 - V_f)} \right]^{1/2} \tag{28}$$

The result for the shear mode is given by:

$$\sigma_c = \frac{G_b}{1 - V_f} \tag{29}$$

These results are plotted in fig. 21 for E-glass fibers imbedded in an epoxy matrix. The compressive strength of the composite is plotted as a function of the fiber volume fraction. The two curves represent the two failure modes considered. It is seen that for the low fiber volume fractions the extension mode is the lower stress, while for high volume fractions of fibers the shear mode predominates. The compressive strength of reasonable glass reinforced plastic containing fiber volume fractions on the order of 0.6 to 0.7 is seen to be on the order of 450 to 600 ksi. Values of this magnitude do not appear to have been measured for any realistic specimens. However, the achievement of a strength of half a million psi in a composite of this type would require an average shortening of greater than 5%. For the epoxy materials used, such a shortening would result in a decrease in the effective shear stiffness of the binder material because the proportional limit of the matrix would be exceeded. It does appear necessary to modify the analysis to consider inelastic deformation of the matrix material. A first simple approximation to this has been provided by replacing the binder modulus in the formulas previously shown by a modulus which varies linearly for the epoxy from its elastic value at 1% strain to a zero value at 5% strain. The result of this assumption is the curve labeled inelastic in fig. 21. Here it is seen that for very high fiber volume fractions the strength is bounded and,

although higher than any results obtained to date, they are not unreasonably high. The results of this study are presented in a somewhat different form in fig. 22 where the average compressive strain at failure is plotted as a function of the fiber volume fraction for composites having two different ratios of fiber Young's modulus to binder shear modulus. Curves for the two failure modes, that is extension and shear, are presented. The strength of the composite is obtained simply from these curves by multiplying the shortening by the product of fiber volume fraction and fiber Young's modulus. These curves again indicate that the shear instability mode is predominant over the major range of interest for these ratios of fiber to binder moduli. Also indicated is the fact that a substantial difference in the result is achieved for a change in the ratio of fiber to binder moduli Thus, the factor of 2 utilized in the example here results in almost a factor of 2 on the results for the shear mode. Thus, changes in the effective value of the shear stiffness of the binder when stressed beyond the elastic limit of the material can have a substantial effect on the predicted value of the composite.

The results presented so far are based on strain energy computations which have involved some assumptions regarding the displacements, and hence, it is no longer valid to treat the stress obtained as an upper bound of the buckling stress. In order to investigate the nature of the approximation made in the strain energy a more precise model must be considered. This is done by treating the boundary value problem defined by considering an elastic domain subjected to sinusoidal normal displacements on the boundary. The strain energy in the binder material is evaluated by considering this strip as

a two dimensional elastic domain. The equilibrium equation expressed in terms of displacements can be used to obtain a solution to this problem by following an approach used by Timoshenko (ref. 10 ) for the related traction boundary value problem. That is the displacements $u_x$ and $u_y$ can be assumed to be arbitrary functions of y multiplied by trigonometic functions of the longitudinal direction x. Substitution of these displacements into the equilibrium equations can be shown to yield an ordinary differential equation for the function of y. The constants in this solution are evaluated by considering the boundary conditions on the displacements. From this the strain energy can be found and this strain energy can be used in the expression shown previously to obtain a true bound on the compressive critical buckling stress. This can be done again under the assumption that the fiber is sufficiently rigid so that shear deformations of the fiber can be neglected. It is also possible to relax even this constraint and consider two adjacent elastic domains; one representing the binder and one representing the fiber and to have boundary conditions in the form of continuity of displacements and normal tractions across the surface rather than in the form of prescribed sinusoidal deformations. This approach requires further study.

Another assessment of the results of the present analysis with experiment can be obtained by utilizing existing results (ref. 11) for hollow glass fiber composites. These results are shown in fig. 23. Here a set of short compression columns fabricated from hollow glass fibers imbedded in an epoxy matrix and tested in compression are plotted in the form of the

ratio of the strength to density ratio for a hollow glass fiber composite normalized with respect to a composite containing solid E-glass fibers with the same binder volume fraction. Each experimental point here is for a composite containing a 30% binder on a volume basis and each point represents the average of at least 5 tests of nominally identical specimens. The fiber radius ratio, that is the ratio of the inner to the outer radii of the hollow glass fibers, is the independent variable. The analysis indicates that the stress to density curve would increase monotonically with the fiber radius ratio over the range of $\alpha < 0.9$. It is seen that the experimental data appear to have the analytical result as an upper bound.

## Conclusions Regarding Compressive Strengths

It appears that the compressive strength of a fibrous composite loaded in a direction parallel to the fibers is governed by an instability mode analogous to the buckling of a column on an elastic foundation. An analysis to assess the quantitative effect of the influence of constituent properties upon this buckling stress has been presented.

The compression model indicates that the matrix shear stiffness is the material property which has the most significant effect on composite compressive strength. The choice of the failure mode is supported qualitatively by experimental results for the compressive strength of hollow glass fiber composites.

It appears that the use of matrix materials having shear moduli which are moderate rather than small with respect to the fiber Young's modulus can yield composites, of high modulus fibers, which have extremely high compressive strength. Of course the binder must have these values at the high strains associated with the very high composite compressive strengths.

## Transverse Strength

The problem of the strength of fiber reinforced materials and composite media in general is one of the most important aspects of the study of mechanical behavior of such media. Ideally speaking the aim is to predict mechanical behavior and strength of the composite on the basis of the known mechanical behavior and the geometry of the constituents. The present investigation is concerned with limited treatment of this problem by use of the theorems of limit analysis of the theory of plasticity, for cases where the load is applied in a direction such that there is no continuous load path through the inclusions.

### Theorems of Limit Analysis

The theorems of limit analysis are concerned with the evaluation of the limiting or ultimate load which can be carried by plastic bodies. The limiting load is defined as that load at which the deformation of the body can increase without increase in load. This load may be defined as the failure load of the body.

One way to find the limiting load is to find the stresses and deformations in the body during a loading program which carries it from an elastic state into an elasto-plastic state and finally into a fully ideally plastic state, when deformation continues without load increase and the limiting load is thus attained. However, such an analysis is extremely difficult to perform and it is the great advantage of the theorems of limit analysis that the limiting load can be estimated by bounding from above and below without reference

to the loading program by which the limiting load is attained. The limit analysis theorems have been discussed and proved in several plasticity texts. For the theorems in the plane strain case, which is of importance for the following treatment of fiber reinforced materials, see Ref. 12. For very general treatment in the three dimensional case see Ref. 13.

Fiber Reinforced Materials

Consider a fiber reinforced cylindrical specimen consisting of an ideally plastic binder and elastic-brittle fibers which are parallel to the specimen generators. The assumption of elastic-brittle fibers is certainly valid for the commonly used glass fibers.

It is assumed that the specimen is in plane strain. Under these conditions the commonly used Tresca and Mises yield conditions are the same (Ref. 12). The specimen is referred to a cartesian system of axes where the $x_1$ axis is in fiber direction and $x_2x_3$ are in the transverse plane normal to the fibers.

The yield condition for the binder material then assumes the form

$$(\sigma_{22} - \sigma_{33})^2 + 4\sigma_{23}^2 = \sigma_y^2 \qquad (30)$$

where $\sigma_y$ is the yield stress of the matrix in simple tension. For convenience let the cross section of the fiber reinforced specimen be chosen rectangular and let a simple tension $\sigma_{22} = \sigma^o$ be applied to two opposite faces (fig. 24a). The limiting load $\sigma^L$ is defined as that value of $\sigma^o$ for which the deformation of the specimen increases without increase in load. This load may be defined as the strength of the specimen for the loading

described. The theorems of limit analysis provide a method for bounding $\sigma^L$ from below and above. To find a lower bound on $\sigma^L$ one has first to construct what is known as a statically admissible stress system (Ref. 1,4). It is easily realized that the stress system

$$\sigma_{22} = \sigma^o \qquad (\sigma^o \leq \sigma_y) \tag{31a}$$

$$\sigma_{33} = \sigma_{23} = 0 \tag{31b}$$

in binder and fibers is statically admissible since it satisfies the boundary conditions, equilibrium equations, traction continuity at fiber-binder interfaces and nowhere violates the yield condition (eq. 30). Accordingly, any $\sigma^o \leq \sigma_y$ is a lower bound on $\sigma^L$ and the best lower bound associated with (eq. 31) is $\sigma_y$ itself. Consequently

$$\sigma_y \leq \sigma^L \tag{32}$$

Thus the yield stress of the binder is a lower bound for the strength of the specimen under the loading described.

It follows in a completely analogous way that when the specimen surface is subjected to pure shear $\tau^o$ in the $x_2x_3$ plane, the strength in shear $\tau^L$ is bounded from below by $\sigma_{y/2}$, thus

$$\frac{\sigma_y}{2} \leq \tau^L \tag{33}$$

Finally if the specimen is subjected on its boundaries to biaxial stress

$$\sigma_{22} = \sigma_2^o$$

$$\sigma_{33} = \sigma_3^o \qquad (34)$$

$$\sigma_{23} = 0$$

the limiting load is bounded from below according to the condition

$$\sigma_y \leq |\sigma_3^o - \sigma_2^o| \qquad (35)$$

the lower bounds are geometry independent.

For upper bound construction it is necessary to construct what is known as a kinematically admissible velocity field. Consider again the specimen shown in fig. 24a under the same loading. However, in the subsequent treatment a geometrical restriction has to be introduced. It has to be assumed that it is possible to put a plane (normal to the $x_2x_3$ plane) through the specimen which does not cut through any fiber. Let the inclination of this plane to the $x_1x_2$ plane be denoted by $\alpha$ (fig. 24a).

The kinematically admissible velocity field chosen is defined by a constant velocity v of the part $\overline{aefd}$ relative to the part $\overline{efcb}$, in the direction of the cut $\overline{ef}$. Thus the velocity field is a sliding rigid body motion of one part relative to the other. There is a tangential velocity discontinuity, only, of the velocity at $\overline{ef}$ which is permitted in a kinematically admissible field.

In cartesian components the velocity field is given as follows:

$$\left.\begin{aligned} v_2 &= 0 \\ v_3 &= 0 \end{aligned}\right\} \quad \text{in } \overline{efcb} \qquad (36)$$

$$\left.\begin{aligned} v_2 &= -v\cos\alpha \\ v_3 &= -v\sin\alpha \end{aligned}\right\} \text{ in } \overline{aefd} \qquad (37)$$

Since the velocities are constant they satisfy the incompressibility condition. Also rigid body motions are permitted for a kinematically admissible fields at those parts of the boundary where tractions are prescribed, (ref. 13). Consequently the velocity field (eq. 36, 37) is kinematically admissible.

Proceeding now according to ref. 12, Chapter 7, the kinematically admissible multiplier $m_k$ is defined by

$$m_k = \frac{\sigma_Y}{2} \quad \frac{\int_A \dot{\Gamma}\, dA + \int_{\overline{ef}} \Delta v\, ds}{\int_C (T_2 v_2 + T_3 v_3) ds} \qquad (38)$$

Here A is the area abcd, $\dot{\Gamma}$ is the plastic dissipation function which depends only upon the strain rates derived from the kinematically admissible field, $\Delta v$ is the tangential discontinuity in the velocity across $\overline{ef}$, ds is an element of length, C the boundary $\overline{abcd}$ and $T_2$ and $T_3$ are components of traction on the boundary. The meaning of $m_k$ is explained by the statement that $m_k \sigma^o$ is an upper bound on $\sigma^L$. Because of the nature of eq. 36 & 37 the strain rates vanish and thus vanishes. Introducing eq. 36 & 37 into eq. 38 and using the present particular boundary loading, one finds

$$m_k = \frac{\sigma_Y}{\sigma_\infty} \quad \frac{1}{\sin 2\alpha} \qquad (39)$$

and accordingly

$$\sigma^L \leq \frac{\sigma_Y}{\sin 2\alpha} \tag{40}$$

The maximum of sin 2 is unity, for $\alpha = 45^\circ$. In that case, combining eq. 20 with eq. 32 it follows that

$$\sigma_L = \sigma_Y \tag{41}$$

Thus, in the event that it is possible to put a $45^\circ$ plane through the specimen without cutting any fibers, the strength of the fiber reinforced specimen is just the strength of the binder, independently of the shape or stiffness of the fibers.

The same situation is valid for biaxial applied stress of the type of eq. 34. In the event of applied uniform shear stress, the limiting shear stress $\tau^L$ is $\sigma_Y/2$ if it is possible to put a plane through the specimen, without cutting fibers, which is perpendicular to the direction of one of the shear stresses.

The preceding results are chiefly important for regular arrays of fibers of equal cross section. Consider for instance a square array of fibers of equal circular sections. The most unfavorable situation for uniaxial stress is at $45^\circ$ to the array side (fig. 24c), for in this case it is always possible to put a $45^\circ$ plane through the binder alone. However, if the array is oriented as in Figure 3d, the possibility of putting a $45^\circ$ plane through the binder alone depends on the fractional volume of fibers. It is easily found that this is possible only for a fractional volume smaller than $\frac{\pi}{8} = 0.392$.

Particle Reinforced Materials

The preceding analysis is easily carried out for the three-dimensional case of a plastic binder which is reinforced by elastic-brittle particles. In this case the theorems of limit analysis have to be used in their three dimensional form (compare ref. 13). However, in three dimensions the Tresca and Mises yield conditions are not the same, and accordingly the results are somewhat modified.

For lower bound construction the results (eq. 32, 33 and 35) are recovered identically for both yield conditions. Again the results are independent of the geometry.

For upper bound construction, the Tresca yield condition leads again to coincidence of upper and lower bounds with a geometrical restriction similar to the one used before. Thus for uniaxial stress eq. 40 is found again if it is possible to put a plane through the binder which makes an angle $\alpha$ with the direction of the stress. For $\alpha = 45^{\circ}$, eq. 41 is found again and analogously for biaxial stress the limiting load is defined by

$$|\sigma_i^{\circ} - \sigma_j^{\circ}| = \sigma_y \tag{42}$$

where i and j are any perpendicular directions.

For applied shear again

$$\tau^{\circ} = \sigma_y/2 \tag{43}$$

if it is possible to put a plane entirely through the binder which is normal to one of the shear stresses.

For the Mises yield condition the bounds do not coincide. Thus for simple tension with the 45° plane condition

$$\sigma_y \leq \sigma^u \leq \frac{2\sigma_y}{\sqrt{3}} = 1.15\,\sigma_y \tag{44}$$

Analogously for biaxial stress

$$\sigma_y \leq |\sigma_1^0 - \sigma_2^0| \leq 1.15\,\sigma_y \tag{45}$$

and for pure shear

$$\frac{\sigma_y}{2} \leq \tau^u \leq \frac{\sigma_y}{\sqrt{3}}$$

Conclusion

It has been shown that under certain geometrical conditions, the strength of an ideally plastic binder is not increased (or increased at most by 15%) by reinforcement with elastic-brittle fibers or particles. However, the geometrical restriction that a plane can be passed through the binder without cutting the reinforcement is severe, and in the more common case, where this condition is not fulfilled, the effect upon strength is uncertain.

## STRUCTURAL EFFICIENCY OF COMPOSITE MATERIALS - FIRST ASSESSMENT

If composites can provide weight savings for structures subjected to compressive loadings as well as for the tensile loadings of pressure vessels to which they have thus far been primarily applied, they will be much more valuable as aerospace materials. Many structural elements in aerospace vehicles are designed by compressive loadings, and as will be seen, eventually complete evaluations are desirable for the variety of elements - columns, plates, and shells - of which aerospace vehicles are comprised, to determine the suitability of composites for use throughout the structure. For a first assessment the main structural shell of launch vehicles has been chosen as representative of a major class of applications for which improved materials may lead to significant structural advances. This section of this report is concerned with this assessment.

In order to accomplish an adequate structural-efficiency evaluation a number of factors must be properly combined. Heretofore some of these factors, e.g. the elastic constants of composites, have not been defined with sufficient precision to permit a reasonable quantitative determination of the merit of composite materials for shell-buckling applications. Thus the assessment that follows is a first assessment; in consequence, the procedures used are developed in some detail so that their validity can be estimated, and so that subsequent further evaluations may derive therefrom with confidence. The sequence of exposition is:

1. Derivation of structural-efficiency-evalution shell analysis

2. Determination of the range of loadings and geometries of interest for launch vehicles
3. Calculation of structural efficiencies of representative metal shells to use as a basis for comparison
4. Compilation of elastic constants of composites of a variety of filaments and binders
5. Calculation of structural efficiencies of composite shells, and comparisons among materials relative to the metallic constructions.

These steps are presented in the following sections.

## Analysis of the Structural Efficiency of Cylindrical Shells

In order to evaluate the structural efficiency of various materials for use in the cylindrical-shell-in-axial-compression application which is the launch vehicle, the loading-index approach, developed in this country by Shanley (Ref. 3) and others, is used. In this approach a non-dimensional measure of the structural weight is plotted against a non-dimensional measure of the design load in such fashion that the structure having the least value of the ordinate at any value of the abscissa is the one of minimum weight for that design load. Use of this approach requires first the derivation of the non-dimensional parameters to be plotted, and second the development of procedures for determining their relationships for the structures to be examined. This derivation and development is given in the following section.

### Derivation of Structural-Efficiency Parameters for Cylindrical Shells in Axial Compression

The structural-index plot used for the efficiency evaluations herein will first be derived for the simple case of isotropic, monocoque shells. Its extension to orthotropic and sandwich shells follows directly, as will be shown.

(a) The shell weight per unit surface area is

$$W = \rho t \tag{46}$$

where

| | |
|---|---|
| $W$ | weight per unit area of shell |
| $\rho$ | shell density |
| $t$ | shell thickness |

(b) In simplest form the formula for the compressive buckling stress of a thin-walled shell is

$$\sigma_{cr} = K \frac{E}{\sqrt{3(1-\nu^2)}} \left(\frac{t}{R}\right) \tag{47}$$

where

$\sigma_{cr}$ critical stress

$K$ a constant

$E$ Young's modulus

$\nu$ Poisson's ratio

$R$ radius of shell

(c) The stress is also related to the design loading by

$$\sigma = \frac{N_x}{t} \tag{48}$$

where

$N_x$ design compressive loading intensity (compressive load per unit length circumference of the shell)

(d) If the structure is made only just thick enough to achieve the design load at the buckling stress (with normal factors of safety applied)

$$\sigma = \sigma_{cr} \tag{49}$$

and so combining equations (47) and (48)

$$\frac{N_x}{t} = K \frac{E}{\sqrt{3(1-\nu^2)}} \left(\frac{t}{R}\right) \tag{50}$$

(e) Solving for $t$

$$t = \sqrt{\frac{N_x R}{\frac{KE}{\sqrt{3(1-\nu^2)}}}} \tag{51}$$

(f) Substituting (51) in (46) and dividing by R:

$$\frac{W}{R} = \frac{\rho}{\sqrt{\frac{KE}{\sqrt{3(1-\nu^2)}}}} \sqrt{\frac{N_x}{R}} \tag{52}$$

Or, for a given material

$$\frac{W}{R} = C \sqrt{\frac{N_x}{R}} \tag{53}$$

where

$C$ incorporates the material properties and the $K$ from the shell-buckling formula

Equation (53) relates the non-dimensional shell weight to the design conditions of load and size, and a plot of $\frac{W}{R}$ vs. $\frac{N_x}{R}$ is the desired, non-dimensional efficiency representation. As will be seen, the same parameters will apply in the case of the more complicated composite sandwich shells. The equations for these cases will now be described.

Development of Structural-Efficiency Equations for Composite-Sandwich Shells

For anisotropic shells such as composite laminates, it is shown in Appendix 3 that the expression equivalent to equation 47 is

$$\sigma_{cr} = \left[ \sqrt{\frac{K' E_L E_T}{3(1-\nu_{LT}\nu_{TL})} \left\{ \frac{\sqrt{E_L E_T} + \nu_{LT} E_L + 2(1-\nu_{LT}\nu_{TL}) G_{LT}}{\sqrt{E_L E_T} - \nu_{LT} E_L + \frac{E_L E_T}{2G_{LT}}} \right\}} \right] \left(\frac{t}{R}\right) \tag{54}$$

where now

| | |
|---|---|
| $E_L$ | longitudinal Young's modulus |
| $E_T$ | transverse Young's modulus |
| $\nu_{LT}, \nu_{TL}$ | Poisson's ratios |
| $G_{LT}$ | shear modulus in plane of filaments |

Thus the efficiency equation for the anisotropic shell is

$$\frac{W}{R} = \frac{\rho \sqrt{\frac{N_x}{R}}}{\left[ \frac{K' E_L E_T}{3(1-\nu_{LT}\nu_{TL})} \left\{ \frac{\sqrt{E_L E_T} + \nu_{LT} E_L + 2(1-\nu_{LT}\nu_{TL}) G_{LT}}{\sqrt{E_L E_T} - \nu_{LT} E_L + \frac{E_L E_T}{2G_{LT}}} \right\} \right]^{1/4}} \tag{55}$$

instead of equation (52).

Because the bending stiffness of a sandwich plate is given by

$$D_{sand} = \frac{E_S}{1-\nu^2} \left[ (t_c + 2t_s)^3 - t_c^3 \right] \tag{56}$$

where

| | |
|---|---|
| $D_{sand}$ | plate bending stuffness of sandwich |
| $E_S$ | Young's modulus of faces of sandwich |
| $\nu$ | Poisson's ratio for faces of sandwich |
| $t_c$ | core thickness |

$t_s$ face thickness

if the core is of negligible stiffness, the general efficiency equation for a composite sandwich shell with a flexible core may be derived from (55) as:

$$\frac{W}{R} = \frac{\rho_s + \rho_c\left(\frac{t_c}{2t_s}\right)}{\left[\left(\frac{t_c}{2t_s}+1\right)^3 - \left(\frac{t_c}{2t_s}\right)^3\right]^{1/4}} \left\{ \frac{\sqrt{\frac{N_x}{R}}}{\left[\frac{K' E_L E_T}{3(1-\nu_{LT}\nu_{TL})}\left\{\frac{\sqrt{E_L E_T} + \nu_{LT} E_L + 2(1-\nu_{LT}\nu_{TL})G_{LT}}{\sqrt{E_L E_T} - \nu_{LT} E_L + \frac{E_L E_T}{2G_{LT}}}\right\}\right]^{1/4}} \right\} \tag{57}$$

(If the sandwich faces are isotropic, equation (57) reduces to

$$\frac{W}{R} = \frac{\rho_s + \rho_c\left(\frac{t_c}{2t_s}\right)}{\left[\left(\frac{t_c}{2t_s}+1\right)^3 - \left(\frac{t_c}{2t_s}\right)^3\right]^{1/4}} \left\{ \frac{\sqrt{\frac{N_x}{R}}}{\sqrt{\frac{K' E}{\sqrt{3(1-\nu^2)}}}} \right\} \tag{57a}$$

For minimum weight the core thickness to face thickness ratio must be optimized. Optimum values of $\frac{t_c}{2t_s}$ are readily found by differentiation of (57) to be obtainable from the expression

$$\frac{\rho_c}{\rho_s} = \frac{2\left(\frac{t_c}{2t_s}\right) + 1}{2\left(\frac{t_c}{2t_s}\right)^2 + 3\left(\frac{t_c}{2t_s}\right) + \frac{4}{3}} \tag{58}$$

Equations (52), (55), or (57) apply when the stresses are low enough to not exceed the elastic limit of the material. For simplicity in this study all materials are assumed to behave elastically below their "yield stress," $\sigma_y$, and incapable of achieving stresses above their "yield" values. ("Yield stresses" for the reference metals were arbitrarily selected; methods for computing the "yield stresses" for the composites are discussed in another section.) With this yield criterion, the efficiency above the elastic limit is described by the two equations

$$\frac{N_x}{R} = \frac{\sigma_y^2}{\sqrt{\left[\left(\frac{t_c}{2t_s}+1\right)^3 - \left(\frac{t_c}{2t_s}\right)^3\right]\left[\frac{K' E_L E_T}{3(1-\nu_{LT}\nu_{TL})}\left\{\frac{\sqrt{E_L E_T} + \nu_{LT} E_L + 2(1-\nu_{LT}\nu_{TL})G_{LT}}{\sqrt{E_L E_T} - \nu_{LT} E_L + \frac{E_L E_T}{2G_{LT}}}\right\}\right]}} \tag{59}$$

(or for isotropic faces)

$$\frac{N_x}{R} = \frac{\sigma_y^2}{\sqrt{\left[\left(\frac{t_c}{2t_s}+1\right)^3 - \left(\frac{t_c}{2t_s}\right)^3\right]\left\{\frac{K' E}{\sqrt{3(1-\nu^2)}}\right\}}} \tag{59a}$$

and

$$\frac{W}{R} = \frac{\rho_s + \rho_c\left(\frac{t_c}{2t_s}\right)}{\sigma_y}\left(\frac{N_x}{R}\right) \tag{60}$$

where

$$\frac{t_c}{2t_s} < \left(\frac{t_c}{2t_s}\right)_{Optimum}$$

For the present evaluations, arbitrarily the values of K and $K'$ were selected to be equal to unity. Thus the efficiencies for all materials are uniformly higher than might be expected to be realized in practise, but the relative efficiencies are probably in the proper proportions.

Determination of Range of Loadings of Interest for Launch Vehicles

Values of thrust and diameter for the United States launch vehicles (from Ref.14) are given in Table 2. Also given are the available values of the loading index $\frac{N_x}{R}$ (from Ref. 15). The values of $\frac{N_x}{R}$ given here are somewhat higher than are obtained as in Ref. 14, simply by dividing the thrust by $2\pi R^3$. The larger values take into account such factors as increased loads resulting from bending due to wind shears.

Although data in Table 2 are far from comprehensive, they do indicate the approximate range encompassed by present launch vehicles. For the purposes of this report this range will be considered to be from 10 to 1000 $\frac{kN}{m^2}$ (approximately 1 to 100 psi).

Calculation of Efficiencies of Metal Shells for Reference

In order to have a basis for comparison, the structural efficiencies of a family of idealized monocoque metal shells were calculated using the procedures previously developed (Eq. 52). In addition to the idealization of the material stress-strain curves into two straight lines as described before, the mechanical properties assigned to the metals are somewhat advanced from current technology (properties used are given in Table 3). The curves of $\frac{W}{R^2}$ vs. $\frac{N_x}{R}$ resulting from these calculations are presented in fig. 25.

The range of loadings of interest for boost vehicles is indicated on fig. 25 by the grid lines on the graph. In this range the monocoque metal shells in general buckle elastically, as indicated by the slope of

1/2 of the curves on the log-log plot (i.e. in this region $\frac{W}{R} \sim \sqrt{\frac{N_x}{R}}$ ). Partial exceptions are: (1) the magnesium-lithium alloy, which reaches its yield stress at loadings just slightly in excess of those representative of the Scout vehicle, and (2) beryllium, which becomes plastic just at the edge of the arbitrarily selected "range of interest".

The efficiency of monocoque shells which buckle elastically can be increased by an appropriate form of stiffening. To extend the reference efficiencies of metal shells into this stiffened-shell regime, the metals were hypothesized into ideal sandwich shells, having non-load bearing cores of 277, 27.7, and 2.77 $\frac{kg}{m^3}$ (0.01, 0.001, and 0.0001 pci). The cores were assumed to stabilize the sandwich faces so that they would not wrinkle below the yield stress, and the shear stiffnesses of the cores were assumed adequate to approximate infinite shear-stiffness behavior. While such ideal stabilization would hardly be attainable with actual construction, especially for the lower core densities, it does provide a useful lower limit to the weights of metal sandwich shells against which to measure other materials. These lower limit weights (calculated via eqs. (57a) and (59a) and employing optimum core proportions as given by fig. 26) are compared to the monocoque shell weights in fig. 27.

Figure 27 shows that in the range of loadings of interest for boost vehicles there are only relatively small differences in weight among the common metals if effective stiffening, comparable to the intermediate density sandwich core, is employed. Beryllium permits appreciable

weight savings at the lower loadings; titanium is slightly superior at the higher loadings. Accordingly, these two metals are selected as the standards against which the composite efficiencies will be measured. For clarity the curves for beryllium and titanium are, therefore, separated out from fig. 27 and replotted as fig. 28.

Several measures useful not only for the evaluation of composites but also to help guide the advancement of boost-vehicle shell technology in general are evident in fig. 28.

1. Weight can be saved as effectively by improvements in stiffening (e.g. better core materials) as by improvements in face materials.
2. Even for the low loadings typical of boost vehicles, effective stiffening permits the achievement of efficiencies approaching the ultimate represented by the yield stress/density ratio of the material ( $\frac{W}{R} = \frac{\rho}{\sigma_y} \frac{N_x}{R}$ ).
3. Relative to such boosters as the Scout for which

   $\frac{W}{R} \gtrapprox 16.2 \frac{kg}{m^3} \left(.079 \frac{psf}{in}\right)$ @ $\frac{N_x}{R} = 469 \frac{kN}{m^2}$ (68 psi)

   substantially reduced weights may potentially be accessible, [$\frac{W}{R} < 2 \frac{kg}{m^3}$ $\left(.01 \frac{psf}{in}\right)$ in a titanium sandwich or $\frac{W}{R} \approx 3 \frac{kg}{m^3}$ $\left(.015 \frac{psf}{in}\right)$ in a monocoque beryllium construction .]

Calculation of Elastic Constants for Composites and Use in Efficiency Evaluations

With the curves of fig. 28 for metals established, a yardstick is

available for the measurement of possible combinations of materials for filaments and binders in composites. Accordingly, a comprehensive survey of available or potential combinations was undertaken. Both realistic and idealistic material properties were considered to provide a study of the effects of systematic variations, such as:

1. A variation in Young's modulus of the binder material for constant density.

and 2. A variation in Young's modulus of the binder for constant modulus/density ratio.

or 3. A variation in density of the binder for constant Young's modulus.

In all, eight filamentary materials and eight binder materials were considered in all combinations. The mechanical properties of these materials are given in Table 4. The binder materials are listed in quotation marks because they are hypothetical materials to a degree, because their properties have been adjusted somewhat from the normal values to provide the proper constant ratios to the other binder materials. The material properties summarized in Table 4 are also repeated in Tables 5-12 as the values for $V_b$ = 0 or 1, -i.e. the properties of composites at zero or one hundred percent binder.

In Tables 5-12 are presented the elastic constants calculated from the equations developed in Reference 1 and herein. These values are presented in comprehensive detail because they are the first such

available, and as such may be of use for other studies as well as this first evaluation for shell buckling for which they were primarily generated.

No attempt is made to draw general conclusions from the elastic-constant values calculated. These values are only an intermediate step in the evaluation, and it is through their employement in further analysis like that for shell buckling that their implications become evident.

In the following section the results of the employment of these elastic-constant values in shell buckling efficiency evaluations are presented. Eqs. (57) and (59) were used together with values of $\sigma_y$ calculated as follows.

The compressive strength of a fibrous composite was calculated on the basis of elastic instability of the fibers. The transverse Young's modulus, $E_2$, was treated as the foundation modulus and strengths for all materials were related to those experimentally obtained for glass reinforced plastics. Thus, the "yield strength", $\sigma_{yo}$, for uniaxial composites is given by:

$$\frac{\sigma_{yo}}{\sigma_{y_{ref}}} = \frac{V_f (E_f E_2)^{1/2}}{\{ V_f (E_f E_2)^{1/2} \}_{ref.}}$$

where the following reference values were used:

$\sigma_{y_{ref}}$ = 150,000 psi

$V_{f\ ref}$ = 0.7

$E_{f\ ref}$ = $10.5 \times 10^6$ psi

$E_{2\ ref}$ = $2.32 \times 10^6$ psi

For laminates having stiffening in more than one direction compressive failure was assumed to occur at the same strain as for the uniaxial laminate. Thus;

$$\frac{\sigma_y}{\sigma_{y0}} = \frac{E_L}{E_1}$$

The efficiency procedure is similar to that used for the reference efficiency evaluations for the metal shells (figs. 27 and 28), and comparisons to the metal shells are used to assess the merits of the various composite combinations.

Efficiencies of Composite Shells

The end objective of this study is the derivation of quantatative guidelines for the further development of most promising composite materials for aerospace structural applications. The scope of the problem is indicated to a degree by the numbers of constants to be evaluated (Table 5 - 12 ) and the complexity of the interrelations among the elastic constants and the efficiency of the structure to which they apply (as suggested by equations like 57). In this section the results of the employment of the newly available values of elastic constants in an arbitrarily selected first structural application analysis, namely that of cylindrical shells in axial compression for boost vehicles, are contemplated. As will be seen, a number of guidelines for future directions of research emphasis are generated in this first evaluation; not the least of these are toward other types of structural applications which need to be evaluated in similar fashion to this study of shells. Accordingly, the results will be presented and assessed first directly for their implications for the boost-vehicle case, and second for their possible extension to other structures. The sequence of presentation is: first, a survey of the possibilities associated with the use of a variety of filaments in an epoxy binder; second, a study of the effects of changes in binder material; third, a review of some of the complications associated with composites of the various types considered; and finally, consideration of extensions to other applications than boost vehicle shells.

Various filaments in epoxy binder

(a) Steel. The problems inherent in the use of filamentary materials for shell structures are brought out by the use of steel filaments in epoxy binder. Typical results for this combination are presented in Figure 29.

(In Figure 29(as in subsequent figures) the results for titanium and beryllium shells for the loadings of interest are repeated from Figure 28 for comparison. They are identified by the grid lines between the upper-long-dash-curves for titanium and lower short-dash curves for beryllium.)

The following results appear in Figure 29.

(1) The uniaxial nature of the steel filaments causes them to be much less efficient for shell buckling applications than the reference sheet metal shells, except at the highest loadings and for the extremely low density sandwich core.

(2) Some of the lack of bi-axiality associated with filaments is made up by the use of a $\pm 30^{\circ}$, $90^{\circ}$ laminate to provide essentially isotropic properties in the plane of the composite. Associated with the isotropic configuration, however, is a loss in axial stiffness compared to the $0^{\circ}$ configuration. This loss of axial stiffness leads to yielding at lower compressive loads, making the isotropic case less efficient than the $0^{\circ}$ orientation at the higher loading intensities (i.e. for non-elastic buckling).

(3) The $\pm 30^{o}$ comfiguration is less efficient than the isotropic configuration for all loading intensities. (This result was found to apply to all combinations of materials, not just to steel in epoxy.)

(4) There is no indication of a direction for development pointing toward a steel-in-epoxy composite having efficient characteristics for boost-vehicle shells.

(b) E-Glass. Effects of the use of hollow filaments and the general potential of E-Glass in epoxy is brought out in Figure 30, as follows:

(1) Hollow filaments (inside radius equal to 0.8 of the outside radius) are effective in increasing the efficiency of monocoque but not sandwich shells when epoxy resin is used as a binder.

(2) E-Glass reinforced epoxy is potentially competitive with metal for boost-vehicle sandwich shells only if substantially advanced sandwich core materials become available, and then only at the higher loading intensities.

(c) Hi-Modulus Glass and Asbestos. High modulus glass and asbestos filaments are perhaps more nearly "available" than the more advanced filaments like boron or alumina. The suitability of their application for the reinforcement of epoxy is evaluated in Figure 31 with the following results:

(1) While high-modulus glass reinforced epoxy is competitive

with the metals for shells only at low sandwich core densities and the highest compressive loading intensities, asbestos appears to be a highly competitive reinforcement. Asbestos in epoxy is more efficient than the metals like titanium for all core densities, and better even than beryllium at high loadings and low core densities.

(d) Boron and Alumina. Boron and alumina filaments have as advanced mechanical properties as any materials projected as likely candidates for near future use in composites. Their efficiencies in epoxy are evaluated in Figure 32 as follows:

(1) For monocoque shells for boost vehicles both boron and alumina bonded with 30 volume percent epoxy in an isotropic laminate configuration are substantially more efficient than the metals like titanium; they are not competitive with beryllium.

(2) Both boron and alumina reinforced epoxies become more attractive relative to metal construction when used as sandwich facings on ideal cores of lower and lower density. With present day core densities and loading intensities comparable to those for the Saturn V, for example, the boron reinforced epoxy sandwich considered should provide about 30 percent weight saving over the best metal construction.

(e) Epoxy Binder - elastic buckling. The results of Figures 29-32 have considered only the technologically reasonable case of 30 percent volume fraction binder and 70 percent volume fraction filaments. This packing density is representative of current practice for glass-reinforced plastics, but particularly in view of the rapid increases in transverse stiffness with better packing noted in Reference 1, study of the effects of changes in packing density is desirable. To this end Figures 33 and 34 have been prepared.

In Figures 33 and 34 are plotted values of $F = \frac{W/R}{\sqrt{N_x/R}}$ for the cylindrical shells against the volume fraction of binder $v_b$ in the composite. The values of F represent the elastic-buckling efficiencies; thus the lower the F value the higher the efficiency at the low loading intensities for which elastic buckling governs the design. For comparison the F-values for titanium and beryllium shells are included (the horizontal lines on the figures).

Figure 33 considers the monocoque shell (core density $\rho_c = \infty$ ). As would be expected, the composites increase in efficiency with increasing filament content and with increasing modulus-to-density ratio for the filamentary materials. The universally better efficiency of the isotropic laminate compared to the $0^\circ$ configuration is evidenced by the marked differences in the sets of curves for the two cases. Of interest is the marked effectiveness of small volume fractions of boron or alumina in the isotropic arrangement. With the $0^\circ$ configuration, high packing

ratios are evidently essential to make reinforced epoxy efficient as a monocoque shell; not so for the isotropic case, indeed for this application there is little to be gained by increasing the packing from the conventional 30 percent binder to the 9 percent or so maximum achieveable with perfect packing of round filaments.

Figure 34 considers the sandwich shell of core density perhaps achieveable by best present technology ( $\rho_c = 27.7 \frac{kg}{m^3}$ or .001 pci ). The results are qualitatively the same as for the monocoque shells but quantitatively less favorable to the composites. In the $0^o$ configuration only the best filaments in very high volume fractions (volume fractions so high as to be perhaps not practically attainable) are competitive; in the isotropic arrangement, however, asbestos, alumina, and boron are competitive with the metals, but for purely elastic buckling they show no liklihood of surpassing the beryllium sandwich. (It must be remembered, however, that for the boost-vehicle application the beryllium sandwich is not elastic, Figure 28, and boron filaments even in epoxy binder are indeed competitive or superior, Figure 32).

(f) Epoxy binder - general. The low Young's modulus of epoxy appears to impose a severe handicap to the development of composites for structurally efficient shells. Both Figures 33 and 34 show clearly the long way that the reinforcement has to go in reducing the F value from that for the epoxy (the end points, at $v_b = 1$ ) toward the much lower values representative of the better filamentary materials (the other end points

at $v_b = 0$ ). Clearly the use of a binder with better properties than epoxy should be helpful in improving the composite efficiencies at all packing ratios. Effects of the use of other binders than epoxy are considered in the following section.

Alumina and Boron Filaments in Various Binders

(a) Alumina filaments in binders of varying modulus and constant density.

In order to study the effects of improved binder materials the stiffest fibers (alumina) were considered in binders of the hypothetical "magnesium", "light-alloy II", "light-alloy III", and "boron" of Table 4. Results are shown as the F values for sandwich shells of reasonably advanced core densities in Figure 35. The vast improvement over the epoxy binder is immediately evident from the reduced abscissa scale from that of Figure 34. The isotropic configuration is now only very slightly more efficient than the axially stiffer $0^{\circ}$ configuration, and in first approximation the F values for both arrangements vary linearly with binder content between the end points for filaments and binders. Remembering that for launch vehicles beryllium metal is generally less efficient than is indicated by its elastic F-value, we conclude that for this application reasonable concentration of alumina fibers in any of these binders in any orientation should have the potential to surpass available structural metals.

(b) Boron filaments in various binders. Figure 36 shows that boron filaments have even greater potential for launch-vehicle shells than the alumina filaments of Figure 35. Here a variety of binder materials

are surveyed, and the results for epoxy resin are used as a reference. All binders considered are superior to the epoxy for all packing ratios. The best are the hypothetical "light-alloys" with "magnesium" not far behind. Quantitatively, 70 percent boron filaments in an isotropic array in a binder like the (heavy) "magnesium" of Figure 36 should have an elastic buckling efficiency (F value) as a sandwich shell 27 percent less than that for beryllium. For loadings of practical interest (as for the Saturn V) such a boron-magnesium composite should weigh less than one-half (44.5%) of the best metal construction.

Special stress conditions in composites

Because of the inherent non-homogeneity of composite materials, internal stress conditions are encountered that are not found in homogeneous metals. To a degree these special stresses are acceptable because of the high strength properties of filamentary reinforcements. Often, however, the binder material may be critical, as in the failure mode discussed in the section "

In any event attention must be paid to the possibility of inordinately high stresses within the composite.

In this section only the effects of various composition factors for the composites on some of the special stress conditions will be evaluated, for further guidance toward the development of improved composite materials. Typical variations in compressive strengths and

maximum shear stresses with composition will be considered.

(a) Compressive strengths. The variation of compressive strengths with configuration, binder content, and filament material for the binder with the poorest properties (epoxy) is presented in Figure 37. Values plotted were calculated as described in the section "

Despite the limitations noted for the method of calculation, the following trends are evident:

(1) The $0^{o}$ orientation is substantially stronger than the isotropic configuration.

(2) The advanced filaments (boron, alumina) have the highest strengths.

(3) The strengths increase substantially at the higher packing ratios.

Not shown, but evident from the analysis of the section " is the fact that the strengths should increase with improvements in binder properties over those for epoxy. The combination of all of these factors suggests that boron or alumina in an advanced matrix with reasonably high filament concentration will have high compressive strengths. The only factor which operates differently for providing strength than for providing elastic buckling efficiency is that of configuration, i.e. the $0^{o}$ orientation is strongest, but the isotropic array is the most efficient for elastic buckling.

(b) Maximum shear stresses. The compression of laminated plates having anisotropic laminae with principal stiffness directions at various angles can produce a maximum shear stress appreciably different from the maximum shear in an isotropic plate in compression. The magnitude of the maximum shear stress in the laminate is a function of the angles and anisotropies of the laminae. That these shear stresses may be appreciable is shown in Figures 38 and 39 (calculated as described in Reference 1).

In epoxy binder the maximum shear stresses approach 1.4 times the applied compressive stress in the alumina-reinforced epoxy with the isotropic configuration (Figure 38). These values are approximately halved if a binder material like "magnesium" is used (Figure 39). For the $\pm 30^{\circ}$ configuration the shear stresses are much smaller, and, of course, they revert to the normal factor of 1/2 of the compressive stress for the $0^{\circ}$ orientation.

Extensions of Efficiency Analyses to Other than Shell Buckling Applications

Really not much can be said with confidence a priori about the extension of the results of the studies of the efficiencies of composite materials for the boost-vehicle shell buckling application to other aerospace structural components with different loading conditions. For example, the similarity of the efficiency equation for the buckling of flat sandwich plates in compression, vis.

$$\frac{W}{b} = \frac{\rho_s + \rho_c \left(\frac{t_c}{2t_s}\right)}{\left[\left(\frac{t_c}{2t_s}+1\right)^3 - \left(\frac{t_c}{2t_s}\right)^3\right]} \left\{ \frac{\left(\frac{N_x}{b}\right)^{1/3}}{\left[\frac{\pi^2}{6(1-\nu_{LT}\nu_{TL})}\left(\sqrt{E_L E_T} + \nu_{LT} E_L + 2\{1-\nu_{LT}\nu_{TL}\}G_{LT}\right)\right]^{1/3}} \right\}$$

where b:plate width

to that for the cylindrical shell (equation 57 ) would appear to suggest the possibility of a similarity in the results for the two cases. The fact that the buckling of flat plates with integral, waffle-like stiffening (Ref. 5) has shown that the isotropic ($\pm 30^\circ$, $90^\circ$) configuration for the stiffening is not optimum for that case - whereas it was found to be for the composite shell - however, reduces confidence in the parallelism of the results.

Further, for most applications other than the boost-vehicle shell, strength rather than elastic buckling may well be the dominant factor, as it has been in the pressure vessel application to which most past composites have been applied. Indeed if any conclusion of this nature can be drawn from the results of this first study of efficiency of application, it is that the results

reinforce the inference that efficiency studies must be carried out in detail for other applications to evaluate the directions for most fruitful development of composites therefor.

## Concluding Remarks on Efficiencies

In this concluding section an attempt will be made to review the significant results that came out of the rather specific analysis made herein of the efficiency of composite material in as general a way as feasible, for guidance toward most fruitful directions for future emphasis. These remarks will endeavor to emphasize (1) results that were surprising (2) results that showed up areas which were considered unimportant and hence were not adequately explored, and (3) results of most significance for further research. Where possible the general factors which operated to produce these results will also be identified.

### Unexpected Results

The most unexpected beneficent result was that of the effectiveness of small percentages of boron or alumina filaments in epoxy binder in the isotropic configuration (see figs. 33 and 34). The resulting composite is apparently competitive with structural metals (except beryllium) at the low-loading intensities of the boost-vehicle shell application. There may well be other applications for which it has especial merit.

A most disappointing result was the failure of the hollow glass filaments to show greater advantages compared to solid glass (fig. 30). Evidently the very low transverse effectiveness of the hollow is more harmful than anticipated.

Unexpectedly large were the maximum shear stresses for the isotropic ($\pm 30^{\circ}$, $90^{\circ}$) configuration with epoxy resin (fig. 38). The magnitude of these

shear stresses may well be a limiting factor in the use of epoxy to yield an efficient sandwich shell.

The fact that $\pm 30^{o}$ configuration provides generally less axial stiffness than the isotropic ($\pm 30^{o}$, $90^{o}$) arrangement (Tables 5 to 12 ) was not anticipated and is intuitively repugnant. This result may derive from the still inexactly defined method of calculation (average of upper and lower bounds) of the transverse Young's modulus of a uni-directionally reinforced composite. While not anticipated, the effect is not of sufficient magnitude to be disturbing.

Unobtainable Results

Because of the unexpected good performance of the low percentage of boron or alumina in epoxy in the isotropic array, it is now apparent that investigation of more extreme combinations even than alumina and epoxy might be illuminating. The use of a hypothetical binder of the same modulus as epoxy and lower density, or both lower modulus and density, would have helped to clarify this interesting result.

In like fashion the unexpectedly high shear stresses in the $\pm 30^{o}$, $90^{o}$ configuration lead to a desire for knowledge of the corresponding stresses if isotropy is obtained with a $0^{o}$, $\pm 45^{o}$, $90^{o}$ array. The question whether the beneficent result with boron and alumina in epoxy is practically negated by the accompanying shear stresses or can be circumvented can not immediately be answered.

Perhaps of lesser interest because there in no sign that it may be profitable is the question whether hollow filaments other than E-glass lead to better efficiencies. The question was not explored in the present study, and on the basis of the results for the hollow glass there is no reason to explore it unless a hollow with better transverse stiffness is discovered.

## Significant Results

Three results of this study are of general significance - one is perhaps new, the others are perhaps more in the area of knowledge that should be common and has been here re-emphasized.

The first significant result is the demonstration of the importance of isotropy to the development of efficiency in the buckling of shells under axial compression. The isotropic configuration was universally the best for all reinforcements; similarly the achievement of near isotropy by the use of stiffer binder materials than epoxy generally improved the efficiency. Because of the effectiveness of the isotropic shells, perhaps the importance of isotropy for other buckling structures needs to be re-examined.

The second important result (somewhat related to the first) is that a better binder than epoxy is needed to take advantage of the improved properties becoming available in filaments. As shown in several facets of the study, boron filaments in a binder like magnesium hold much more structural promise than boron filaments in epoxy.

Finally the fact that all related elements of a structure contribute to the overall structural efficiency has been demonstrated again in this study,

and the improvement of one alone (such as the composite shell) may not be as effective as a lesser change in related areas (such as sandwich core). In general, the better the core material for the sandwich considered here, the more effective the improvement of the composite material to use for the sandwich faces.

## HIGH-MODULUS BINDER STUDIES

Experimental studies, described in detail in Appendix 5, were undertaken to survey the possibilities of effecting increases in Young's modulus of the binder materials now available for filamentary composites. These studies were divided into two areas: (1) investigations of the mechanical properties of the binders alone, and (2) tests of strength of filament wound rings utilizing the binders. The results are summarized as follows:

Binder Systems

Both filled and unfilled binders were investigated. Starting with a standard epoxy resin (Kopoxite 159) and a new resin of somewhat higher initial Young's modulus (Cyclopentenyl-Oxide-Ether, $E = 4.5 \frac{GN}{m^2}$ or 650 psi) a series of modified formulations were made. These formulations were used for the study of possibilities of particle fillers for raising the binder system modulus. In general these modified formulations had lower moduli and greater elongations than the parent resin.

Several types of fillers were used in an attempt to produce a high-modulus binder system. These fillers included aluminum and alumina powders, aluminum needles, and calcium carbonate powder. Highest values of Young's modulus were obtained with the least ductile modification of the parent resin; a value of $E = 13.8 \frac{GN}{m^2}$ (2000 ksi) was achieved at a volume fraction of 66% by weight aluminum powder. None of the filled resins achieved the tensile strength of the unmodified, unfilled resins from which they were compounded. In one case, however (the surface-modified aluminum powder) the filled resin strength was greater than that for the modified resin used for that specific combination. Both strength and ductility of the aluminum-filled resins were dependent upon the surface treatment of the particles. Highest filled strength was achieved with the calcium carbonate at 48.3% by weight filler.

Three Phase (Powder-filled Resin, Filament) Systems

Filament-wound rings were made incorporating the alumina and calcium-carbonate-filled resins and 12-end E-Glass rovings. As

might be expected, the filled resin did not infiltrate into the rovings so that an inhomogeneous ring resulted. Tensile strengths from split disk tests were less for the three-phase rings than for control rings wound with the same rovings and unfilled resins. The calcium carbonate filled system, however, produced rings stronger than a comparable ring bounded with the unfilled "high-modulus" cyclopentenyl-oxide-ether" resin.

## Concluding Remarks

Results obtained in this exploration of three-phase composite systems neither confirm nor deny the possibility of success for such an approach. While the strengths in tension attained were less than for good, normal two-phase systems, they were not so low that they could not be explained by the inevitable faultiness (use of 12-end roving instead of monofilaments, non-optimization of filler, etc.) of such exploratory tests. Through the use of fillers (either aluminum powder or calcium-carbonate) binder systems of substantially enhanced stiffness were achieved. In one case (the degreased aluminum powder - see Appendix 5 - in the most ductile resin) the filled resin had an appreciable elongation. In two cases (the conversion-coated aluminum powder and the calcium carbonate fillers) the ultimate tensile strengths were only somewhat less than for the parent resin. Thus, perhaps in view of the desirability of improved stiffness binders as demonstrated in the previous section of this report, further investigations in this area are warranted.

## GENERAL CONCLUSIONS

Detailed, specific conclusions derived from the several studies of which this report is comprised are given in the sections of the report to which they apply. In this section more generalized conclusions will be drawn, particularly regarding recommendations for directions for future work based on the results thus far achieved. These concluding recommendations are divided into three areas relating to (1) further evaluations of the potentials of various combinations and new combinations to be evaluated, (2) further developments in supporting analysis, and (3) supporting experiments.

Evaluations - With the bases available (elastic constants, strengths) efficiency analyses can be made for all types of structural applications. This effort can be made less onerous if the results of the shell buckling study contained herein are used as a guide for the selection of material combinations and configurations for evaluation. Thus, for example, the generalization where possible of such results as the importance of improved binder materials can reduce the combinations of filaments and binders that need to be studied. Certainly the determination of the generality of application of the $\pm 30^{\circ}$, $90^{\circ}$ (isotropic) configuration, found most suitable for cylindrical shells in axial compression herein, should be most useful for expediting evaluations of composites for other structural applications.

Yet to be evaluated at all are the effects of filament cross-sectional geometry on the efficiency of application, with the exception of the hollow-glass filaments investigated here. The merit of elliptical shapes for increasing the transverse stiffness (reported in Ref. 1) is an example of the type of advance that needs to be assessed. The hollow, as pointed out in the text also deserves further attention.

Supporting analyses - Analyses of elastic constants appear adequate for the guidance of future development of circular-filament reinforced composites. Effects of geometry of filament now need to be determined.

Perhaps most vitally needed are adequate strength criteria with consideration for the various combinations of stress possible within the composite. Thus the effects of the possibly large maximum shear stresses noted in the shell evaluation need to be evaluated and combined with analyses like those reported for tensile and compressive strength to provide insight into the ultimate material behavior.

Experiments - Experimental data are needed in all areas. Not only the three-phase composite system but all the attractive systems considered require further experimental investigation. The types of tests needed range from materials tests to assess mechanisms of failure to structural tests to assess validity of concepts. Thus, the tests must range, for example, from photoelastic tests of stresses in the

vicinity of a fiber to static tests to confirm or deny the validity of the isotropic configuration as outstanding for shells in compression.

REFERENCES


1. Rosen, B. Walter; Dow, Norris F.; and Hashin, Zvi: "Mechanical Properties of Fibrous Composites". NASA CR-31, April, 1964.

2. Stein, Manuel; and Mayers, J.: "Compressive Buckling of Simply Supported Curved Plates and Cylinders of Sandwich Construction". NACA TN-2601, Jan. 1952.

3. Shanley, F.R.: "Weight-Strength Analysis of Aircraft Structures", Dover Publications, Inc., New York, 1960.

4. Hashin, Zvi; and Rosen, B. Walter: "The Elastic Moduli of Fiber-Reinforced Materials". Journal of Applied Mechanics, Vol. 31E, pp. 223-232, June, 1964.

5. Tsai, S. W.: "Structural Behavior of Composite Materials", NASA CR-71, July, 1964.

6. Hashin, Z. and Shtrikman, S.: "On Some Variational Principles in Non-Homogeneous and Anisotropic Elasticity". Journal of Mech. Phys. Solids, Vol. 10, pp. 335-342, 1962.

7. Rosen, B. W.: "Tensile Failure of Fibrous Composites", AIAA preprint No. 64-73, Jan. 1964.

8. Metcalfe, A. G.; and Schmitz, G. K.: "Effect of Length on the Strength of Glass Fibers", ASTM 1964 preprint No. 87, June, 1964.

9. Dow, N. F. and Gruntfest, I. J.: "Determination of Most Needed Potentially Possible Improvements in Materials for Ballistic and Space Vehicles", GE TIS 60SD389, June, 1960.

10. Timoshenko, S.: "Theory of Elastic Stability", Section 21, McGraw-Hill, New York, 1936.

11. Rosen, B. W.; and Ketler, A. E. Jr.: "Hollow Glass Fiber Reinforced Plastics", GE-TIS R63SD41, May, 1963.

12. Prager, W.; and Hodge, P. G.: "Theory of Perfectly Plastic Solids", J. Wiley and Sons, 1951.

13. Koiter, W. T.: "General Theorems for Elastic-Plastic Solids", Chapter IV in "Progress in Solid Mechanics". Sneddon and Hill, Eds., North Holland, 1960.

14. Gerard, George; and Paperino, Ralph: "Minimum Weight Design of Stiffened Cylinders for Launch Vehicle Applications", Allied Research Associates Tech. Rept. No. 235-5, March, 1964.

15. Anderson, Roger A.: Private communication, Feb. 5, 1964.

16. Dong, S. B.; Matthiesen, R. B.; Pister, K.S.; and Taylor, R. L.; "Analysis of Structural Laminates", ARL report #76, USAF, September, 1961.

## APPENDIX 1

### Statistical Models for Fiber Strength

A frequently used model for the distribution function for strength of brittle fibers is the Weibull distribution, which may be written as:

$$g(\sigma) = L\alpha\beta\sigma^{\beta-1} exp(-L\alpha\sigma^{\beta}) \qquad (1\text{-}1)$$

where L is the specimen length and $\alpha$ and $\beta$ are the two parameters of the distribution function. For fibers whose strength is governed by this function, a logarithmic plot of mean fiber strength as a function of fiber length would be a straight line. Experimental data for glass fibers (e.g. ref. 8 ) indicate that such a plot should be bi-linear with the smaller slope in the very short gage-length region. The following work is the analysis of a simple model designed to illustrate a possible cause for this bi-linear behavior. The model is presented to indicate how the behavior of such fibers in a composite can be treated by the method of ref. 7 .

Brittle fibers shall be considered to consist of a series of fixed length fiber elements. The strength distribution for these elements shall be related to that for the fiber in the same fashion that the strength distributions of links and chains are related. Thus if the fiber links are characterized by a distribution function, $f(\sigma)$, the fibers will be characterized by $g(\sigma)$ given by:

$$g(\sigma) = n f(\sigma) \left[1 - F(\sigma)\right]^{n-1} \tag{1-2}$$

where

$$F(\sigma) = \int_0^{\sigma} f(\sigma)\, d\sigma \tag{1-3}$$

Consider a rectangular distribution as shown in fig. 14a. For this:

$$f(\sigma) = \frac{1}{b-a} \qquad a \le \sigma \le b$$

$$f(\sigma) = 0 \qquad \begin{cases} \sigma < a \\ \sigma > b \end{cases} \tag{1-4}$$

From (1-3) and (1-4):

$$F(\sigma) = \frac{\sigma - a}{b-a} \qquad a \le \sigma \le b$$

$$F(\sigma) = 0 \qquad \sigma < a \tag{1-5}$$

$$F(\sigma) = 1 \qquad \sigma > b$$

Substituting (1-4) and (1-5) into eq. (1-2) yields:

$$g(\sigma) = 0 \qquad \begin{cases} \sigma < a \\ \sigma > b \end{cases}$$

$$g(\sigma) = \frac{n}{b-a}\left(\frac{b-\sigma}{b-a}\right)^{n-1} \qquad a \le \sigma \le b \qquad (1\text{-}6)$$

The mode of $g(\sigma) = \sigma^* = a$

Next consider the double rectangular distribution shown in fig. 15a.

Here:

$$\left.\begin{array}{ll} f(\sigma) = 0 & \sigma < \sigma_1 \\ f(\sigma) = \dfrac{p}{\sigma_2 - \sigma_1} & \sigma_1 \le \sigma \le \sigma_2 \\ f(\sigma) = 0 & \sigma_2 < \sigma < \sigma_3 \\ f(\sigma) = \dfrac{1-p}{\sigma_4 - \sigma_3} & \sigma_3 \le \sigma \le \sigma_4 \\ f(\sigma) = 0 & \sigma > \sigma_4 \end{array}\right\} \qquad (1\text{-}7)$$

Substituting eqs. (1-7) into eq. (1-3) yields:

$$\left.\begin{array}{ll} F(\sigma) = 0 & \sigma < \sigma_1 \\ F(\sigma) = p\left(\dfrac{\sigma - \sigma_1}{\sigma_2 - \sigma_1}\right) & \sigma_1 \le \sigma \le \sigma_2 \\ F(\sigma) = p & \sigma_2 < \sigma < \sigma_3 \\ F(\sigma) = p + (1-p)\left(\dfrac{\sigma - \sigma_3}{\sigma_4 - \sigma_3}\right) & \sigma_3 \le \sigma \le \sigma_4 \\ F(\sigma) = 1 & \sigma > \sigma_4 \end{array}\right\} \qquad (1\text{-}8)$$

For the chain, substitution of eqs. (1-7) and (1-8) into eq. (1-2) yields:

$$
\left.
\begin{aligned}
g(\sigma) &= 0 && \sigma < \sigma_1 \\
g(\sigma) &= \frac{np}{\sigma_2 - \sigma_1}\left[1 - p\left(\frac{\sigma - \sigma_1}{\sigma_2 - \sigma_1}\right)\right]^{n-1} && \sigma_1 \le \sigma \le \sigma_2 \\
g(\sigma) &= 0 && \sigma_2 < \sigma < \sigma_3 \\
g(\sigma) &= \frac{n(1-p)}{\sigma_4 - \sigma_3}\left[(1-p) - (1-p)\left(\frac{\sigma - \sigma_3}{\sigma_4 - \sigma_3}\right)\right]^{n-1} && \sigma_3 \le \sigma \le \sigma_4 \\
g(\sigma) &= 0 && \sigma > \sigma_4
\end{aligned}
\right\} \quad (1\text{-}9)
$$

This yields the distribution function shown in fig. 15c. The values of the two peaks are:

$$g(\sigma_1) = \frac{np}{\sigma_2 - \sigma_1} \qquad (1\text{-}10)$$

$$g(\sigma_3) = \frac{n(1-p)^n}{\sigma_4 - \sigma_3} \qquad (1\text{-}11)$$

It is seen that the mode changes from $\sigma_3$ to $\sigma_1$ at some value of n. The value at which they are equal is plotted in fig. 16 and is obtained by setting:

$$g(\sigma_1) = g(\sigma_3) \qquad (1\text{-}12)$$

From eqs. (1-10) to (1-12):

$$n = \frac{\log\left[\rho\left(\frac{\sigma_4-\sigma_3}{\sigma_2-\sigma_1}\right)\right]}{\log(1-\rho)} \tag{1-13}$$

The average strength for a given length fiber composed of n links taken from the population characterized by eqs. (1-7) is found as follows:

$$\bar{\sigma} = \int_0^\infty \sigma\, g(\sigma)\, d\sigma \tag{1-14}$$

$$\therefore \bar{\sigma} = \int_{\sigma_1}^{\sigma_2} \frac{n\sigma\rho}{\sigma_2-\sigma_1}\left[1-\rho\left(\frac{\sigma-\sigma_1}{\sigma_2-\sigma_1}\right)\right]^{n-1} d\sigma + \int_{\sigma_3}^{\sigma_4} \frac{n\sigma(1-\rho)^n}{\sigma_4-\sigma_3}\left(\frac{\sigma_4-\sigma}{\sigma_4-\sigma_3}\right)^{n-1} d\sigma \tag{1-15}$$

which yields

$$\bar{\sigma} = \left[\sigma_1-\sigma_2(1-\rho)^n\right] + \frac{\sigma_2-\sigma_1}{\rho(n+1)}\left[1-(1-\rho)^{n+1}\right] + (1-\rho)^n\sigma_3 + \frac{\sigma_4-\sigma_3}{n+1}(1-\rho)^n \tag{1-16}$$

Eq. (1-16) is plotted in fig. 17 for selected values of p and $\sigma_i$. It is seen that the bi-linear distribution is very well simulated.

## APPENDIX 2

### Compressive Strength of Fibrous Composites

The compressive strength of a fibrous composite is evaluated by treating the elastic stability of a two-dimensional array of layers of fiber and matrix material. The fibers are considered to be relatively stiff as compared to the binder and hence shear deformations of the fiber are neglected. Instability will be evaluated by utilizing the energy method. The change in strain energy for the fiber, $\Delta V_f$, and the binder, $\Delta V_b$, as the composite changes from a compressed but unbuckled configuration to the buckled state will be equated to the work, $\Delta T$, done by the fiber loads. Thus,

$$\Delta V_f + \Delta V_b = \Delta T \tag{2-1}$$

For the two dimensional case the load per running inch on each fiber can be expressed as the produce of fiber stress, $\sigma_f$, and fiber thickness, h:

$$P = \sigma_f h \tag{2-2}$$

The procedure then is to assume various buckle patterns and find the lowest buckling load. If all terms in the strain energy are appropriately considered each of these buckling stresses will provide an upper bound; and the lowest

of these values may be taken as a buckling load. The cases to be considered herein are the two cases shown in fig. 3 where the buckling pattern in all fibers is of the same wavelength with adjacent fibers either in or out of phase with one another. The mixture of the two can be expected to have a buckling stress larger than the smaller load for the two individual modes. Each fiber will be assumed to buckle into the sinusoidal pattern expressed by the following series in v, the displacement in the y direction:

$$V = \sum_{n} a_n \sin \frac{n\pi x}{L} \tag{2-3}$$

For the extension mode, the transverse strain is assumed to be independent of the y direction so that:

$$\epsilon_y = \frac{v}{c} \tag{2-4}$$

and

$$\sigma_y = E_b \frac{v}{c} \tag{2-5}$$

The changes in strain energy associated with the axial and shear stresses are considered negligible with respect to those due to the transverse stresses. Thus

$$\Delta V_b = \frac{1}{2} \int_V \sigma_y \epsilon_y \, dV \tag{2-6}$$

Substituting eqs. (2-3) to (2-5) into (2-6) yields:

$$\Delta V_b = \frac{E_b L}{2c} \sum_n a_n^2 \tag{2-7}$$

From ref. 10 (in the present nomenclature)

$$\Delta V_f = \frac{\pi^4 E_f h^3}{48 L^3} \sum_n n^4 a_n^2 \tag{2-8}$$

and

$$\Delta T = \frac{P\pi^2}{4L} \sum_n n^2 a_n^2 \tag{2-9}$$

Substituting eqs. (2-7) to (2-9) into (2-1):

$$P = \frac{\pi^2 E_f h^3}{12 L^2} \; \frac{\sum_n n^4 a_n^2 + \frac{24 L^4 E_b}{\pi^4 c h^3 E_f} \sum_n a_n^2}{\sum_n n^2 a_n^2} \tag{2-10}$$

Expression (2-10) is a minimum for one value of n, say m, hence

$$\sigma_{f_{cr}} = \frac{\pi^2 E_f h^2}{12 L^2} \left[ m^2 + \frac{24 L^4 E_b}{\pi^4 c h^3 E_f} \left( \frac{1}{m^2} \right) \right] \tag{2-11}$$

Since m is large it may be treated as a continuous variable and eq. (2-11) can be minimized by setting

$$\frac{\partial \sigma_{f_{cr}}}{\partial m^2} = 0 \tag{2-12}$$

This yields

$$\sigma_{f_{cr}} = 2 \left[ \frac{V_f E_b E_f}{3(1-V_f)} \right]^{1/2} \tag{2-13}$$

where $$V_f = \frac{h}{h+2c} \tag{2-14}$$

and for the composite stress, $\sigma_c$ ,

$$\sigma_c = V_f \sigma_{f_{cr}}$$

$$\therefore \sigma_c = 2 V_f \left[ \frac{V_f E_b E_f}{3(1-V_f)} \right]^{1/2} \tag{2-15}$$

The critical strain, $\epsilon_{cr}$ , can be evaluated from eq. (2-13). Thus,

$$\epsilon_{cr} = 2 \left[ \frac{V_f}{3(1-V_f)} \right]^{1/2} \left( \frac{E_b}{E_f} \right)^{1/2} \tag{2-16}$$

The shear instability mode is evaluated in a similar fashion. Here the displacements of all fibers are assumed to be of the same amplitude and

in phase with one another. The shear strains are assumed to be a function of only the longitudinal coordinate. In the binder:

$$\gamma_{xy} = \frac{\partial u_y}{\partial x} + \frac{\partial u_x}{\partial y} \tag{2-17}$$

Since the transverse displacement is independent of the transverse coordinate, y:

$$\left.\frac{\partial u_y}{\partial x}\right|_b = \left.\frac{du_y}{dx}\right|_f \tag{2-18}$$

Since the shear strain is independent of y:

$$\frac{du_x}{dy} = \frac{1}{2c}\left[u_x(c) - u_x(-c)\right] \tag{2-19}$$

Since the fiber shear deformation is negligible:

$$u_x(c) = \frac{h}{2}\left.\frac{du_y}{dx}\right|_f \tag{2-20}$$

Substituting (2-19) into (2-18):

$$\frac{du_x}{dy} = \frac{h}{2c}\left.\frac{du_y}{dx}\right|_f \tag{2-21}$$

Substituting (2-21) and (2-18) into (2-17):

$$\gamma_{xy} = \left(1 + \frac{h}{2c}\right) \frac{du_y}{dx}\Big|_f \tag{2-22}$$

and

$$\tau_{xy} = G_b \gamma_{xy} \tag{2-23}$$

The changes in strain energy associated with the extensional stresses are considered negligible for this case. Thus:

$$\Delta V_b = \frac{1}{2} \int_V \tau_{xy} \gamma_{xy} \, dV \tag{2-24}$$

Substituting eqs. (2-3), (2-22) and (2-23) into (2-24) yields:

$$\Delta V_b = G_b c \left(1 + \frac{h}{2c}\right)^2 \left(\frac{\pi^2}{2L}\right) \sum_n a_n^2 n^2 \tag{2-25}$$

Using eq. (2-25) in place of eq. (2-7) in eq. (2-1) and proceeding as for the extension mode,

$$\sigma_{f_{cr}} = \frac{G_b}{v_f(1-v_f)} + \frac{\pi^2 E_f}{12} \left(\frac{mh}{L}\right)^2 \tag{2-26}$$

Since L/m is the buckle wavelength, the second term in eq. (2-26) is small for wavelengths large compared with the fiber diameter, and the buckling stress is given approximately by:

$$\sigma_{f_{cr}} = \frac{G_b}{V_f (1-V_f)} \tag{2-27}$$

and

$$\sigma_o = \frac{G_b}{1-V_f} \tag{2-28}$$

$$\epsilon_{cr} = \frac{1}{V_f (1-V_f)} \left( \frac{G_b}{E_f} \right) \tag{2-29}$$

The lower of the values given by eqs. (2-15) and (2-28) is the best estimate for the compressive strength.

## APPENDIX 3

### Laminate Stress Analysis

The analysis of stresses in a laminate follows that of Ref. 16 but is modified to evaluate elastic constants and simplified to neglect coupling between bending and extension. The laminate is considered to have a large number of symmetric laminae so that the bending stiffness and extensional stiffness are related in the same fashion as they are for an homogeneous material. This also results in bending and extensional stresses being uncoupled. Transverse shear is also neglected.

The stress-strain law for each layer relative to the lamina principal axes is:

$$\sigma_i = c_{ij} \epsilon_j \qquad ij = 1, 2, 3 \qquad (3\text{-}1)$$

$\sigma_i$ = stress
$\epsilon_j$ = strain
$c_{ij}$ = elastic constants
- and a repeated index denotes summation

For the orthotropic lamina of a filament wound material:

$$c_{ij} = \begin{bmatrix} c_{11} & c_{12} & 0 \\ c_{12} & c_{22} & 0 \\ 0 & 0 & c_{33} \end{bmatrix} \qquad (3\text{-}2)$$

where these stiffnesses are related to the conventional elastic constants by

$$c_{11}^{(k)} = \frac{E_1^{(k)}}{1 - \nu_{21}^{(k)} \nu_{12}^{(k)}}$$

$$c_{22}^{(k)} = \frac{E_2^{(k)}}{1 - \nu_{21}^{(k)} \nu_{12}^{(k)}} \qquad (3\text{-}3)$$

$$c_{12}^{(k)} = c_{21}^{(k)} = \frac{\nu_{21}^{(k)} E_2^{(k)}}{1 - \nu_{12}^{(k)} \nu_{21}^{(k)}}$$

$$c_{33}^{(k)} = 2G_{12}$$

$E_1$ = Young's modulus in fiber direction
$E_2$ = Young's modulus normal to fiber direction
$G_{12}$ = Shear modulus in fiber plane
$\nu_{21}$ = Ratio of strain in the 1 direction to strain in the 2 direction for uniaxial stress in the 2 direction

The elastic constants in the principal laminae directions are defined by:

$$\bar{\sigma}_i = c_{ij} \bar{\epsilon}_j \qquad (3\text{-}4)$$

where the overbar denotes quantities referenced to the laminate axes. These constants can be obtained from the lamina constants by coordinate

transformations of the stress and strain as follows:

$$\sigma_i = T_{ij}\,\sigma_j \qquad (3\text{-}5)$$

$$\epsilon_i = T_{ij}\,\epsilon_j$$

where

$$T_{ij} = [T] = \begin{bmatrix} \cos^2\theta & \sin^2\theta & 2\sin\theta\cos\theta \\ \sin^2\theta & \cos^2\theta & -2\sin\theta\cos\theta \\ -\sin\theta\cos\theta & \sin\theta\cos\theta & \cos^2\theta - \sin^2\theta \end{bmatrix}$$

Substitution of (3-5) and (3-4) into (3-1) yields:

$$\bar{c}_{ij} = L_{im}\, c_{mn}\, T_{nj} \qquad (3\text{-}6)$$

where the $L_{ij}$ are the elements of the inverse of the $T_{ij}$ matrix.

Consider a laminate of n layers subject to in-plane loads. Since transverse shear and coupling between bending and extension have been neglected the strains in all layers will be the same and the average stresses, $\bar{\tau}_i$, will be:

$$\bar{\tau}_i = \sum_{k=1}^{n} \sigma_i^{(k)} t_k$$

$$\bar{\tau}_i = \sum_{k=1}^{n} c_{ij}^{(k)} \bar{\epsilon}_j\, t_k \qquad (3\text{-}7)$$

$$\bar{\tau}_i = \bar{\epsilon}_j \bar{A}_{ij}$$

where $t_k$ = fraction of total thickness in kth layer and

$$\overline{A}_{ij} = \sum_{k=1}^{n} \bar{c}_{ij}^{(k)} t_k$$

Equations (3-7) may be rewritten

$$\bar{\epsilon}_j = \overline{B}_{ij} \bar{\tau}_i \qquad (3\text{-}8)$$

where the $B_{ij}$ are the elements of the inverse of the $A_{ij}$ matrix.

This is the solution for lamina strains as a function of applied stresses, $\sigma_i$.

From Equation (3-8) the desired elastic constants can be defined as follows:

$$E_L = \frac{1}{\overline{B}_{11}}$$

$$E_T = \frac{1}{\overline{B}_{22}} \qquad (3\text{-}9)$$

$$G_{LT} = \frac{1}{\overline{B}_{33}}$$

$$\nu_{TL} = \frac{\overline{B}_{12}}{\overline{B}_{11}}$$

$$\nu_{LT} = \frac{\overline{B}_{12}}{\overline{B}_{22}}$$

The stresses in the kth lamina are now given by

$$\bar{\sigma}_i^{(k)} = \bar{c}_{ij}^{(k)} \bar{\epsilon}_j \tag{3-10}$$

and the stress components within any lamina referenced to axes making an angle, $\alpha$, with the longitudinal and transverse axes are given by:

$$\sigma_i^{(k)} = T_{ij} \bar{\sigma}_j^{(k)} \tag{3-11}$$

where the $T_{ij}$ contain $\alpha$ in place of $\theta$.

The elastic constants of equation (3-9) and the stresses of equation (3-11) have been evaluated for various geometries. The results are discussed in the text.

## APPENDIX 4

### Elastic Stability of Filament Wound Cylindrical Shells Under Axial Compression

The stability analysis of filament wound cylindrical shells is a small deflection, classical analysis of anisotropic shells. The work utilizes the results of ref. 2 . Under the assumptions that transverse shear strain is negligible and that each bending stiffness is related to the appropriate extensional stiffness in the same fashion that bending and extensional stiffness of homogeneous materials are related, the buckling stress, $\sigma_{cr}$, is obtained from eq. A4 of ref. 2.

The buckling stress equation can be written in the following form:

$$k = \frac{\sigma_{cr}}{E_L} = m^2 \left(\frac{h}{a}\right)^2 \beta_1 \left\{1 + \beta_2 \phi^2 + \beta_3 \phi^4\right\} + \frac{1}{m^2 \left(\frac{\pi R}{a}\right)^2 \left[\frac{1}{\beta_3} + \beta_4 \phi^2 + \phi^4\right]} \tag{4-1}$$

where

$$\left.\begin{aligned} \phi &= \frac{na}{2\pi Rm} \\ \beta_1 &= \frac{\pi^2}{12(1 - \nu_{TL}\nu_{LT})} \\ \beta_2 &= 2\left[\nu_{LT} + 2(1 - \nu_{TL}\nu_{LT})\frac{G_{LT}}{E_L}\right] \\ \beta_3 &= \frac{E_T}{E_L} \\ \beta_4 &= \frac{E_L}{G_{LT}} - 2\nu_{TL} \end{aligned}\right\} \tag{4-2}$$

$a$ = shell length

$R$ = shell radius

$m$ = longitudinal wave number

$n$ = circumferential wave number

$L$ = longitudinal direction

$T$ = transverse or circumferential direction

For long cylinders, the longitudinal wave number may be treated as a continuous variable and the buckling stress can be analytically minimized with respect to it. For simplicity, $m^2$ and $\phi^2$ will be treated as the independent variables, rather than $m$ and $n$. Thus:

$$\frac{\partial k}{\partial m^2} = 0 \tag{4-3}$$

Substituting eq. (4-1) into eq. (4-3):

$$\left(\frac{h}{a}\right)^2 \beta_1 \left[1 + \beta_2 \phi^2 + \beta_3 \phi^4\right] - \frac{1}{m^4 \left(\frac{\pi R}{a}\right)^2 \left[\frac{1}{\beta_3} + \beta_4 \phi^2 + \phi^4\right]}$$

$$\therefore \quad m^2 = \left\{ \frac{1}{\left(\frac{h}{a}\right)^2 \beta_1 \left[1 + \beta_2 \phi^2 + \beta_3 \phi^4\right] \left(\frac{\pi R}{a}\right)^2 \left[\frac{1}{\beta_3} + \beta_4 \phi^2 + \phi^4\right]} \right\}^{1/2} \tag{4-4}$$

The minimum stress is then defined by substituting eq. (4-4) into eq. (4-1):

$$k = \frac{2h}{\pi R}\left\{\frac{\beta_1\left[1+\beta_2\phi^2+\beta_3\phi^4\right]}{\left[\frac{1}{\beta_3}+\beta_4\phi^2+\phi^4\right]}\right\}^{1/2} \tag{4-5}$$

Next the circumferential wave number will be optimized by assuming that it is valid to treat it as a continuous variable. Thus:

$$\frac{\partial k}{\partial \phi^2} = 0 \tag{4-6}$$

and from eqs. (4-1) and (4-6):

$$\left[1+\beta_2\phi^2+\beta_3\phi^4\right]^{-1/2}\left[\frac{1}{\beta_3}+\beta_4\phi^2+\phi^4\right]^{-3/2}\left[\beta_2-\beta_3\beta_4\right]\left[\frac{1}{\beta_3}-\phi^4\right]=0 \tag{4-7}$$

For an isotropic shell:

$$\beta_2 - \beta_3\beta_4 = 0 \tag{4-8}$$

and any value of $\phi$ along with the $m$ value defined by eqs. (4-4) gives the same buckling stress. When eq. (4-8) is not satisfied one of the following must exist:

$$1+\beta_2\phi^2+\beta_3\phi^4 \longrightarrow \infty \tag{4-9}$$

$$1 + \beta_3 \beta_4 \phi^2 + \beta_3 \phi^4 \longrightarrow \infty \tag{4-10}$$

$$\phi^4 = \frac{1}{\beta_3} \tag{4-11}$$

Also the case

$$\phi = 0 \tag{4-12}$$

must be considered as it is the value at one end of the allowable range. For either (4-9), (4-10) or (4-12) it is apparent that eq. (4-5) reduced to:

$$k = \frac{2h}{\pi R} \left(\beta_1 \beta_3\right)^{1/2} \tag{4-13}$$

From eqs. (4-11) and (4-5):

$$k = \frac{2h}{\pi R} \left(\beta_1 \beta_3\right)^{1/2} \left[ \frac{2 + \frac{\beta_2}{\beta_3^{1/2}}}{2 + \beta_4 \beta_3^{1/2}} \right] \tag{4-14}$$

Substituting eqs. (4-2) into eq. (4-13) yields:

$$\sigma_{cr} = \sqrt{E_L E_T} \left(\frac{h}{R}\right) \left[ \frac{1}{3(1 - \nu_{LT} \nu_{TL})} \right]^{1/2} \tag{4-15}$$

Substituting eqs. (4-2) into eq. (4-14) yields:

$$\sigma_{cr} = \sqrt{E_L E_T}\left(\frac{h}{R}\right)\left[\frac{1}{3(1-\nu_{LT}\nu_{TL})}\right]^{1/4}\left\{\frac{1+\sqrt{\frac{E_L}{E_T}}\left[\nu_{LT}+2(1-\nu_{LT}\nu_{TL})\frac{G_{LT}}{E_L}\right]}{1+\frac{1}{2}\sqrt{\frac{E_T}{E_L}}\left[\frac{E_L}{G_{TL}}-2\nu_{TL}\right]}\right\}^{1/2} \qquad (4\text{-}16)$$

The lower of the values obtained from eqs. (4-15) and (4-16) is the small deflection theory result for orthotropic cylinders and this is the value used in the studies described in the body of this report.

Recent attempts to evaluate the wave numbers implicitly in the above minimization have indicated the existance of a branch of the curve not previously considered. This is presently being studied to determine if this results in lower buckling stress values for any of the ranges of parameters considered.

# APPENDIX 5

## Experimental Investigations of Binder Systems for Composite Materials

by
P. Juneau

Details of the experiments on binder systems directed toward the development of binders of Young's moduli greater than those for available epoxy resins are described in the following sections.

### Resin Studies

#### Resorcinol Diglycidyl Ether Based Resins

Preliminary investigations were made on the following formulations:

| Series | Kopoxite 159 | MNA | EM207 | BDMA |
|---|---|---|---|---|
| 17 | 100 | 125 | --- | 1 |
| (PJ122A) 1&2 | 100 | 125 | 25 | 1 |
| (PJ122B) 14 | 100 | 125 | 50 | 1 |
| (PJ122C) 19 | 100 | 125 | 75 | 1 |

Since Kopoxite 159 (a relatively pure resorcinol diglycidyl ether) tended to crystallize on standing at room temperature, the formulations were made by first melting the Kopoxite 159, then stirring in the other components until a homogeneous mixture was achieved. The formulations were then vacuum de-aerated and cast in a mold 1/4" x 8" x 11". After curing the 1/4" sheet of plastic was cut into tensile specimens and tested.

Further investigations were undertaken using Kopoxite 159 and curing agents other than MNA ("Nadic Methyl Anhydride"). The following table lists

two formulations of interest:

| Series | Kopoxite 159 | Methyl Nadic Anhydride | BDMA | Moleic Anhydride | Harcure E |
|---|---|---|---|---|---|
| 20 | 100 | | 1 | 65 | |
| 21 | 100 | 80 | 1 | | 102 |

These materials were prepared in order to determine the effect of various molecular constituents on the physical properties of epoxy castings. Formulation 20 darkened considerably upon curing, and was quite brittle. Formulation 21 was soft and flexible.

The tensile data obtained on these materials are outlined in Table A. These data illustrate the range of properties that can be achieved by modifying the constituents of a resin system, and altering reaction ratios in a judicious manner.

Table A. Mechanical Properties of Resorcinol Diglycidyl Ether Formulations

| Series | UTS, psi | Young's Modulus psi | Elongation to Break % |
|---|---|---|---|
| 14 | $9.6\text{-}10.5 \times 10^3$ | $.482\text{-}.534 \times 10^6$ | 2.3 - 2.7 |
| (PJ122A) 1&2 | $9.1\text{-}12.0 \times 10^3$ | $.445\text{-}.490 \times 10^6$ | 1.4 - 2.2 |
| (PJ122B) 14 | $8.1\text{-}8.3 \times 10^3$ | $.331\text{-}.368 \times 10^6$ | 5.2 - 6.5 |
| (PJ122C) 19 | $5.7\text{-}5.9 \times 10^3$ | $.277\text{-}.284 \times 10^6$ | 10 |
| 20 | $13.6\text{-}13.8 \times 10^3$ | $.503\text{-}.557 \times 10^6$ | 5.3 - 8.9 |
| 21 | unable to break | $.095 \times 10^6$ | 25 |

## Cyclopentenyl Oxide Ether Based Resins

Two new epoxide resins were investigated.

ERLA 0400

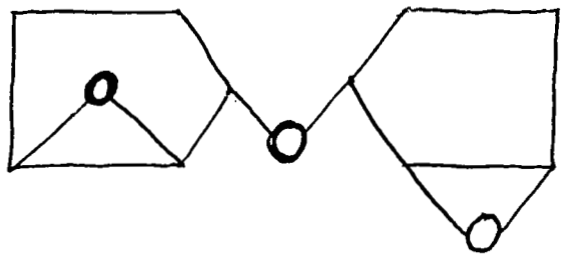

and

ERRA 0300

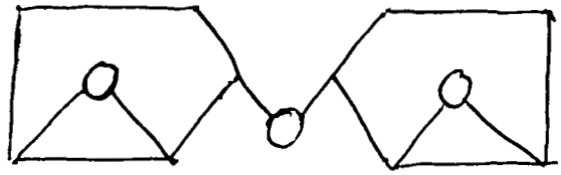

These resins were incorporated in the following formulations, which were cast into 1/4" x 8" x 11" plates, machined and tested.

Cyclopentenyl Oxide Ether Based Formulations

| Series | Resin | Curing Agent | Polyol |
|---|---|---|---|
| 25 | ERRA 0300 94.2 pbw | Moleic Anhydride 83.5 pbw | Trimethylol Propane 9.0 pbw |
| 26 | ERRA 0300 | m-Phenylene Diamine 80 pbw | --- |
| 27 | Repeat of #26 using filtered resin | | |
| 12A-34-2 | ERRA 0300 | m-Phenylene Diamine 108 pbw | --- |
| 12A-34-3 | ERLA 0400 | Curing Agent 2 10.8 pbw | --- |
| 12A-34-4 | ERLA 0400 | m-Phenylene Diamine 108 pbw | --- |

Series 26, 27, and 12A-34-2, upon examination after curing, were found to contain numerous small flakes of brown material, in spite of the great care having been taken during casting to filter the uncured resin. By contrast, 12A-34-4 was free of defects after curing, as was Series 25. An attempt to cure Series 12A-34-3 was met with failure when the cured piece was examined and found to have shattered inthe mold. The two successful pieces and 12A-34-2 (to evaluate the effect of inclusions) were machined into tensile specimens and tested for mechanical properties. Results are outlined in Table B. These data show that the strength characteristics of these resins, using in-phenylene diamine as the curing agent, are only slightly higher than the Kopoxite 159 based resins.

Table B. Physical Properties-Cyclopentenyl Oxide Ether Resins

| Series | UTS, psi | Young's Modulus psi | Elongation to Break % |
|---|---|---|---|
| 25 | $6.15\text{-}715 \times 10^3$ | | 2.4 - 5.4 |
| 12A-34-2 | $9.58\text{-}13.3 \times 10^3$ | $.632\text{-}.676 \times 10^6$ | 1.6 - 2.5 |
| 12A-34-4 | $13.6\text{-}15.0 \times 10^3$ | $.620\text{-}.679 \times 10^6$ | 2.3 - 2.7 |

Filler Studies

Aluminum Fillers

Aluminum flake, aluminum powder, and aluminum needles were investigated. Leafing grade aluminum flake was incorporated into series PJ122A resin to the extent of 30% by volume (approximately 50% by weight). The result was a very thick pasty mass that was impossible to de-aerate

using vacuum techniques, or centrifugation to 20,000 RPM. These difficulties were attributed to the tendency of the flake aluminum to overlap and link in addition to the thixotropic effect of the finely divided particles. Due to these difficulties, no flake aluminum filler pieces were produced that were suitable for fabrication into test specimens.

Alweg PF aluminum needles have undergone experimentation in which specimens of the needles (0.27" length by 0.028" to 0.032" diameter) were encapsulated in Series PJ122C resin. Encapsulation was accomplished by first spreading a layer of needles 1/2" deep in a flat pan, pouring resin on top, then de-aerating under vacuum. After curing the casting was machined into tensile specimens and tested.

Aluminum powder, approximately 325 mesh, was incoporated into series PJ122C resin to the extent of 11% by weight of aluminum, and 34% resin. Since the aluminum powder was suspected of being coated with oil and other contaminants, experiments were performed in which solvent cleaned aluminum was used as the filler. The use of two surface active agents, 26020 and A1100, was investigated in an attempt to improve adhesion between the filler particles and resin matrix. Finally, the use of a chromite/phosphate etch to conversion coat the aluminum particles was attempted in an effort to improve composite properties.

Solvent cleaning of the aluminum powder was accomplished by washing the material several times in ligroine and decanting off the excess, then washing with acetone and removing the excess by suction through a Buchner funnel. If the powder was to be used as the filler in a system containing a surface active

agent such as 26020 or A1100, the agent was mixed into the resin before the aluminum was added, then the filled formulation was handled in the usual manner.

Chromate/phosphate etching was done by first pouring approximately 500 g aluminum powder into 1000 cc of 5% Detrex solution at 110°F, and allowing this mixture to stand 15-30 minutes. The excess solution was then decanted off, and the aluminum washed with water several times, using a Buchner funnel to pull off the last traces of liquid. The aluminum was then poured into a cold solution of 4500 cc $H_2O$, 750 cc 98% $H_2SO_4$, 150 g $Na_2Cr_2O_7$ and allowed to stand ten minutes, at the end of which period the excess chromic acid was poured off, and the aluminum powder washed with water, then acetone, and dried by suction using a Buchner funnel. It was necessary to exercise a great deal of caution during the chromic acid wash, since the large surface area of aluminum exposed tended to cause violent reactivity and generation of $H_2$ gas.

Alumina and Calcium Carbonate Fillers

In view of the problems associated with using aluminum fillers, such as the difficulties involved in de-aerating aluminum filled composites containing very fine particles, some investigations were performed using 900 mesh $Al_2O_3$ (15 micron maximum particle size) and Surfex MM $CaCO_3$ (3 micron maximum particle size).

The following table summarizes the experiments performed on resin filler combinations, giving details of the formulation. All formulations were vacuum de-aerated prior to casting. Curing was accomplished in a circulating

air oven at 250°F for 16 hours. After curing, the 1/4" x 8" x 11" plates were out into tensile specimens and tested on the Instron machine at ambient temperature, using .05"/min rate. An examination of the data in Table C discloses a number of interesting characteristics relating to the several fillers, surface active agents, etc. Of the aluminum powder filler materials, Series 24 displays the lowest strength and highest elongation to failure, in spit of having incorporated into it both degreased aluminum and A1100 surface active agent. This implies poor adhesion of the A1100 to the aluminum particles since Series 23, which was made using a silicone grease coated aluminum powder filler displayed slightly better physical properties. The best surface treatment for the aluminum appears to be the chromate/phosphate etch, which was used to make the Series 30 formulation, and which displays the best strength characteristics of the aluminum filler composites, indicating good adhesion of the resin to the aluminum particles. It is of interest to compare Series 30 made with a relatively low modulus resin, and Series 12A-29-5, which was made with a slightly higher modulus resin, and the same filler, treatment, and cure cycle. The disparity in physical properties may be attributed to the inability of the more rigid resin to adjust to small changes in dimension, plus its greater match sensitivity and decreased resistance to crack propagation. The poorest performance of all the aluminum filled materials was displayed by 12A-28-3, which was filled with aluminum "needles". This performance may be due to the shape of the aluminum particles, which are shaped more like spindles than needles, and have a relatively small length to diameter ratio.

Filament Wound Composites

Seven filament wound structures were made, using HTS-E 12 end fiberglass roving as the reinforcement, and both unfilled and filled (with fine particle fillers) resins as binders. The winding machine was programmed to position the roving at the rate of twenty to twenty two strands per inch, producing circumferentially wound cylinder having an eight inch inside diameter, 3.75 inches long. All the cylinders had six layers of glass roving in the structure, but wall thickness varied depending on resin viscosity and filler concentration. After winding, the cylinders were cured, while rotating, at 250°F for sixteen hours. The cured cylinders were then machined into 1/4" rings for testing using a split disc technique. Fig. 40 illustrates the test set up, with a ring in testing position. Table D outlines the data gathered on the filament wound composite structures tested in this program. An examination of the tensile strength characteristics of these composites shows that cylinders "A" and "B" displayed the greatest hoop stress values. Cylinder "B" was the more uniform of the two, but values are very similar for both pieces.

Cylinders "C" and "D" employed the same resin system as cylinder "A", but in addition contained a quantity of 900 mesh alumina filler in order to increase the modulus of the binder. The tensile strengths of these test specimens bear a direct relationship to the quantity of particulate filler added to the resin system, and indicate that increased filler content decreases composite strength. Both "C" and "D" composites are much weaker than the

"A" composite, which contains the same resin, but no particulate filler. The decrease in strength of the filler system may be attributed in part to the abrasive character of the alumina filler, and in part to the increase in stress area occasioned by the bulking of the entire system by the addition of the filler.

Cylinders "E" and "F" have comparable hoop tensile strengths. These specimens used "Surfex MM" filler in place of alumina, incorporated into resins identical with the binders used in "A" and "B". It is interesting to note that the tensile strength values of "E" and "F" are lower than "A" and "B", but higher than "C" and "D", indicating that the "Surfex MM" filler is less abrasive than alumina, and the decrease in strength upon comparison with "A" and "B" is due primarily to the bulking of the resin system by the filler.

Cylinder "G" was made using a cyclopentenyl oxide resin system cured with meta phenylene diamine. In spite of the relatively good physical properties of the unreinforced resin (identified as 12A-34-4) the filament wound composite displayed tensile strength characteristics that were not as good as those specimens made with resorcinol diglycidyl ether. This disappointing result may be attributed to the fact that there appeared to be poor adhesion between the resin and the glass fibers, since the strands of glass in the rings were easily separated by a moderate twisting action.

Microscopic Examination of Filament Wound Rings

Specimens of all filament wound pieces were encapsulated in resin, cross sectioned, polished, and the polished surfaces examined under the

microscope for details of structure. Visual observations of these pieces are recorded as follows:

Specimens "A" and "B": These specimens appeared to be very uniformly wound of close packed sets of fiber bundles, with good resin wetting throughout. The adhesion between fiber and resin was excellent, and there appeared to be few included air bubbles.

Specimens "C" and "D": The structures of these rings were quite similar, in that both appeared to be composed of fairly discrete bundles of glass fibers separated by areas of filled resin. The bundles of fibers appeared to act as strainers to filter out the particles of alumina, so that the fiber bundles themselves were stuch together with fairly pure resin, while around each bundle was a sheath of filler epoxy resin. The bundles appeared to be dispersed in a random fashion throughout the resin matrix. Many air bubbles were present.

Specimens "E" and "F": The cross sections of these rings looked very similar to those of specimens "C" and "D".

Specimen "G": This cross section appeared to have a uniform array of glass fibers throughout, with few air bubbles noticeable.

Table C

Filled Resins

| Series | Resin Component | Filler | UTS, PSI | Young's Modulus PSI | Elongation to Failure % |
|---|---|---|---|---|---|
| 18 | PJ 122C (34% by weight) | Al powder - as received | $4.8 - 5.2 \times 10^3$ | $0.88 - 1.26 \times 10^6$ | 0.87 - 1.12 |
| 22 | PJ 122C " " " | " " - as degreased | $5.1 - 5.6 \times 10^3$ | $1.08 - 1.32 \times 10^6$ | 0.67 - 0.83 |
| 23 | PJ 122C " " " | " " - coated with mold release | $3.5 - 4.6 \times 10^3$ | $0.89 - 1.31 \times 10^6$ | 0.35 - 0.66 |
| 24 | PJ 122C + 1.5 pbw A1100 | " " - degreased | $2.4 - 2.7 \times 10^3$ | $0.50 - 0.56 \times 10^6$ | 5.3 - 9.7 |
| 29 | PJ 122C + 1.5 pbw 26020 | " " - " | $4.5 - 4.5 \times 10^3$ | $0.91 - 1.04 \times 10^6$ | 0.9 - 1.0 |
| 30 | PJ 122C " " " | " " - conversion coated | $7.1 - 7.4 \times 10^3$ | $0.83 - 1.20 \times 10^6$ | 1.8 - 2.3 |
| 12A-29-5 | PJ 122A " " " | " " - " " | $5.5 - 6.1 \times 10^3$ | $1.61 - 2.28 \times 10^6$ | 0.5 - 0.6 |
| 12A-28-3 | PJ 122A " " " | Almeg Needles - Conversion coated | $2.5 - 2.7 \times 10^3$ | $0.89 - 1.09 \times 10^6$ | 0.42 - 0.5 |
| 12A-35-2 | PJ 122A (70% by weight) | $Al_2O_3$ 900 mesh (30% by weight) | | | |
| 12A-35-4 | PJ 122A (37% by weight) | $Al_2O_3$ 900 mesh (63% by weight) | $8.0 \times 10^3$ | | |
| 34 | PJ 122A (51.7% by wt.) | Surfex MM (48.3% by weight) | $7.9 - 8.4 \times 10^3$ | $0.91 - 1.01 \times 10^6$ | 1.05 - 1.17 |
| 35 | PJ 122C (51.7% by wt.) | Surfex MM (48.3% by weight) | $6.8 - 8.4 \times 10^3$ | $0.65 - 0.84 \times 10^6$ | 0.96 - 1.96 |

Table D. Properties of Filament Wound Composites

Tensile Data on Eight Inch Rings - Modified Resins Using Wet Filament Winding Technique

| Desig. | Resin System | | Resin Cont. by weight | Filler Cont. by weight | Glass Cont. by weight | Density g/cc | Wall. Thick. | Hoop Stress PSI |
|---|---|---|---|---|---|---|---|---|
| A | 100 pbw Kopoxite 159<br>125 " MNA<br>25 " Thiokol EM 207<br>1 " BDA | | 22% | ----- | 78% | 1.9268 | .056"-.060" | $1.75\text{-}2.14 \times 10^5$ |
| B | 100 pbw Kopoxite 159<br>125 " MNA<br>75 " Thiokol EM 207<br>1 " BDA | | 20% | ----- | 80% | 1.9462 | .055"-.056" | $2.06\text{-}2.12 \times 10^5$ |
| C | Resin as in "A" (PJ122A)<br>$Al_2O_3$ 900 mesh | 70 pbw<br>30 pbw | 29.1% | 11.9% | 59% | 2.0029 | .078"-.080" | $0.67\text{-}0.69 \times 10^5$ |
| D | Resin as in "A" (PJ122A)<br>$Al_2O_3$ 900 mesh | 37 pbw<br>63 pbw | 21.5% | 40% | 38.5% | 2.3611 | .077"-.108" | $0.51\text{-}0.53 \times 10^5$ |
| E | Resin as in "A" (PJ122A)<br>Surfex MM | 51.7 pbw<br>48.3 pbw | 22.0% | 22.5% | 55.5% | 2.0005 | .074"-.079" | $1.43\text{-}1.52 \times 10^5$ |
| F | Resin as in "B" (PJ122C)<br>Surfex MM | 51.7 pbw<br>48.3 pbw | 20.3% | 21.7% | 58.0% | 1.9751 | .074"-.076" | $1.42\text{-}1.47 \times 10^5$ |
| G | ERLA 0400<br>m-phenylene diamine | 404 pbw<br>108 pbw | 18.0% | ----- | 82.0% | 1.9282 | .053"-.054" | $1.12\text{-}1.46 \times 10^5$ |

NOTE: MNA = Methyl Nadic Anhydride
BDA = Benzyl Dimethyl Amine

Table 1
Thin Fibrous Composite Tensile Tests

| Specimen Number | Maximum Number of Breaks | Maximum Load | Number of Fibers | Fiber Area ($in^2$) | Maximum Fiber Stress (ksi) |
|---|---|---|---|---|---|
| B1 | 37 | 210 | 125 | $1.272 \times 10^{-3}$ | 165.1 |
| B2 | 31 | 222 | 130 | 1.323 | 167.8 |
| B3 | 34 | 221 | 130 | 1.323 | 167.0 |
| B4 | 13 | 207 | 131 | 1.333 | 155.3 |
| B5 | 24(36)* | 197 | 129 | 1.313 | 150.0 |
| | | | | Average stress | 161.0 |
| | | | | Standard deviation | 7.1 |
| C1 | 21 | 195 | 125 | $1.272 \times 10^{-3}$ | 153.3 |
| C2 | 28 | 181 | 124 | 1.262 | 143.4 |
| C3 | 19(37)* | 184 | 126 | 1.283 | 143.4 |
| C4 | 33 | 196 | 126 | 1.283 | 152.8 |
| C5 | -- | 200 | | | |
| C6 | 22 | 206 | 128 | 1.303 | 158.1 |
| C7 | 20 | 203 | 122 | 1.242 | 163.4 |
| | | | | Average stress | 152.4 |
| | | | | Standard deviation | 7.1 |

* Number in parentheses observed after maximum load.

TABLE 2. Compressive loadings for launch vehicles.

| Vehicle | Thrust, kN (lbs.) | Diameter, m (in.) | $\frac{N_x}{R}$, $\frac{kN}{m^2}$ (psi) |
|---|---|---|---|
| Redstone | 347 (78,000) | 1.778 (70) | |
| Scout | 383 (86,000) | 0.991 (39) | 469 (68) |
| Thor | 756 (170,000) | 2.438 (96) | |
| Atlas | 1730 (389,000) | 3.048 (120) | 51.75 (7.5) |
| Minuteman | 756 (170,000) | 1.803 (71) | |
| Titan I | 1334 (300,000) | 3.048 (120) | |
| Titan II | 1913 (430,000) | 3.048 (120) | |
| Saturn V | 33,360 (7,500,000) | 10.160 (400) | 302 (43.8) |
| Nova | 111,200 (25,000,000) | 24.38 (960) | |

TABLE 3. Mechanical properties assigned to idealized metals for comparison with composites.

| Material | Density $Mg/m^3$ (pci) | Young's Modulus $GN/m^2$ (ksi) | Yield Stress $GN/m^2$ (ksi) | Poisson's Ratio |
|---|---|---|---|---|
| Steel | 7.89 (0.285) | 207 (30,000) | 2.07 (300) | 0.25 |
| Titanium | 4.82 (0.174) | 103 (15,000) | 1.38 (200) | 0.145 |
| Aluminum | 2.80 (0.100) | 73.8 10,700) | 0.483 (70) | 0.315 |
| Magnesium -Lithium | 1.34 (0.0485) | 42.75 (6200) | 0.124 (18) | 0.43 |
| Beryllium | 1.83 (0.066) | 293 (42,500) | 4.00 (58) | 0.09 |

TABLE 4. Mechanical properties used for filamentary and binder materials surveyed for composites.

| | Young's Modulus $GN/m^2$ (ksi) | Density $Mg/m^3$ (pci) | Poisson's Ratio |
|---|---|---|---|
| **Filaments** | | | |
| Hollow E-Glass | 72.45 (10,500) | 2.56 (0.0914) | 0.20 |
| Solid E-Glass | 72.45 (10,500) | 2.56 (0.0914) | 0.20 |
| Hi-Modulus Glass | 110 (16,000) | 2.56 (0.0914) | 0.20 |
| Asbestos | 183 (26,500) | 2.44 (0.087) | 0.20 |
| Steel | 207 (30,000) | 7.9 (0.283) | 0.25 |
| Beryllium | 276 (40,000) | 1.85 (0.066) | 0.09 |
| Boron | 414 (60,000) | 2.32 (0.083) | 0.20 |
| Alumina | 518 (75,000) | 4.0 (0.143) | 0.20 |
| **Binders** | | | |
| "Epoxy" | 3.45 (500) | 1.40 (0.050) | 0.35 |
| "Light-Alloy I" | 103.5 (15,000) | 1.40 (0.050) | 0.30 |
| "Magnesium" | 51.75 (7500) | 2.10 (0.075) | 0.30 |
| "Light-Alloy II" | 103.5 (15,000) | 2.10 (0.075) | 0.30 |
| "Light-Alloy III" | 207 (30,000) | 2.10 (0.075) | 0.30 |
| "Boron" | 414 (60,000) | 2.10 (0.075) | 0.30 |
| "Titanium" | 103.5 (15,000) | 4.20 (0.150) | 0.30 |
| "Steel" | 207 (30,000) | 8.40 (0.300) | 0.30 |

Table 5. ELASTIC CONSTANTS OF FIBROUS COMPOSITES

Uniaxial Laminates
Epoxy Matrix

| $v_b$ | Property | Fiber Materials: Hollow E-glass | Solid E-glass | Hi Mod. Glass | Asbes - tos | Steel | Beryl- lium | Boron | Alumina |
|---|---|---|---|---|---|---|---|---|---|
| 0 | $E^*$ | --- | 10.500 | 16.000 | 26.500 | 30.000 | 40.000 | 60.000 | 75.000 |
| | $\nu$ | --- | 0.200 | 0.200 | 0.200 | 0.250 | 0.090 | 0.200 | 0.200 |
| | $\rho$+ | --- | 0.0914 | 0.0914 | 0.0870 | 0.2830 | 0.0660 | 0.0830 | 0.1430 |
| 0.15 | $E_1$* | 3.289 | 9.001 | 13.676 | 22.601 | 25.575 | 34.078 | 51.076 | 63.826 |
| | $E_2$* | 0.560 | 3.784 | 4.318 | 4.839 | 4.944 | 5.170 | 5.402 | 5.504 |
| | $G_{12}$* | 0.695 | 1.543 | 1.754 | 1.955 | 1.983 | 2.102 | 2.168 | 2.206 |
| | $\nu_{21}$ | 0.213 | 0.211 | 0.211 | 0.211 | 0.256 | 0.114 | 0.211 | 0.211 |
| | $\rho$ | 0.0355 | 0.0852 | 0.0852 | 0.0814 | 0.248 | 0.0636 | 0.0805 | 0.129 |
| 0.30 | $E_1$ | 2.797 | 7.501 | 11.351 | 18.701 | 21.150 | 28.156 | 42.151 | 52.651 |
| | $E_2$ | 0.506 | 2.229 | 2.394 | 2.538 | 2.564 | 2.624 | 2.676 | 2.700 |
| | $G_{12}$ | 0.529 | 0.879 | 0.941 | 0.995 | 1.002 | 1.031 | 1.046 | 1.054 |
| | $\nu_{21}$ | 0.226 | 0.224 | 0.224 | 0.224 | 0.262 | 0.140 | 0.224 | 0.224 |
| | $\rho$ | 0.0380 | 0.0790 | 0.0790 | 0.0759 | 0.213 | 0.0612 | 0.0830 | 0.115 |
| 0.45 | $E_1$ | 2.305 | 6.002 | 9.027 | 14.802 | 16.725 | 22.232 | 33.227 | 41.477 |
| | $E_2$ | 0.525 | 1.508 | 1.576 | 1.633 | 1.642 | 1.666 | 1.684 | 1.693 |
| | $G_{12}$ | 0.415 | 0.583 | 0.608 | 0.628 | 0.631 | 0.641 | 0.647 | 0.650 |
| | $\nu_{21}$ | 0.240 | 0.237 | 0.237 | 0.237 | 0.269 | 0.168 | 0.237 | 0.237 |
| | $\rho$ | 0.0406 | 0.0728 | 0.0728 | 0.0703 | 0.178 | 0.0588 | 0.0681 | 0.101 |
| 0.60 | $E_1$ | 1.813 | 4.502 | 6.702 | 10.902 | 12.300 | 16.307 | 24.302 | 30.302 |
| | $E_2$ | 0.543 | 1.086 | 1.117 | 1.142 | 1.146 | 1.158 | 1.165 | 1.169 |
| | $G_{12}$ | 0.332 | 0.415 | 0.426 | 0.434 | 0.436 | 0.440 | 0.442 | 0.444 |
| | $\nu_{21}$ | 0.255 | 0.252 | 0.252 | 0.252 | 0.276 | 0.199 | 0.252 | 0.252 |
| | $\rho$ | 0.0432 | 0.0666 | 0.0666 | 0.0648 | 0.143 | 0.0564 | 0.0632 | 0.0872 |
| 0.75 | $E_1$ | 1.321 | 3.001 | 4.376 | 7.001 | 7.875 | 10.381 | 15.376 | 19.126 |
| | $E_2$ | 0.542 | 0.810 | 0.825 | 0.837 | 0.838 | 0.844 | 0.848 | 0.849 |
| | $G_{12}$ | 0.269 | 0.307 | 0.311 | 0.315 | 0.315 | 0.317 | 0.318 | 0.318 |
| | $\nu_{21}$ | 0.271 | 0.269 | 0.269 | 0.268 | 0.284 | 0.234 | 0.268 | 0.268 |
| | $\rho$ | 0.0457 | 0.0603 | 0.0603 | 0.0592 | 0.108 | 0.540 | 0.0582 | 0.0732 |
| 0.90 | $E_1$ | 0.829 | 1.501 | 2.051 | 3.101 | 3.450 | 4.453 | 6.451 | 7.951 |
| | $E_2$ | 0.525 | 0.617 | 0.625 | 0.633 | 0.634 | 0.638 | 0.640 | 0.641 |
| | $G_{12}$ | 0.220 | 0.231 | 0.232 | 0.233 | 0.234 | 0.234 | 0.234 | 0.234 |
| | $\nu_{21}$ | 0.288 | 0.287 | 0.287 | 0.287 | 0.293 | 0.272 | 0.287 | 0.287 |
| | $\rho$ | 0.0483 | 0.0541 | 0.0541 | 0.0537 | 0.0733 | 0.0516 | 0.0533 | 0.0593 |
| 1.00 | E | 0.500 | 0.500 | 0.500 | 0.500 | 0.500 | 0.500 | 0.500 | 0.500 |
| | $\nu$ | 0.300 | 0.300 | 0.300 | 0.300 | 0.300 | 0.300 | 0.300 | 0.300 |
| | $\rho$ | 0.0500 | 0.0500 | 0.0500 | 0.0500 | 0.0500 | 0.0500 | 0.0500 | 0.0500 |

* $10^6$ psi ; + $\#/in^3$

Table 5A. ELASTIC CONSTANTS OF FIBROUS COMPOSITES

Isotropic Laminates
Epoxy Matrix

| $v_b$ | Property | Fiber Material: Hollow E-glass | Solid E-glass | Hi Mod. Glass | Asbestos | Steel | Beryllium | Boron | Alumina |
|---|---|---|---|---|---|---|---|---|---|
| 0 | E* | --- | 10.500 | 16.000 | 26.500 | 30.000 | 40.000 | 60.000 | 75.000 |
| | $\nu$ | --- | 0.200 | 0.200 | 0.200 | 0.250 | 0.090 | 0.200 | 0.200 |
| | $\rho$+ | --- | 0.0914 | 0.0914 | 0.0870 | 0.2830 | 0.0660 | 0.0830 | 0.1430 |
| 0.15 | E | 1.803 | 5.494 | 7.398 | 10.711 | 11.764 | 14.782 | 20.567 | 24.883 |
| | $\nu$ | 0.124 | 0.251 | 0.264 | 0.280 | 0.297 | 0.270 | 0.303 | 0.308 |
| | $\rho$ | 0.0355 | 0.0852 | 0.0852 | 0.0814 | 0.248 | 0.0636 | 0.0805 | 0.129 |
| 0.30 | E | 1.507 | 3.947 | 5.335 | 7.876 | 8.706 | 11.097 | 15.781 | 19.296 |
| | $\nu$ | 0.155 | 0.275 | 0.287 | 0.301 | 0.311 | 0.297 | 0.316 | 0.319 |
| | $\rho$ | 0.0380 | 0.0790 | 0.0790 | 0.0759 | 0.213 | 0.0612 | 0.0830 | 0.115 |
| 0.45 | E | 1.268 | 2.970 | 4.020 | 5.980 | 6.626 | 8.484 | 12.154 | 14.910 |
| | $\nu$ | 0.188 | 0.288 | 0.299 | 0.309 | 0.316 | 0.308 | 0.321 | 0.323 |
| | $\rho$ | 0.0406 | 0.0728 | 0.0728 | 0.0703 | 0.178 | 0.0588 | 0.0681 | 0.101 |
| 0.60 | E | 1.050 | 2.195 | 2.946 | 4.361 | 4.829 | 6.174 | 8.842 | 10.844 |
| | $\nu$ | 0.218 | 0.296 | 0.304 | 0.313 | 0.319 | 0.313 | 0.323 | 0.325 |
| | $\rho$ | 0.0432 | 0.0666 | 0.0666 | 0.0648 | 0.143 | 0.0564 | 0.0632 | 0.0872 |
| 0.75 | E | 0.839 | 1.517 | 1.983 | 2.864 | 3.156 | 3.994 | 5.661 | 6.912 |
| | $\nu$ | 0.245 | 0.299 | 0.307 | 0.315 | 0.319 | 0.315 | 0.324 | 0.326 |
| | $\rho$ | 0.0457 | 0.0603 | 0.0603 | 0.0592 | 0.108 | 0.0540 | 0.0582 | 0.0732 |
| 0.90 | E | 0.634 | 0.894 | 1.080 | 1.431 | 1.548 | 1.883 | 2.550 | 3.050 |
| | $\nu$ | 0.275 | 0.300 | 0.306 | 0.313 | 0.316 | 0.315 | 0.322 | 0.324 |
| | $\rho$ | 0.0483 | 0.0541 | 0.0541 | 0.0537 | 0.0733 | 0.0516 | 0.0533 | 0.0593 |
| 1.00 | E | 0.500 | 0.500 | 0.500 | 0.500 | 0.500 | 0.500 | 0.500 | 0.500 |
| | $\nu$ | 0.300 | 0.300 | 0.300 | 0.300 | 0.300 | 0.300 | 0.300 | 0.300 |
| | $\rho$ | 0.0500 | 0.0500 | 0.0500 | 0.0500 | 0.0500 | 0.0500 | 0.0500 | 0.0500 |

* $10^6$ psi ; + $\#/in^3$

Table 6. ELASTIC CONSTANTS OF FIBROUS COMPOSITES

Uniaxial Laminates
Magnesium Matrix

| | | Fiber Material | | | | | | | |
|---|---|---|---|---|---|---|---|---|---|
| $v_b$ | Property | Hollow E-glass | Solid E-glass | Hi Mod. Glass | Asbes-tos | Steel | Beryl-lium | Boron | Alumina |
| 0 | E* | --- | 10.500 | 16.000 | 26.500 | 30.000 | 40.000 | 60.000 | 75.000 |
| | $\nu$ | --- | 0.200 | 0.200 | 0.200 | 0.250 | 0.090 | 0.200 | 0.200 |
| | $\rho$+ | --- | 0.0914 | 0.0914 | 0.0870 | 0.2830 | 0.0660 | 0.0830 | 0.1430 |
| 0.15 | $E_1$* | 4.347 | 10.061 | 14.736 | 23.661 | 26.628 | 35.173 | 52.136 | 64.886 |
| | $E_2$* | 1.441 | 10.007 | 14.177 | 20.981 | 22.901 | 28.254 | 36.123 | 40.882 |
| | $G_{12}$* | 1.163 | 4.104 | 5.812 | 8.605 | 9.148 | 12.260 | 14.820 | 16.761 |
| | $\nu_{21}$ | 0.229 | 0.215 | 0.214 | 0.213 | 0.256 | 0.116 | 0.212 | 0.212 |
| | $\rho$ | 0.0392 | 0.0889 | 0.0889 | 0.0852 | 0.252 | 0.0673 | 0.0818 | 0.133 |
| 0.30 | $E_1$ | 4.908 | 9.617 | 13.468 | 20.818 | 23.255 | 30.331 | 44.269 | 54.769 |
| | $E_2$ | 1.978 | 9.540 | 12.669 | 17.206 | 18.322 | 21.547 | 25.344 | 27.466 |
| | $G_{12}$ | 1.388 | 3.853 | 5.097 | 6.894 | 7.213 | 8.885 | 10.085 | 10.907 |
| | $\nu_{21}$ | 0.250 | 0.230 | 0.228 | 0.226 | 0.263 | 0.144 | 0.225 | 0.224 |
| | $\rho$ | 0.0455 | 0.0914 | 0.0865 | 0.0834 | 0.221 | 0.0687 | 0.0806 | 0.123 |
| 0.45 | $E_1$ | 5.467 | 9.170 | 12.196 | 17.972 | 19.881 | 25.474 | 36.398 | 44.648 |
| | $E_2$ | 2.722 | 9.085 | 11.340 | 14.304 | 14.950 | 16.928 | 18.862 | 19.915 |
| | $G_{12}$ | 1.639 | 3.619 | 4.491 | 5.626 | 5.815 | 6.740 | 7.348 | 7.741 |
| | $\nu_{21}$ | 0.266 | 0.245 | 0.242 | 0.240 | 0.270 | 0.173 | 0.238 | 0.238 |
| | $\rho$ | 0.0518 | 0.0840 | 0.0840 | 0.0816 | 0.189 | 0.0700 | 0.0794 | 0.112 |
| 0.60 | $E_1$ | 6.023 | 8.720 | 10.921 | 15.122 | 16.506 | 20.599 | 28.523 | 34.523 |
| | $E_2$ | 3.706 | 8.636 | 10.138 | 11.952 | 12.307 | 13.477 | 14.450 | 14.983 |
| | $G_{12}$ | 1.922 | 3.401 | 3.970 | 4.650 | 4.756 | 5.256 | 5.556 | 5.757 |
| | $\nu_{21}$ | 0.278 | 0.260 | 0.257 | 0.255 | 0.277 | 0.205 | 0.253 | 0.253 |
| | $\rho$ | 0.0582 | 0.0816 | 0.0816 | 0.0798 | 0.158 | 0.0714 | 0.0782 | 0.102 |
| 0.75 | $E_1$ | 6.578 | 8.265 | 9.642 | 12.268 | 13.130 | 15.705 | 20.644 | 24.394 |
| | $E_2$ | 4.931 | 8.196 | 9.050 | 10.013 | 10.183 | 10.807 | 11.258 | 11.517 |
| | $G_{12}$ | 2.243 | 3.197 | 3.158 | 3.874 | 3.928 | 4.169 | 4.311 | 4.397 |
| | $\nu_{21}$ | 0.288 | 0.275 | 0.273 | 0.271 | 0.285 | 0.239 | 0.270 | 0.269 |
| | $\rho$ | 0.0645 | 0.0791 | 0.0791 | 0.0780 | 0.127 | 0.0727 | 0.0770 | 0.0920 |
| 0.90 | $E_1$ | 7.131 | 7.807 | 8.358 | 9.409 | 9.752 | 10.790 | 12.759 | 14.260 |
| | $E_2$ | 6.384 | 7.771 | 8.079 | 8.411 | 8.466 | 8.701 | 8.861 | 8.965 |
| | $G_{12}$ | 2.610 | 3.006 | 3.122 | 3.244 | 3.261 | 3.336 | 3.386 | 3.407 |
| | $\nu_{21}$ | 0.295 | 0.290 | 0.289 | 0.288 | 0.294 | 0.275 | 0.287 | 0.287 |
| | $\rho$ | 0.0708 | 0.0766 | 0.0766 | 0.0762 | 0.0958 | 0.0741 | 0.0758 | 0.0818 |
| 1.00 | E | 7.500 | 7.500 | 7.500 | 7.500 | 7.500 | 7.500 | 7.500 | 7.500 |
| | $\nu$ | 0.300 | 0.300 | 0.300 | 0.300 | 0.300 | 0.300 | 0.300 | 0.300 |
| | $\rho$ | 0.0750 | 0.0750 | 0.0750 | 0.0750 | 0.0750 | 0.0750 | 0.0750 | 0.0750 |

* $10^6$ psi ; + $\#/in^3$

Table 6A. ELASTIC CONSTANTS OF FIBROUS COMPOSITES

Isotropic Laminates
Magnesium Matrix

| | | Fiber Material | | | | | | | |
|---|---|---|---|---|---|---|---|---|---|
| $v_b$ | Property | Hollow E-glass | Solid E-glass | Hi Mod. Glass | Asbes - tos | Steel | Beryl- lium | Boron | Alumina |
| 0 | $E^*$ | --- | 10.500 | 16.000 | 26.500 | 30.000 | 40.000 | 60.000 | 75.000 |
| | $\nu$ | --- | 0.200 | 0.200 | 0.200 | 0.250 | 0.090 | 0.200 | 0.200 |
| | $\rho^+$ | --- | 0.0914 | 0.0914 | 0.0870 | 0.2830 | 0.0660 | 0.0830 | 0.1430 |
| 0.15 | E | 2.817 | 10.014 | 14.336 | 21.815 | 24.099 | 30.388 | 41.293 | 48.667 |
| | $\nu$ | 0.142 | 0.216 | 0.216 | 0.218 | 0.258 | 0.141 | 0.227 | 0.232 |
| | $\rho$ | 0.0392 | 0.0889 | 0.0889 | 0.0852 | 0.252 | 0.0673 | 0.0818 | 0.133 |
| 0.30 | E | 3.376 | 9.545 | 12.877 | 18.275 | 19.984 | 24.163 | 31.319 | 36.704 |
| | $\nu$ | 0.164 | 0.232 | 0.232 | 0.236 | 0.267 | 0.180 | 0.249 | 0.254 |
| | $\rho$ | 0.0455 | 0.0914 | 0.0865 | 0.0834 | 0.221 | 0.0687 | 0.0806 | 0.123 |
| 0.45 | E | 4.036 | 9.089 | 11.554 | 15.367 | 16.443 | 19.441 | 24.356 | 27.756 |
| | $\nu$ | 0.192 | 0.247 | 0.248 | 0.251 | 0.275 | 0.211 | 0.264 | 0.269 |
| | $\rho$ | 0.0518 | 0.0840 | 0.0840 | 0.0816 | 0.189 | 0.0700 | 0.0794 | 0.112 |
| 0.60 | E | 4.811 | 8.641 | 10.334 | 12.867 | 13.573 | 15.563 | 18.243 | 21.158 |
| | $\nu$ | 0.222 | 0.262 | 0.262 | 0.264 | 0.282 | 0.236 | 0.275 | 0.279 |
| | $\rho$ | 0.0582 | 0.0816 | 0.0816 | 0.0798 | 0.158 | 0.0714 | 0.0782 | 0.102 |
| 0.75 | E | 5.709 | 8.203 | 9.203 | 10.666 | 11.071 | 12.232 | 14.165 | 15.523 |
| | $\nu$ | 0.253 | 0.276 | 0.276 | 0.276 | 0.288 | 0.258 | 0.284 | 0.287 |
| | $\rho$ | 0.0645 | 0.0791 | 0.0791 | 0.0780 | 0.127 | 0.0727 | 0.0770 | 0.0920 |
| 0.90 | E | 6.733 | 7.776 | 8.154 | 8.699 | 8.851 | 9.291 | 10.032 | 10.572 |
| | $\nu$ | 0.282 | 0.290 | 0.290 | 0.289 | 0.294 | 0.281 | 0.292 | 0.293 |
| | $\rho$ | 0.0708 | 0.0766 | 0.0766 | 0.0762 | 0.0958 | 0.0741 | 0.0758 | 0.0818 |
| 1.00 | E | 7.500 | 7.500 | 7.500 | 7.500 | 7.500 | 7.500 | 7.500 | 7.500 |
| | $\nu$ | 0.300 | 0.300 | 0.300 | 0.300 | 0.300 | 0.300 | 0.300 | 0.300 |
| | $\rho$ | 0.0750 | 0.0750 | 0.0750 | 0.0750 | 0.0750 | 0.0750 | 0.0750 | 0.0750 |

* $10^6$ psi ; + $\#/in^3$

Table 7. ELASTIC CONSTANTS OF FIBROUS COMPOSITES

Uniaxial Laminates
"Light Alloy I" Matrix

| $v_b$ | Property | Fiber Material: Hollow E-glass | Solid E-glass | Hi Mod. Glass | Asbestos | Steel | Beryllium | Boron | Alumina |
|---|---|---|---|---|---|---|---|---|---|
| 0 | $E^*$ | --- | 10.500 | 16.000 | 26.500 | 30.000 | 40.000 | 60.000 | 75.000 |
| | $\nu$ | --- | 0.200 | 0.200 | 0.200 | 0.250 | 0.090 | 0.200 | 0.200 |
| | $\rho^+$ | --- | 0.0914 | 0.0914 | 0.0870 | 0.2830 | 0.0660 | 0.0830 | 0.1430 |
| 0.15 | $E_1^*$ | 5.478 | 11.195 | 15.871 | 24.796 | 27.755 | 36.344 | 53.272 | 66.022 |
| | $E_2^*$ | 1.786 | 11.080 | 15.888 | 24.301 | 26.832 | 34.142 | 45.942 | 53.709 |
| | $G_{12}^*$ | 1.409 | 4.562 | 6.523 | 9.963 | 10.669 | 14.959 | 18.846 | 22.039 |
| | $\nu_{21}$ | 0.241 | 0.218 | 0.216 | 0.214 | 0.257 | 0.119 | 0.213 | 0.212 |
| | $\rho$ | 0.0355 | 0.0852 | 0.0852 | 0.0814 | 0.248 | 0.0636 | 0.0780 | 0.129 |
| 0.30 | $E_1$ | 7.164 | 11.882 | 15.734 | 23.085 | 25.509 | 32.657 | 46.537 | 57.037 |
| | $E_2$ | 2.756 | 11.695 | 15.763 | 22.370 | 24.174 | 29.379 | 36.833 | 41.291 |
| | $G_{12}$ | 1.922 | 4.757 | 6.383 | 9.015 | 9.522 | 12.405 | 14.744 | 16.498 |
| | $\nu_{21}$ | 0.263 | 0.235 | 0.232 | 0.229 | 0.264 | 0.148 | 0.226 | 0.225 |
| | $\rho$ | 0.0380 | 0.0790 | 0.0790 | 0.0759 | 0.213 | 0.0612 | 0.0731 | 0.115 |
| 0.45 | $E_1$ | 8.846 | 12.561 | 15.589 | 21.367 | 23.261 | 28.939 | 39.795 | 48.045 |
| | $E_2$ | 4.108 | 12.340 | 15.623 | 20.587 | 21.823 | 25.684 | 30.079 | 32.678 |
| | $G_{12}$ | 2.514 | 4.958 | 6.246 | 8.174 | 8.526 | 10.411 | 11.813 | 12.798 |
| | $\nu_{21}$ | 0.276 | 0.251 | 0.247 | 0.243 | 0.271 | 0.179 | 0.240 | 0.239 |
| | $\rho$ | 0.0405 | 0.0728 | 0.0728 | 0.0703 | 0.178 | 0.0588 | 0.0681 | 0.101 |
| 0.60 | $E_1$ | 10.526 | 13.234 | 15.438 | 19.641 | 21.011 | 25.186 | 33.045 | 39.045 |
| | $E_2$ | 6.029 | 13.014 | 15.469 | 18.911 | 19.695 | 22.247 | 25.756 | 26.215 |
| | $G_{12}$ | 3.204 | 5.168 | 6.112 | 7.424 | 7.652 | 8.811 | 9.615 | 10.153 |
| | $\nu_{21}$ | 0.286 | 0.266 | 0.262 | 0.258 | 0.279 | 0.211 | 0.255 | 0.254 |
| | $\rho$ | 0.0432 | 0.0666 | 0.0666 | 0.0648 | 0.143 | 0.0564 | 0.0632 | 0.0872 |
| 0.75 | $E_1$ | 12.205 | 13.901 | 15.279 | 17.907 | 18.758 | 21.398 | 26.286 | 30.037 |
| | $E_2$ | 8.696 | 13.720 | 15.301 | 17.339 | 17.764 | 19.211 | 20.460 | 21.194 |
| | $G_{12}$ | 4.020 | 5.386 | 5.981 | 6.751 | 6.878 | 7.499 | 7.906 | 8.167 |
| | $\nu_{21}$ | 0.292 | 0.279 | 0.277 | 0.274 | 0.286 | 0.243 | 0.271 | 0.270 |
| | $\rho$ | 0.0457 | 0.0603 | 0.0603 | 0.0592 | 0.108 | 0.0540 | 0.0582 | 0.0732 |
| 0.90 | $E_1$ | 13.882 | 14.562 | 15.114 | 16.166 | 16.504 | 17.572 | 19.518 | 21.018 |
| | $E_2$ | 12.178 | 14.469 | 15.123 | 15.888 | 16.034 | 16.560 | 16.973 | 17.231 |
| | $G_{12}$ | 5.000 | 5.613 | 5.853 | 6.143 | 6.189 | 6.404 | 6.538 | 6.622 |
| | $\nu_{21}$ | 0.297 | 0.292 | 0.291 | 0.289 | 0.294 | 0.277 | 0.288 | 0.288 |
| | $\rho$ | 0.0483 | 0.0541 | 0.0541 | 0.0537 | 0.0733 | 0.0516 | 0.0533 | 0.0593 |
| 1.00 | E | 15.000 | 15.000 | 15.000 | 15.000 | 15.000 | 15.000 | 15.000 | 15.000 |
| | $\nu$ | 0.300 | 0.300 | 0.300 | 0.300 | 0.300 | 0.300 | 0.300 | 0.300 |
| | $\rho$ | 0.0500 | 0.0500 | 0.0500 | 0.0500 | 0.0500 | 0.0500 | 0.0500 | 0.0500 |

* $10^6$ psi ; + #/in$^3$

Table 7A. ELASTIC CONSTANTS OF FIBROUS COMPOSITES

Isotropic Laminates
"Light Alloy I" Matrix

| $v_b$ | Property | Fiber Material: Hollow E-glass | Solid E-glass | Hi Mod. Glass | Asbestos | Steel | Beryllium | Boron | Alumina |
|---|---|---|---|---|---|---|---|---|---|
| 0 | E* | --- | 10.500 | 16.000 | 26.500 | 30.000 | 40.000 | 60.000 | 75.000 |
| | $\nu$ | --- | 0.200 | 0.200 | 0.200 | 0.250 | 0.090 | 0.200 | 0.200 |
| | $\rho$+ | --- | 0.0914 | 0.0914 | 0.0870 | 0.2830 | 0.0660 | 0.0830 | 0.1430 |
| 0.15 | E | 3.506 | 11.128 | 15.875 | 24.429 | 27.115 | 34.712 | 48.245 | 57.625 |
| | $\nu$ | 0.153 | 0.218 | 0.216 | 0.216 | 0.257 | 0.218 | 0.219 | 0.221 |
| | $\rho$ | 0.0355 | 0.0852 | 0.0852 | 0.0814 | 0.248 | 0.0636 | 0.0780 | 0.129 |
| 0.30 | E | 4.816 | 11.772 | 15.742 | 22.531 | 24.555 | 30.302 | 39.749 | 46.121 |
| | $\nu$ | 0.175 | 0.235 | 0.232 | 0.232 | 0.265 | 0.164 | 0.237 | 0.240 |
| | $\rho$ | 0.0380 | 0.0790 | 0.0790 | 0.0759 | 0.213 | 0.0612 | 0.0731 | 0.115 |
| 0.45 | E | 6.329 | 12.430 | 15.599 | 20.752 | 22.220 | 26.401 | 32.945 | 37.325 |
| | $\nu$ | 0.198 | 0.250 | 0.248 | 0.247 | 0.273 | 0.195 | 0.252 | 0.256 |
| | $\rho$ | 0.0405 | 0.0728 | 0.0728 | 0.0703 | 0.178 | 0.0588 | 0.0681 | 0.101 |
| 0.60 | E | 8.134 | 13.103 | 15.446 | 19.068 | 20.058 | 22.919 | 27.191 | 30.078 |
| | $\nu$ | 0.225 | 0.265 | 0.263 | 0.262 | 0.280 | 0.225 | 0.265 | 0.268 |
| | $\rho$ | 0.0432 | 0.0666 | 0.0666 | 0.0648 | 0.143 | 0.0564 | 0.0632 | 0.0872 |
| 0.75 | E | 10.321 | 13.795 | 15.285 | 17.469 | 18.045 | 19.726 | 22.171 | 23.845 |
| | $\nu$ | 0.254 | 0.278 | 0.277 | 0.276 | 0.287 | 0.252 | 0.277 | 0.279 |
| | $\rho$ | 0.0457 | 0.0603 | 0.0603 | 0.0592 | 0.108 | 0.0540 | 0.0582 | 0.0732 |
| 0.90 | E | 12.952 | 14.508 | 15.116 | 15.957 | 16.172 | 16.806 | 17.713 | 18.345 |
| | $\nu$ | 0.282 | 0.291 | 0.291 | 0.290 | 0.294 | 0.280 | 0.290 | 0.290 |
| | $\rho$ | 0.0483 | 0.0541 | 0.0541 | 0.0537 | 0.0733 | 0.0516 | 0.0533 | 0.0593 |
| 1.00 | E | 15.000 | 15.000 | 15.000 | 15.000 | 15.000 | 15.000 | 15.000 | 15.000 |
| | $\nu$ | 0.300 | 0.300 | 0.300 | 0.300 | 0.300 | 0.300 | 0.300 | 0.300 |
| | $\rho$ | 0.0500 | 0.0500 | 0.0500 | 0.0500 | 0.0500 | 0.0500 | 0.0500 | 0.0500 |

* $10^6$ psi ; + #/in$^3$

Table 8. ELASTIC CONSTANTS OF FIBROUS COMPOSITES

Uniaxial Laminates
"Light Alloy II" Matrix

| | | Fiber Materials | | | | | | | |
|---|---|---|---|---|---|---|---|---|---|
| $v_b$ | Property | Hollow E-glass | Solid E-glass | Hi Mod. Glass | Asbes-tos | Steel | Beryl-lium | Boron | Alumina |
| 0 | E* | --- | 10.500 | 16.000 | 26.500 | 30.000 | 40.000 | 60.000 | 75.000 |
| | $\nu$ | --- | 0.200 | 0.200 | 0.200 | 0.250 | 0.090 | 0.200 | 0.200 |
| | $\rho$+ | --- | 0.0914 | 0.0914 | 0.0870 | 0.2830 | 0.0660 | 0.0830 | 0.1430 |
| 0.15 | $E_1$* | 5.478 | 11.195 | 15.871 | 24.796 | 27.755 | 36.344 | 53.272 | 66.022 |
| | $E_2$* | 1.786 | 11.080 | 15.888 | 24.303 | 26.832 | 34.142 | 45.942 | 53.709 |
| | $G_{12}$* | 1.409 | 4.562 | 6.523 | 9.963 | 10.669 | 14.959 | 18.846 | 22.039 |
| | $\nu_{21}$ | 0.241 | 0.218 | 0.216 | 0.214 | 0.257 | 0.119 | 0.213 | 0.212 |
| | $\rho$ | 0.0392 | 0.0889 | 0.0889 | 0.0852 | 0.252 | 0.0673 | 0.0818 | 0.133 |
| 0.30 | $E_1$ | 7.164 | 11.882 | 15.734 | 23.085 | 25.509 | 32.657 | 46.537 | 57.037 |
| | $E_2$ | 2.756 | 11.695 | 15.763 | 22.370 | 24.174 | 29.579 | 36.833 | 41.291 |
| | $G_{12}$ | 1.922 | 4.757 | 6.383 | 9.015 | 9.523 | 12.405 | 14.744 | 16.498 |
| | $\nu_{21}$ | 0.263 | 0.235 | 0.232 | 0.229 | 0.264 | 0.148 | 0.226 | 0.225 |
| | $\rho$ | 0.0455 | 0.0865 | 0.0865 | 0.0834 | 0.221 | 0.0687 | 0.0806 | 0.123 |
| 0.45 | $E_1$ | 8.846 | 12.561 | 15.589 | 21.367 | 23.261 | 28.939 | 39.795 | 48.045 |
| | $E_2$ | 4.108 | 12.340 | 15.632 | 20.587 | 21.823 | 25.684 | 30.079 | 32.678 |
| | $G_{12}$ | 2.514 | 4.958 | 6.246 | 8.174 | 8.526 | 10.411 | 11.813 | 12.798 |
| | $\nu_{21}$ | 0.276 | 0.251 | 0.247 | 0.243 | 0.271 | 0.179 | 0.240 | 0.239 |
| | $\rho$ | 0.0518 | 0.0840 | 0.0840 | 0.0816 | 0.189 | 0.0700 | 0.0794 | 0.112 |
| 0.60 | $E_1$ | 10.526 | 13.234 | 15.438 | 19.641 | 21.011 | 25.186 | 33.045 | 39.045 |
| | $E_2$ | 6.029 | 13.014 | 15.469 | 18.911 | 19.695 | 22.247 | 24.756 | 26.215 |
| | $G_{12}$ | 3.204 | 5.168 | 6.112 | 7.424 | 7.652 | 8.811 | 9.615 | 10.153 |
| | $\nu_{21}$ | 0.286 | 0.266 | 0.262 | 0.258 | 0.279 | 0.211 | 0.255 | 0.254 |
| | $\rho$ | 0.0582 | 0.0914 | 0.0816 | 0.0798 | 0.158 | 0.0714 | 0.0782 | 0.102 |
| 0.75 | $E_1$ | 12.205 | 13.901 | 15.279 | 17.907 | 18.758 | 21.398 | 26.286 | 30.037 |
| | $E_2$ | 8.696 | 13.720 | 15.301 | 17.339 | 17.764 | 19.211 | 20.460 | 21.194 |
| | $G_{12}$ | 4.020 | 5.386 | 5.981 | 6.751 | 6.878 | 7.499 | 7.906 | 8.167 |
| | $\nu_{21}$ | 0.292 | 0.279 | 0.277 | 0.274 | 0.286 | 0.243 | 0.271 | 0.270 |
| | $\rho$ | 0.0645 | 0.0791 | 0.0791 | 0.0780 | 0.127 | 0.0727 | 0.0770 | 0.0920 |
| 0.90 | $E_1$ | 13.882 | 14.562 | 15.114 | 16.166 | 16.504 | 17.572 | 19.518 | 21.018 |
| | $E_2$ | 12.178 | 14.469 | 15.123 | 15.888 | 16.034 | 16.560 | 16.973 | 17.231 |
| | $G_{12}$ | 5.000 | 5.613 | 5.853 | 6.143 | 6.189 | 6.404 | 6538 | 6.622 |
| | $\nu_{21}$ | 0.297 | 0.292 | 0.291 | 0.289 | 0.294 | 0.277 | 0.288 | 0.288 |
| | $\rho$ | 0.0708 | 0.0766 | 0.0766 | 0.0762 | 0.0958 | 0.0741 | 0.0758 | 0.0818 |
| 1.00 | E | 15.000 | 15.000 | 15.000 | 15.000 | 15.000 | 15.000 | 15.000 | 15.000 |
| | $\nu$ | 0.300 | 0.300 | 0.300 | 0.300 | 0.300 | 0.300 | 0.300 | 0.300 |
| | $\rho$ | 0.0750 | 0.0750 | 0.0750 | 0.0750 | 0.0750 | 0.0750 | 0.0750 | 0.0750 |

* $10^6$ psi ; + #/in$^3$

Table 8A. ELASTIC CONSTANTS OF FIBROUS COMPOSITES

Isotropic Laminates
"Light Alloy II" Matrix

| | | Fiber Material | | | | | | | |
|---|---|---|---|---|---|---|---|---|---|
| $v_b$ | Property | Hollow E-glass | Solid E-glass | Hi Mod. Glass | Asbes-tos | Steel | Beryl-lium | Boron | Alumina |
| 0 | E* | --- | 10.500 | 16.000 | 26.500 | 30.000 | 40.000 | 60.000 | 75.000 |
| | $\nu$ | --- | 0.200 | 0.200 | 0.200 | 0.250 | 0.090 | 0.200 | 0.200 |
| | $\rho$+ | --- | 0.0914 | 0.0914 | 0.0870 | 0.2830 | 0.0660 | 0.0830 | 0.1430 |
| 0.15 | E | 3.506 | 11.128 | 15.875 | 24.429 | 27.115 | 34.712 | 48.245 | 57.625 |
| | $\nu$ | 0.153 | 0.218 | 0.216 | 0.216 | 0.257 | 0.128 | 0.219 | 0.221 |
| | $\rho$ | 0.0392 | 0.0889 | 0.0889 | 0.0852 | 0.252 | 0.0673 | 0.0818 | 0.133 |
| 0.30 | E | 4.816 | 11.772 | 15.742 | 22.531 | 24.555 | 30.302 | 39.749 | 46.121 |
| | $\nu$ | 0.175 | 0.235 | 0.232 | 0.232 | 0.265 | 0.164 | 0.237 | 0.240 |
| | $\rho$ | 0.0455 | 0.0865 | 0.0865 | 0.0834 | 0.221 | 0.0687 | 0.0806 | 0.123 |
| 0.45 | E | 6.329 | 12.430 | 15.599 | 20.752 | 22.220 | 26.421 | 32.945 | 37.325 |
| | $\nu$ | 0.198 | 0.250 | 0.248 | 0.247 | 0.273 | 0.195 | 0.252 | 0.256 |
| | $\rho$ | 0.0518 | 0.0840 | 0.0840 | 0.0816 | 0.189 | 0.0700 | 0.0794 | 0.112 |
| 0.60 | E | 8.134 | 13.103 | 15.446 | 19.068 | 20.058 | 22.919 | 27.191 | 30.078 |
| | $\nu$ | 0.225 | 0.265 | 0.263 | 0.262 | 0.280 | 0.225 | 0.265 | 0.268 |
| | $\rho$ | 0.0582 | 0.0914 | 0.0816 | 0.798 | 0.158 | 0.0714 | 0.0782 | 0.102 |
| 0.75 | E | 10.321 | 13.795 | 15.285 | 17.469 | 18.045 | 19.726 | 22.171 | 23.845 |
| | $\nu$ | 0.254 | 0.278 | 0.277 | 0.276 | 0.287 | 0.252 | 0.277 | 0.279 |
| | $\rho$ | 0.0645 | 0.0791 | 0.0791 | 0.0780 | 0.127 | 0.0727 | 0.0770 | 0.0920 |
| 0.90 | E | 12.952 | 14.508 | 15.116 | 15.957 | 16.172 | 16.806 | 17.713 | 18.345 |
| | $\nu$ | 0.282 | 0.291 | 0.291 | 0.290 | 0.294 | 0.280 | 0.290 | 0.290 |
| | $\rho$ | 0.0708 | 0.0766 | 0.0766 | 0.0762 | 0.0958 | 0.0741 | 0.0758 | 0.0818 |
| 1.00 | E | 15.000 | 15.000 | 15.000 | 15.000 | 15.000 | 15.000 | 15.000 | 15.000 |
| | $\nu$ | 0.300 | 0.300 | 0.300 | 0.300 | 0.300 | 0.300 | 0.300 | 0.300 |
| | $\rho$ | 0.0750 | 0.0750 | 0.0750 | 0.0750 | 0.0750 | 0.0750 | 0.0750 | 0.0750 |

* $10^6$ psi ; + $\#/in^3$

Table 9. ELASTIC CONSTANTS OF FIBROUS COMPOSITES

Uniaxial Laminates
"Light Alloy III" Matrix

| $v_b$ | Property | Fiber Materials: Hollow E-Glass | Solid E-glass | Hi Mod. Glass | Asbes-tos | Steel | Beryl-lium | Boron | Alumina |
|---|---|---|---|---|---|---|---|---|---|
| 0 | E* | --- | 10.500 | 16.000 | 26.500 | 30.000 | 40.000 | 60.000 | 75.000 |
| | $\nu$ | --- | 0.200 | 0.200 | 0.200 | 0.250 | 0.090 | 0.200 | 0.200 |
| | $\rho$+ | --- | 0.0914 | 0.0914 | 0.0870 | 0.2830 | 0.0660 | 0.0830 | 0.1430 |
| 0.15 | $E_1$* | 7.375 | 13.462 | 18.139 | 27.066 | 30.010 | 38.683 | 55.543 | 68.293 |
| | $E_2$* | 2.353 | 12.423 | 17.593 | 27.041 | 30.018 | 38.724 | 53.815 | 64.374 |
| | $G_{12}$* | 1.883 | 5.152 | 7.262 | 11.115 | 11.930 | 17.082 | 22.060 | 26.390 |
| | $\nu_{21}$ | 0.256 | 0.225 | 0.220 | 0.217 | 0.247 | 0.124 | 0.214 | 0.213 |
| | $\rho$ | 0.0392 | 0.0889 | 0.0889 | 0.0852 | 0.251 | 0.0673 | 0.0818 | 0.132 |
| 0.30 | $E_1$ | 11.670 | 16.405 | 20.261 | 27.616 | 30.017 | 37.298 | 51.071 | 61.572 |
| | $E_2$ | 4.086 | 14.684 | 19.365 | 27.575 | 30.029 | 37.389 | 48.586 | 56.054 |
| | $G_{12}$ | 2.953 | 6.009 | 7.898 | 11.188 | 11.860 | 15.918 | 19.558 | 22.522 |
| | $\nu_{21}$ | 0.276 | 0.244 | 0.238 | 0.233 | 0.266 | 0.157 | 0.228 | 0.227 |
| | $\rho$ | 0.0455 | 0.0865 | 0.0865 | 0.0834 | 0.221 | 0.0687 | 0.0806 | 0.123 |
| 0.45 | $E_1$ | 15.601 | 19.334 | 22.368 | 28.151 | 30.020 | 35.847 | 46.585 | 54.837 |
| | $E_2$ | 6.568 | 17.235 | 21.293 | 28.101 | 30.034 | 35.944 | 43.904 | 49.016 |
| | $G_{12}$ | 4.209 | 6.959 | 8.578 | 11.263 | 11.290 | 14.845 | 17.403 | 19.370 |
| | $\nu_{21}$ | 0.285 | 0.260 | 0.254 | 0.249 | 0.273 | 0.189 | 0.243 | 0.242 |
| | $\rho$ | 0.0518 | 0.0840 | 0.0840 | 0.0816 | 0.189 | 0.0700 | 0.0794 | 0.112 |
| 0.60 | $E_1$ | 19.529 | 22.253 | 24.462 | 28.672 | 30.019 | 34.332 | 42.084 | 48.086 |
| | $E_2$ | 10.286 | 20.070 | 23.371 | 28.626 | 30.033 | 34.389 | 39.614 | 42.863 |
| | $G_{12}$ | 5.702 | 8.017 | 9.307 | 11.337 | 11.721 | 13.853 | 15.527 | 16.751 |
| | $\nu_{21}$ | 0.292 | 0.273 | 0.269 | 0.264 | 0.281 | 0.220 | 0.258 | 0.257 |
| | $\rho$ | 0.0582 | 0.0816 | 0.0816 | 0.0798 | 0.158 | 0.0714 | 0.0782 | 0.102 |
| 0.75 | $E_1$ | 23.456 | 25.163 | 26.546 | 29.180 | 30.015 | 32.757 | 37.566 | 41.318 |
| | $E_2$ | 15.829 | 23.243 | 25.623 | 29.144 | 30.025 | 32.754 | 35.682 | 37.455 |
| | $G_{12}$ | 7.508 | 9.204 | 10.091 | 11.412 | 11.652 | 12.932 | 13.880 | 14.542 |
| | $\nu_{21}$ | 0.296 | 0.285 | 0.281 | 0.278 | 0.288 | 0.251 | 0.273 | 0.272 |
| | $\rho$ | 0.0645 | 0.0791 | 0.0791 | 0.0780 | 0.127 | 0.0727 | 0.0770 | 0.0920 |
| 0.90 | $E_1$ | 27.383 | 28.067 | 28.621 | 29.676 | 30.007 | 31.122 | 33.032 | 34.533 |
| | $E_2$ | 23.538 | 26.971 | 28.124 | 29.658 | 30.012 | 31.092 | 32.133 | 32.752 |
| | $G_{12}$ | 9.738 | 10.544 | 10.937 | 11.488 | 11.584 | 12.0771 | 12.421 | 12.653 |
| | $\nu_{21}$ | 0.298 | 0.294 | 0.293 | 0.291 | 0.295 | 0.280 | 0.289 | 0.289 |
| | $\rho$ | 0.0708 | 0.0766 | 0.0766 | 0.0762 | 0.0958 | 0.0741 | 0.0758 | 0.0818 |
| 1.00 | E | 30.000 | 30.000 | 30.000 | 30.000 | 30.000 | 30.000 | 30.000 | 30.000 |
| | $\nu$ | 0.300 | 0.300 | 0.300 | 0.300 | 0.300 | 0.300 | 0.300 | 0.300 |
| | $\rho$ | 0.0750 | 0.0750 | 0.0750 | 0.0750 | 0.0750 | 0.0750 | 0.0750 | 0.0750 |

* $10^6$psi ; + $\#/in^3$

Table 9A. ELASTIC CONSTANTS OF FIBROUS COMPOSITES

Isotropic Laminates
"Light Alloy III" Matrix

| | | Fiber Material | | | | | | | |
|---|---|---|---|---|---|---|---|---|---|
| $v_b$ | Property | Hollow E-glass | Solid E-glass | Hi Mod. Glass | Asbes - tos | Steel | Beryl- lium | Boron | Alumina |
| 0 | E* | --- | 10.500 | 16.000 | 26.500 | 30.000 | 40.000 | 60.000 | 75.000 |
| | $\nu$ | --- | 0.200 | 0.200 | 0.200 | 0.250 | 0.090 | 0.200 | 0.200 |
| | $\rho$+ | --- | 0.0914 | 0.0914 | 0.0870 | 0.2830 | 0.0660 | 0.0830 | 0.1430 |
| 0.15 | E | 4.824 | 12.816 | 17.808 | 27.053 | 30.014 | 38.616 | 54.292 | 65.537 |
| | $\nu$ | 0.163 | 0.223 | 0.220 | 0.217 | 0.258 | 0.126 | 0.216 | 0.217 |
| | $\rho$ | 0.0392 | 0.0889 | 0.0889 | 0.0852 | 0.251 | 0.0673 | 0.0818 | 0.132 |
| 0.30 | E | 7.580 | 15.332 | 19.709 | 27.595 | 30.022 | 37.193 | 49.210 | 57.580 |
| | $\nu$ | 0.180 | 0.242 | 0.237 | 0.233 | 0.267 | 0.160 | 0.232 | 0.233 |
| | $\rho$ | 0.0455 | 0.0865 | 0.0865 | 0.0834 | 0.221 | 0.0687 | 0.0806 | 0.123 |
| 0.45 | E | 10.758 | 17.987 | 21.700 | 28.126 | 30.026 | 35.717 | 44.548 | 50.575 |
| | $\nu$ | 0.198 | 0.258 | 0.253 | 0.249 | 0.273 | 0.193 | 0.247 | 0.248 |
| | $\rho$ | 0.0518 | 0.0840 | 0.0840 | 0.0816 | 0.189 | 0.0700 | 0.0794 | 0.112 |
| 0.60 | E | 14.585 | 20.856 | 23.785 | 28.648 | 30.025 | 34.191 | 40.210 | 44.261 |
| | $\nu$ | 0.222 | 0.270 | 0.267 | 0.263 | 0.281 | 0.224 | 0.262 | 0.262 |
| | $\rho$ | 0.0582 | 0.0816 | 0.0816 | 0.0798 | 0.158 | 0.0714 | 0.0782 | 0.102 |
| 0.75 | E | 19.436 | 23.961 | 25.982 | 29.161 | 30.019 | 32.627 | 36.115 | 38.508 |
| | $\nu$ | 0.251 | 0.281 | 0.279 | 0.278 | 0.288 | 0.253 | 0.276 | 0.276 |
| | $\rho$ | 0.0645 | 0.0791 | 0.0791 | 0.0780 | 0.127 | 0.0727 | 0.0770 | 0.0920 |
| 0.90 | E | 25.273 | 27.407 | 28.325 | 29.667 | 30.009 | 31.048 | 32.371 | 33.249 |
| | $\nu$ | 0.282 | 0.291 | 0.292 | 0.291 | 0.295 | 0.282 | 0.290 | 0.290 |
| | $\rho$ | 0.0708 | 0.0766 | 0.0766 | 0.0762 | 0.0958 | 0.0741 | 0.0758 | 0.0818 |
| 1.00 | E | 30.000 | 30.000 | 30.000 | 30.000 | 30.000 | 30.000 | 30.000 | 30.000 |
| | $\nu$ | 0.300 | 0.300 | 0.300 | 0.300 | 0.300 | 0.300 | 0.300 | 0.300 |
| | $\rho$ | 0.0750 | 0.0750 | 0.0750 | 0.0750 | 0.0750 | 0.0750 | 0.0750 | 0.0750 |

* $10^6$ psi ; + $\#/in^3$

Table 10. ELASTIC CONSTANTS OF FIBROUS COMPOSITES

Uniaxial Laminates
Titanium Matrix

| $v_b$ | Property | Fiber Materials: Hollow E-glass | Solid E-glass | Hi Mod. Glass | Asbestos | Steel | Beryllium | Boron | Alumina |
|---|---|---|---|---|---|---|---|---|---|
| 0 | $E$* | --- | 10.500 | 16.000 | 26.500 | 30.000 | 40.000 | 60.000 | 75.000 |
| | $\nu$ | --- | 0.200 | 0.200 | 0.200 | 0.250 | 0.090 | 0.200 | 0.200 |
| | $\rho$+ | --- | 0.0914 | 0.0914 | 0.0870 | 0.2830 | 0.0660 | 0.0830 | 0.1430 |
| 0.15 | $E_1$* | 5.478 | 11.195 | 15.871 | 24.796 | 27.755 | 36.344 | 53.272 | 66.022 |
| | $E_2$* | 1.786 | 11.080 | 15.888 | 24.303 | 26.382 | 34.142 | 45.942 | 53.709 |
| | $G_{12}$* | 1.409 | 4.562 | 6.523 | 9.963 | 10.669 | 14.959 | 18.846 | 22.039 |
| | $\nu_{21}$ | 0.241 | 0.218 | 0.216 | 0.214 | 0.257 | 0.119 | 0.213 | 0.212 |
| | $\rho$ | 0.0505 | 0.100 | 0.100 | 0.0964 | 0.263 | 0.0786 | 0.0931 | 0.144 |
| 0.30 | $E_1$ | 7.164 | 11.882 | 15.734 | 23.085 | 25.509 | 32.657 | 46.537 | 57.037 |
| | $E_2$ | 2.756 | 11.695 | 15.763 | 22.370 | 24.174 | 29.579 | 36.833 | 41.291 |
| | $G_{12}$ | 1.922 | 4.757 | 6.383 | 9.015 | 9.523 | 12.405 | 14.744 | 16.498 |
| | $\nu_{21}$ | 0.263 | 0.235 | 0.232 | 0.229 | 0.264 | 0.148 | 0.226 | 0.225 |
| | $\rho$ | 0.0680 | 0.109 | 0.109 | 0.106 | 0.243 | 0.0911 | 0.103 | 0.143 |
| 0.45 | $E_1$ | 8.846 | 12.561 | 15.589 | 21.367 | 23.261 | 28.939 | 39.795 | 48.045 |
| | $E_2$ | 4.108 | 12.340 | 15.623 | 20.587 | 21.823 | 25.684 | 30.079 | 32.678 |
| | $G_{12}$ | 2.514 | 4.958 | 6.246 | 8.174 | 8.526 | 10.411 | 11.813 | 12.798 |
| | $\nu_{21}$ | 0.276 | 0.251 | 0.247 | 0.243 | 0.271 | 0.179 | 0.240 | 0.239 |
| | $\rho$ | 0.0856 | 0.118 | 0.118 | 0.115 | 0.223 | 0.102 | 0.113 | 0.146 |
| 0.60 | $E_1$ | 10.526 | 13.234 | 15.438 | 19.641 | 21.011 | 25.186 | 33.045 | 39.045 |
| | $E_2$ | 6.029 | 13.014 | 15.469 | 18.911 | 19.695 | 22.247 | 24.756 | 26.215 |
| | $G_{12}$ | 3.204 | 5.168 | 6.112 | 7.424 | 7.652 | 8.811 | 9.615 | 10.153 |
| | $\nu_{21}$ | 0.286 | 0.266 | 0.262 | 0.258 | 0.279 | 0.211 | 0.255 | 0.254 |
| | $\rho$ | 0.103 | 0.127 | 0.127 | 0.125 | 0.203 | 0.116 | 0.123 | 0.147 |
| 0.75 | $E_1$ | 12.205 | 13.901 | 15.279 | 17.907 | 18.758 | 21.398 | 26.286 | 30.037 |
| | $E_2$ | 8.696 | 13.720 | 15.301 | 17.339 | 17.764 | 19.211 | 20.460 | 21.194 |
| | $G_{12}$ | 4.020 | 5.386 | 5.981 | 6.751 | 6.878 | 7.499 | 7.906 | 8.167 |
| | $\nu_{21}$ | 0.292 | 0.279 | 0.277 | 0.274 | 0.286 | 0.243 | 0.271 | 0.270 |
| | $\rho$ | 0.121 | 0.135 | 0.135 | 0.134 | 0.183 | 0.129 | 0.133 | 0.148 |
| 0.90 | $E_1$ | 13.882 | 14.562 | 15.114 | 16.166 | 16.504 | 17.572 | 19.518 | 21.018 |
| | $E_2$ | 12.178 | 14.569 | 15.123 | 15.888 | 16.034 | 16.560 | 16.973 | 17.231 |
| | $G_{12}$ | 5.000 | 5.613 | 5.853 | 6.143 | 6.189 | 6.404 | 6.538 | 6.622 |
| | $\nu_{21}$ | 0.297 | 0.292 | 0.291 | 0.289 | 0.294 | 0.277 | 0.288 | 0.288 |
| | $\rho$ | 0.138 | 0.144 | 0.144 | 0.144 | 0.163 | 0.142 | 0.143 | 0.149 |
| 1.00 | $E$ | 15.000 | 15.000 | 15.000 | 15.000 | 15.000 | 15.000 | 15.000 | 15.000 |
| | $\nu$ | 0.300 | 0.300 | 0.300 | 0.300 | 0.300 | 0.300 | 0.300 | 0.300 |
| | $\rho$ | 0.150 | 0.150 | 0.150 | 0.150 | 0.150 | 0.150 | 0.150 | 0.150 |

* $10^6$ psi ; + #/in$^3$

Table 10A. ELASTIC CONSTANTS OF FIBROUS COMPOSITES

Isotropic Laminates
Titanium Matrix

| $v_b$ | Property | Fiber Material: Hollow E-glass | Solid E-glass | Hi Mod. Glass | Asbes-tos | Steel | Beryl-lium | Boron | Alumina |
|---|---|---|---|---|---|---|---|---|---|
| 0 | E* | --- | 10.500 | 16.000 | 26.500 | 30.000 | 40.000 | 60.000 | 75.000 |
| | $\nu$ | --- | 0.200 | 0.200 | 0.200 | 0.250 | 0.090 | 0.200 | 0.200 |
| | $\rho$+ | --- | 0.0914 | 0.0914 | 0.0870 | 0.2830 | 0.0660 | 0.0830 | 0.1430 |
| 0.15 | E | 3.506 | 11.128 | 15.875 | 24.429 | 27.115 | 34.712 | 48.245 | 57.625 |
| | $\nu$ | 0.153 | 0.218 | 0.216 | 0.216 | 0.257 | 0.128 | 0.219 | 0.221 |
| | $\rho$ | 0.0505 | 0.100 | 0.100 | 0.0964 | 0.263 | 0.0786 | 0.0931 | 0.144 |
| 0.30 | E | 4.816 | 11.772 | 15.742 | 22.531 | 24.555 | 30.302 | 39.749 | 46.121 |
| | $\nu$ | 0.175 | 0.235 | 0.232 | 0.232 | 0.265 | 0.164 | 0.237 | 0.240 |
| | $\rho$ | 0.0680 | 0.109 | 0.109 | 0.106 | 0.243 | 0.0911 | 0.103 | 0.143 |
| 0.45 | E | 6.329 | 12.430 | 15.599 | 20.752 | 22.220 | 26.421 | 32.945 | 37.235 |
| | $\nu$ | 0.198 | 0.250 | 0.248 | 0.247 | 0.273 | 0.195 | 0.252 | 0.256 |
| | $\rho$ | 0.0856 | 0.118 | 0.118 | 0.115 | 0.223 | 0.102 | 0.113 | 0.146 |
| 0.60 | E | 8.134 | 13.013 | 15.446 | 19.068 | 20.058 | 22.919 | 27.191 | 30.078 |
| | $\nu$ | 0.225 | 0.265 | 0.263 | 0.262 | 0.280 | 0.225 | 0.265 | 0.268 |
| | $\rho$ | 0.103 | 0.127 | 0.127 | 0.125 | 0.203 | 0.116 | 0.123 | 0.147 |
| 0.75 | E | 10.321 | 13.795 | 15.285 | 17.469 | 18.045 | 19.726 | 22.171 | 23.845 |
| | $\nu$ | 0.254 | 0.278 | 0.277 | 0.276 | 0.287 | 0.252 | 0.277 | 0.279 |
| | $\rho$ | 0.121 | 0.135 | 0.135 | 0.134 | 0.183 | 0.129 | 0.133 | 0.148 |
| 0.90 | E | 12.952 | 14.508 | 15.116 | 15.957 | 16.172 | 16.806 | 17.713 | 18.345 |
| | $\nu$ | 0.282 | 0.291 | 0.291 | 0.290 | 0.294 | 0.280 | 0.290 | 0.290 |
| | $\rho$ | 0.138 | 0.144 | 0.144 | 0.144 | 0.163 | 0.142 | 0.143 | 0.149 |
| 1.00 | E | 15.000 | 15.000 | 15.000 | 15.000 | 15.000 | 15.000 | 15.000 | 15.000 |
| | $\nu$ | 0.300 | 0.300 | 0.300 | 0.300 | 0.300 | 0.300 | 0.300 | 0.300 |
| | $\rho$ | 0.150 | 0.150 | 0.150 | 0.150 | 0.150 | 0.150 | 0.150 | 0.150 |

* $10^6$ psi ; + $\#/in^3$

Table 11. ELASTIC CONSTANTS OF FIBROUS COMPOSITES

Uniaxial Laminates
Steel Matrix

| $v_b$ | Property | Fiber Materials: Hollow E-glass | Solid E-glass | Hi Mod. Glass | Asbestos | Steel | Beryllium | Boron | Alumina |
|---|---|---|---|---|---|---|---|---|---|
| 0 | $E$* | --- | 10.500 | 16.000 | 26.500 | 30.000 | 40.000 | 60.000 | 75.000 |
| | $\nu$ | --- | 0.200 | 0.200 | 0.200 | 0.250 | 0.090 | 0.200 | 0.200 |
| | $\rho$ + | --- | 0.0914 | 0.0914 | 0.0870 | 0.2830 | 0.0660 | 0.0830 | 0.1430 |
| 0.15 | $E_1$* | 7.735 | 13.462 | 18.139 | 27.066 | 30.010 | 38.683 | 55.543 | 68.293 |
| | $E_2$* | 2.353 | 12.423 | 17.593 | 27.041 | 30.018 | 38.724 | 53.815 | 64.374 |
| | $G_{12}$* | 1.883 | 5.152 | 7.262 | 11.115 | 11.930 | 17.082 | 22.060 | 27.390 |
| | $\nu_{21}$ | 0.273 | 0.225 | 0.220 | 0.217 | 0.258 | 0.124 | 0.214 | 0.213 |
| | $\rho$ | 0.0729 | 0.123 | 0.123 | 0.119 | 0.286 | 0.101 | 0.116 | 0.167 |
| 0.30 | $E_1$ | 11.670 | 16.405 | 20.261 | 27.616 | 30.017 | 37.298 | 51.071 | 61.572 |
| | $E_2$ | 4.086 | 14.684 | 19.365 | 27.575 | 30.029 | 37.389 | 48.586 | 56.054 |
| | $G_{12}$ | 2.953 | 6.009 | 7.898 | 11.118 | 11.860 | 15.918 | 19.558 | 22.522 |
| | $\nu_{21}$ | 0.276 | 0.244 | 0.238 | 0.233 | 0.266 | 0.157 | 0.228 | 0.227 |
| | $\rho$ | 0.113 | 0.154 | 0.154 | 0.151 | 0.288 | 0.136 | 0.148 | 0.190 |
| 0.45 | $E_1$ | 15.601 | 19.334 | 22.368 | 28.151 | 30.020 | 35.847 | 46.585 | 54.837 |
| | $E_2$ | 6.568 | 17.235 | 21.293 | 28.103 | 30.034 | 35.944 | 43.904 | 49.016 |
| | $G_{12}$ | 4.209 | 6.959 | 8.578 | 11.263 | 11.790 | 14.845 | 17.403 | 19.370 |
| | $\nu_{21}$ | 0.285 | 0.260 | 0.254 | 0.249 | 0.273 | 0.189 | 0.243 | 0.242 |
| | $\rho$ | 0.153 | 0.185 | 0.185 | 0.183 | 0.291 | 0.171 | 0.181 | 0.214 |
| 0.60 | $E_1$ | 19.529 | 22.262 | 24.262 | 28.672 | 30.019 | 34.332 | 42.084 | 48.056 |
| | $E_2$ | 10.286 | 20.070 | 23.371 | 28.626 | 30.033 | 34.339 | 39.614 | 42.863 |
| | $G_{12}$ | 5.702 | 8.017 | 9.307 | 11.337 | 11.701 | 13.853 | 15.527 | 16.751 |
| | $\nu_{21}$ | 0.292 | 0.273 | 0.269 | 0.264 | 0.281 | 0.220 | 0.257 | 0.257 |
| | $\rho$ | 0.193 | 0.217 | 0.217 | 0.215 | 0.293 | 0.206 | 0.213 | 0.237 |
| 0.75 | $E_1$ | 23.456 | 25.123 | 26.546 | 29.180 | 30.015 | 32.757 | 37.566 | 41.318 |
| | $E_2$ | 15.829 | 23.243 | 25.623 | 29.144 | 30.025 | 32.754 | 35.682 | 37.455 |
| | $G_{12}$ | 7.508 | 9.204 | 10.091 | 11.412 | 11.652 | 12.932 | 13.880 | 14.542 |
| | $\nu_{21}$ | 0.296 | 0.285 | 0.281 | 0.278 | 0.288 | 0.251 | 0.273 | 0.272 |
| | $\rho$ | 0.233 | 0.249 | 0.248 | 0.248 | 0.296 | 0.242 | 0.246 | 0.261 |
| 0.90 | $E_1$ | 27.383 | 28.067 | 28.621 | 29.676 | 30.007 | 31.122 | 33.032 | 34.534 |
| | $E_2$ | 23.538 | 26.971 | 28.124 | 29.658 | 30.012 | 31.092 | 32.133 | 32.752 |
| | $G_{12}$ | 0.738 | 10.544 | 10.937 | 11.488 | 11.584 | 12.077 | 12.421 | 12.653 |
| | $\nu_{21}$ | 0.298 | 0.294 | 0.293 | 0.291 | 0.295 | 0.280 | 0.289 | 0.289 |
| | $\rho$ | 0.273 | 0.279 | 0.279 | 0.279 | 0.298 | 0.277 | 0.278 | 0.284 |
| 1.00 | $E$ | 30.000 | 30.000 | 30.000 | 30.000 | 30.000 | 30.000 | 30.000 | 30.000 |
| | $\nu$ | 0.300 | 0.300 | 0.300 | 0.300 | 0.300 | 0.300 | 0.300 | 0.300 |
| | $\rho$ | 0.3000 | 0.3000 | 0.3000 | 0.3000 | 0.3000 | 0.3000 | 0.3000 | 0.3000 |

* $10^6$ psi ; + #/in$^3$

Table 11A. ELASTIC CONSTANTS OF FIBROUS COMPOSITES

Isotropic Laminates
Steel Matrix

| | | Fiber Materials | | | | | | | |
|---|---|---|---|---|---|---|---|---|---|
| $v_b$ | Property | Hollow E-glass | Solid E-glass | Hi Mod. Glass | Asbes-tos | Steel | Beryl-lium | Boron | Alumina |
| 0 | E* | --- | 10.500 | 16.000 | 26.500 | 30.000 | 40.000 | 60.000 | 75.000 |
| | $\nu$ | --- | 0.200 | 0.200 | 0.200 | 0.250 | 0.090 | 0.200 | 0.200 |
| | $\rho$+ | --- | 0.0914 | 0.0914 | 0.0870 | 0.2830 | 0.0660 | 0.0830 | 0.1430 |
| 0.15 | E | 4.824 | 12.816 | 17.808 | 27.053 | 30.014 | 38.161 | 54.292 | 65.537 |
| | $\nu$ | 0.163 | 0.223 | 0.220 | 0.217 | 0.278 | 0.126 | 0.216 | 0.217 |
| | $\rho$ | 0.0729 | 0.123 | 0.123 | 0.119 | 0.286 | 0.101 | 0.116 | 0.167 |
| 0.30 | E | 7.580 | 15.312 | 19.709 | 27.595 | 30.022 | 37.193 | 49.210 | 57.580 |
| | $\nu$ | 0.180 | 0.242 | 0.237 | 0.233 | 0.266 | 0.160 | 0.232 | 0.233 |
| | $\rho$ | 0.113 | 0.154 | 0.154 | 0.151 | 0.288 | 0.136 | 0.148 | 0.190 |
| 0.45 | E | 10.758 | 17.987 | 21.700 | 28.126 | 30.026 | 35.717 | 44.548 | 50.575 |
| | $\nu$ | 0.198 | 0.258 | 0.253 | 0.249 | 0.273 | 0.193 | 0.247 | 0.248 |
| | $\rho$ | 0.153 | 0.185 | 0.185 | 0.183 | 0.291 | 0.171 | 0.181 | 0.214 |
| 0.60 | E | 14.585 | 20.856 | 23.785 | 28.648 | 30.025 | 34.191 | 40.210 | 44.061 |
| | $\nu$ | 0.222 | 0.270 | 0.267 | 0.263 | 0.281 | 0.224 | 0.262 | 0.262 |
| | $\rho$ | 0.193 | 0.217 | 0.217 | 0.215 | 0.293 | 0.206 | 0.213 | 0.237 |
| 0.75 | E | 19.346 | 23.961 | 25.982 | 29.161 | 30.019 | 32.627 | 36.155 | 38.508 |
| | $\nu$ | 0.251 | 0.281 | 0.279 | 0.278 | 0.288 | 0.253 | 0.276 | 0.276 |
| | $\rho$ | 0.233 | 0.249 | 0.248 | 0.248 | 0.296 | 0.242 | 0.246 | 0.261 |
| 0.90 | E | 25.273 | 27.407 | 28.325 | 29.667 | 30.009 | 31.048 | 32.371 | 33.249 |
| | $\nu$ | 0.282 | 0.291 | 0.292 | 0.291 | 0.295 | 0.282 | 0.290 | 0.290 |
| | $\rho$ | 0.273 | 0.279 | 0.279 | 0.279 | 0.298 | 0.277 | 0.278 | 0.284 |
| 1.00 | E | 30.000 | 30.000 | 30.000 | 30.000 | 30.000 | 30.000 | 30.000 | 30.000 |
| | $\nu$ | 0.300 | 0.300 | 0.300 | 0.300 | 0.300 | 0.300 | 0.300 | 0.300 |
| | $\rho$ | 0.3000 | 0.3000 | 0.3000 | 0.3000 | 0.3000 | 0.3000 | 0.3000 | 0.3000 |

* $10^6$ psi ; + #/in$^3$

Table 12. ELASTIC CONSTANTS OF FIBROUS COMPOSITES

Uniaxial Laminates
Boron Matrix

| | | Fiber Material | | | | | | | |
|---|---|---|---|---|---|---|---|---|---|
| $v_b$ | Property | Hollow E-glass | Solid E-glass | Hi Mod. Glass | Asbes-tos | Steel | Beryl-lium | Boron | Alumina |
| 0 | $E$* | --- | 10.500 | 16.000 | 26.500 | 30.000 | 40.000 | 60.000 | 75.000 |
| | $\nu$ | --- | 0.200 | 0.200 | 0.200 | 0.250 | 0.090 | 0.200 | 0.200 |
| | $\rho$ + | --- | 0.0914 | 0.0914 | 0.0870 | 0.2830 | 0.0660 | 0.0830 | 0.1430 |
| 0.15 | $E_1$* | 12.242 | 17.990 | 22.671 | 31.602 | 34.520 | 43.347 | 60.083 | 72.834 |
| | $E_2$* | 3.387 | 14.713 | 20.050 | 30.053 | 33.326 | 42.826 | 60.141 | 72.737 |
| | $G_{12}$* | 2.822 | 6.152 | 8.342 | 12.431 | 13.310 | 18.995 | 24.701 | 29.844 |
| | $\nu_{21}$ | 0.271 | 0.234 | 0.228 | 0.222 | 0.260 | 0.133 | 0.216 | 0.215 |
| | $\rho$ | 0.0392 | 0.0889 | 0.0889 | 0.0852 | 0.252 | 0.0673 | 0.0818 | 0.133 |
| 0.30 | $E_1$ | 20.675 | 25.437 | 29.302 | 36.667 | 39.031 | 46.538 | 60.134 | 70.637 |
| | $E_2$ | 6.577 | 19.939 | 24.933 | 34.116 | 37.078 | 45.686 | 60.230 | 70.515 |
| | $G_{12}$ | 4.996 | 8.174 | 10.218 | 13.937 | 14.721 | 19.662 | 24.406 | 28.509 |
| | $\nu_{21}$ | 0.285 | 0.256 | 0.249 | 0.241 | 0.269 | 0.171 | 0.232 | 0.230 |
| | $\rho$ | 0.0455 | 0.0865 | 0.0865 | 0.0834 | 0.221 | 0.0687 | 0.0806 | 0.123 |
| 0.45 | $E_1$ | 29.103 | 32.861 | 35.906 | 41.703 | 43.535 | 49.598 | 60.155 | 68.411 |
| | $E_2$ | 11.254 | 26.060 | 30.542 | 38.619 | 41.186 | 48.592 | 60.268 | 68.279 |
| | $G_{12}$ | 7.569 | 10.497 | 12.332 | 15.578 | 16.247 | 20.351 | 24.115 | 27.240 |
| | $\nu_{21}$ | 0.292 | 0.271 | 0.264 | 0.257 | 0.277 | 0.204 | 0.248 | 0.246 |
| | $\rho$ | 0.0518 | 0.0840 | 0.0840 | 0.0816 | 0.275 | 0.0700 | 0.0794 | 0.112 |
| 0.60 | $E_1$ | 37.530 | 40.272 | 42.492 | 46.716 | 48.032 | 52.459 | 60.015 | 66.155 |
| | $E_2$ | 18.497 | 32.028 | 36.851 | 43.546 | 45.628 | 51.560 | 60.255 | 66.014 |
| | $G_{12}$ | 10.660 | 13.193 | 14.733 | 17.370 | 17.901 | 21.062 | 23.827 | 26.032 |
| | $\nu_{21}$ | 0.295 | 0.282 | 0.277 | 0.271 | 0.284 | 0.234 | 0.262 | 0.261 |
| | $\rho$ | 0.0582 | 0.0816 | 0.0816 | 0.0798 | 0.158 | 0.0714 | 0.0782 | 0.102 |
| 0.75 | $E_1$ | 45.957 | 47.675 | 49.065 | 51.710 | 52.524 | 55.407 | 60.114 | 63.871 |
| | $E_2$ | 29.783 | 41.014 | 44.004 | 48.978 | 50.458 | 54.613 | 60.194 | 63.735 |
| | $G_{12}$ | 14.446 | 16.360 | 17.482 | 19.337 | 19.700 | 21.796 | 23.543 | 24.881 |
| | $\nu_{21}$ | 0.298 | 0.290 | 0.287 | 0.283 | 0.290 | 0.261 | 0.277 | 0.276 |
| | $\rho$ | 0.0645 | 0.0791 | 0.0791 | 0.0780 | 0.127 | 0.0727 | 0.0770 | 0.0920 |
| 0.90 | $E_1$ | 54.383 | 55.071 | 55.629 | 56.688 | 57.011 | 58.186 | 60.054 | 61.558 |
| | $E_2$ | 46.081 | 50.577 | 52.645 | 55.175 | 55.871 | 57.788 | 60.090 | 61.473 |
| | $G_{12}$ | 19.188 | 20.133 | 20.664 | 21.504 | 21.664 | 22.556 | 23.262 | 23.782 |
| | $\nu_{21}$ | 0.299 | 0.296 | 0.295 | 0.294 | 0.296 | 0.285 | 0.291 | 0.290 |
| | $\rho$ | 0.0708 | 0.0766 | 0.0766 | 0.0762 | 0.0762 | 0.0741 | 0.0758 | 0.0818 |
| 1.00 | $E$ | 60.000 | 60.000 | 60.000 | 60.000 | 60.000 | 60.000 | 60.000 | 60.000 |
| | $\nu$ | 0.300 | 0.300 | 0.300 | 0.300 | 0.300 | 0.300 | 0.300 | 0.300 |
| | $\rho$ | 0.0750 | 0.0750 | 0.0750 | 0.0750 | 0.0750 | 0.0750 | 0.0750 | 0.0750 |

* $10^6$ psi; + $\#/in^3$

Table 12A. ELASTIC CONSTANTS OF FIBROUS COMPOSITES

Isotropic Laminates
Boron Matrix

| | | Fiber Material | | | | | | | |
|---|---|---|---|---|---|---|---|---|---|
| $v_b$ | Property | Hollow E-glass | Solid E-glass | Hi Mod. Glass | Asbes-tos | Steel | Beryl-lium | Boron | Alumina |
| 0 | E* | --- | 10.500 | 16.000 | 26.500 | 30.000 | 40.000 | 60.000 | 75.000 |
| | $\nu$ | --- | 0.200 | 0.200 | 0.200 | 0.250 | 0.090 | 0.200 | 0.200 |
| | $\rho$+ | --- | 0.0914 | 0.0914 | 0.0870 | 0.2830 | 0.0660 | 0.0830 | 0.1430 |
| 0.15 | E | 7.411 | 15.909 | 21.024 | 30.650 | 33.764 | 43.064 | 60.107 | 72.710 |
| | $\nu$ | 0.168 | 0.233 | 0.226 | 0.221 | 0.259 | 0.132 | 0.217 | 0.216 |
| | $\rho$ | 0.0392 | 0.0889 | 0.0889 | 0.0852 | 0.252 | 0.0673 | 0.0818 | 0.133 |
| 0.30 | E | 13.028 | 21.866 | 26.497 | 35.069 | 37.770 | 46.070 | 60.175 | 70.447 |
| | $\nu$ | 0.181 | 0.254 | 0.246 | 0.239 | 0.267 | 0.170 | 0.233 | 0.232 |
| | $\rho$ | 0.0455 | 0.0865 | 0.0865 | 0.0834 | 0.221 | 0.0687 | 0.0806 | 0.123 |
| 0.45 | E | 19.502 | 28.388 | 32.424 | 39.752 | 42.003 | 49.042 | 60.203 | 68.193 |
| | $\nu$ | 0.196 | 0.268 | 0.261 | 0.255 | 0.275 | 0.203 | 0.248 | 0.247 |
| | $\rho$ | 0.0518 | 0.0850 | 0.0840 | 0.0816 | 0.189 | 0.0700 | 0.0794 | 0.112 |
| 0.60 | E | 27.342 | 35.529 | 38.844 | 44.716 | 46.471 | 52.002 | 60.193 | 65.940 |
| | $\nu$ | 0.218 | 0.277 | 0.273 | 0.268 | 0.282 | 0.233 | 0.263 | 0.262 |
| | $\rho$ | 0.0582 | 0.0816 | 0.0816 | 0.0798 | 0.158 | 0.0714 | 0.0782 | 0.102 |
| 0.75 | E | 37.251 | 43.443 | 45.874 | 50.017 | 51.209 | 54.969 | 60.147 | 63.693 |
| | $\nu$ | 0.249 | 0.283 | 0.282 | 0.280 | 0.289 | 0.259 | 0.277 | 0.277 |
| | $\rho$ | 0.0645 | 0.0791 | 0.0791 | 0.0780 | 0.127 | 0.0727 | 0.0770 | 0.0920 |
| 0.90 | E | 49.828 | 52.615 | 53.834 | 55.781 | 56.311 | 57.968 | 60.069 | 61.565 |
| | $\nu$ | 0.281 | 0.291 | 0.291 | 0.292 | 0.295 | 0.284 | 0.291 | 0.291 |
| | $\rho$ | 0.0708 | 0.0766 | 0.0766 | 0.0762 | 0.0958 | 0.0741 | 0.0758 | 0.0818 |
| 1.00 | E | 60.000 | 60.000 | 60.000 | 60.000 | 60.000 | 60.000 | 60.000 | 60.000 |
| | $\nu$ | 0.300 | 0.300 | 0.200 | 0.300 | 0.300 | 0.300 | 0.300 | 0.300 |
| | $\rho$ | 0.0750 | 0.0750 | 0.0750 | 0.0750 | 0.0750 | 0.0750 | 0.0750 | 0.0750 |

* $10^6$ psi ; + $\#/in^3$

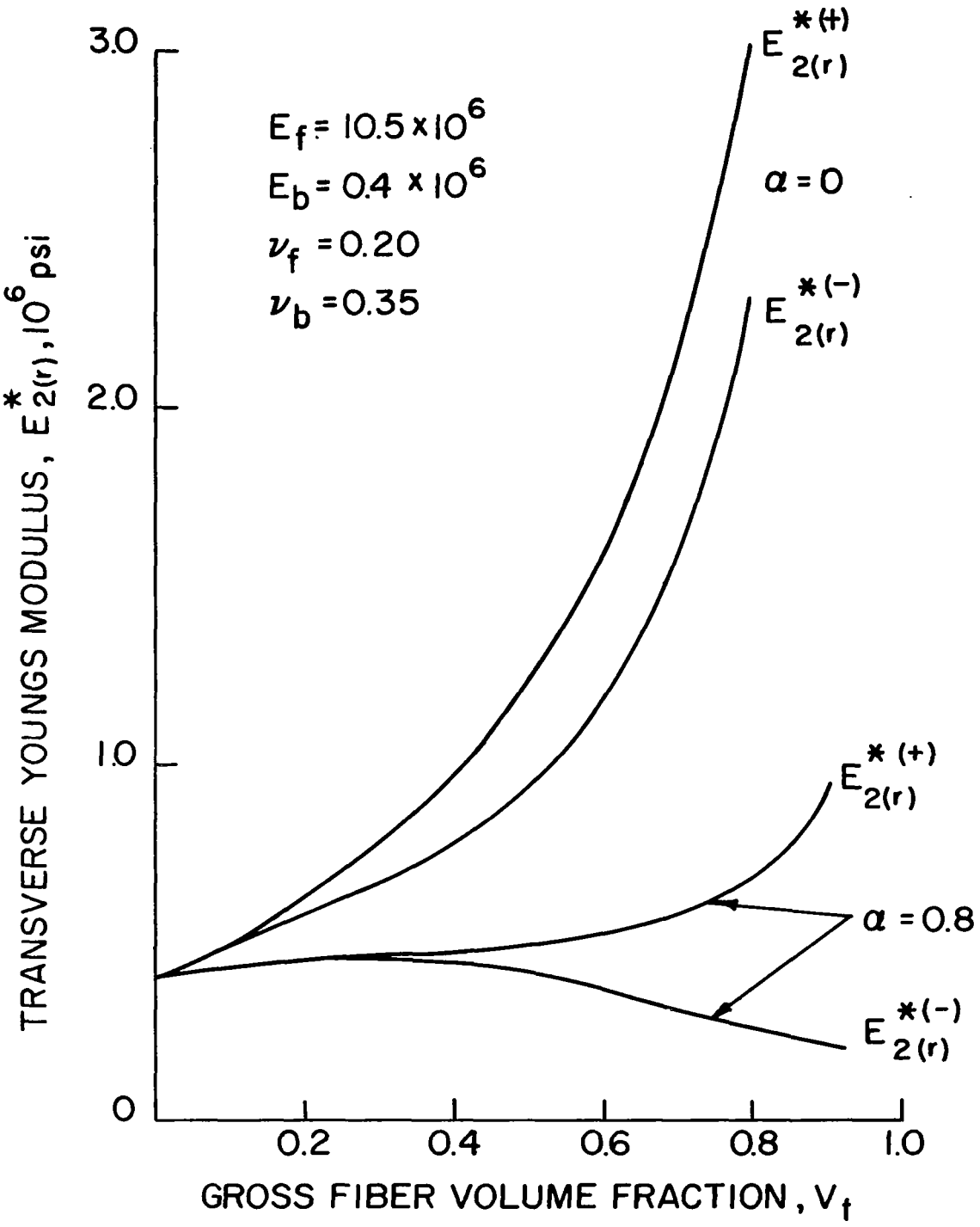


Figure 1. Bounds on the Effective Trasnverse Youngs Modulus for Solid and Hollow Glass Fibers in an Epoxy Matrix. (Parallel fibers, random array)

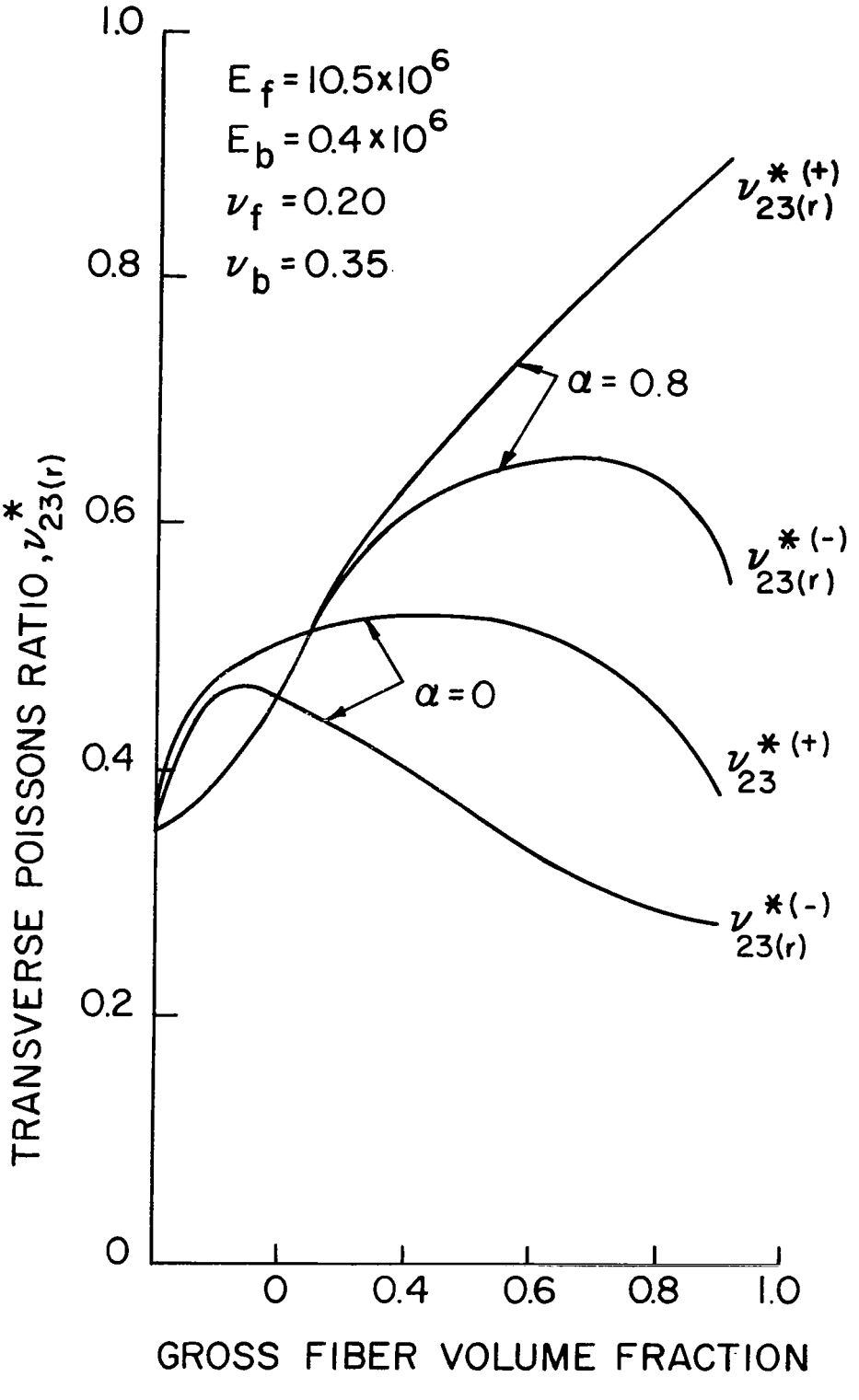


Figure 2. Bounds on the Effective Transverse Poissons Ratio for Solid and Hollow Glass Fibers in a Plastic Matrix (parallel fibers, random array).

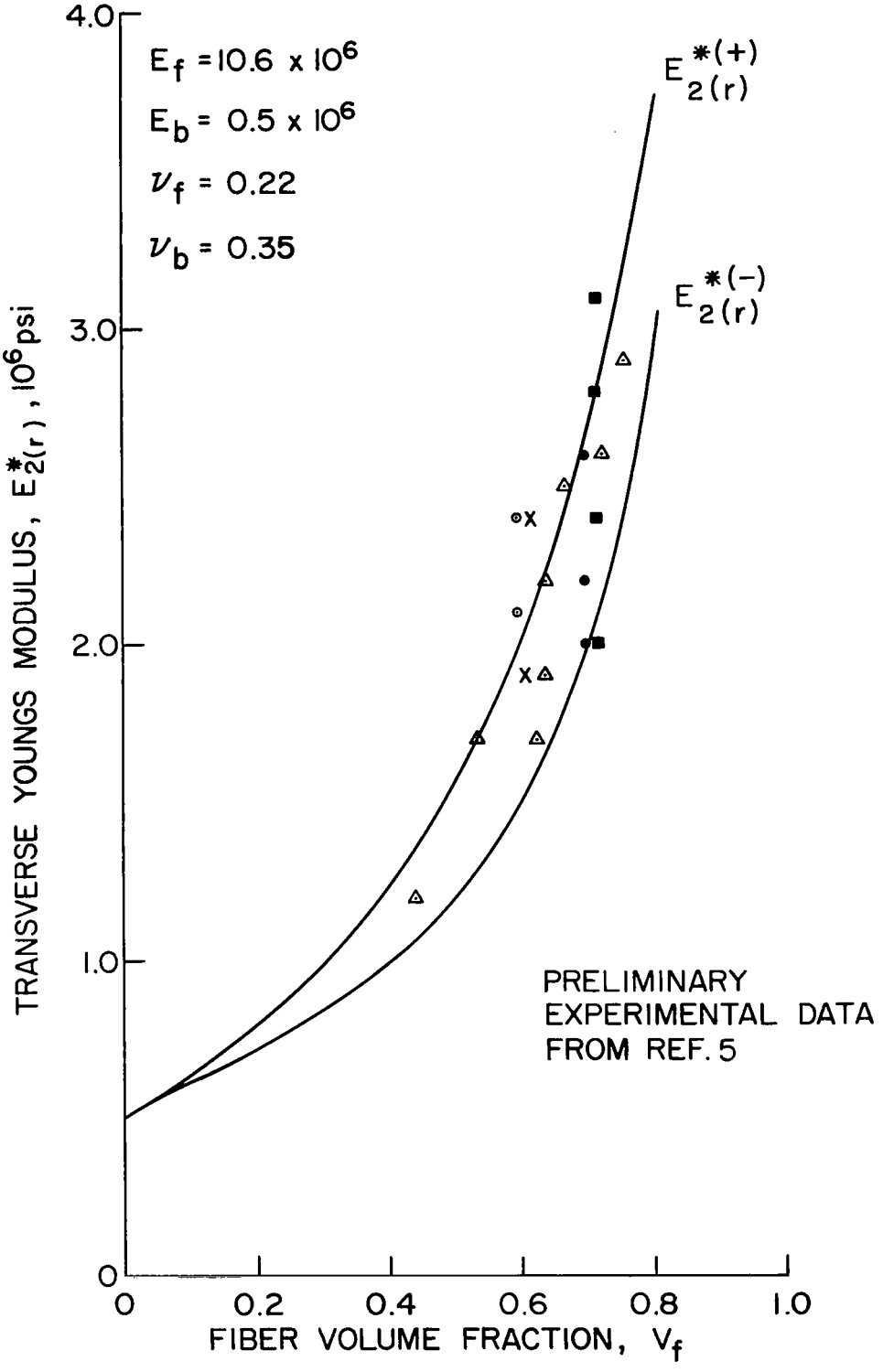


Figure 3. Comparison of Theoretical and Experimental Results for Transverse Youngs Modulus.

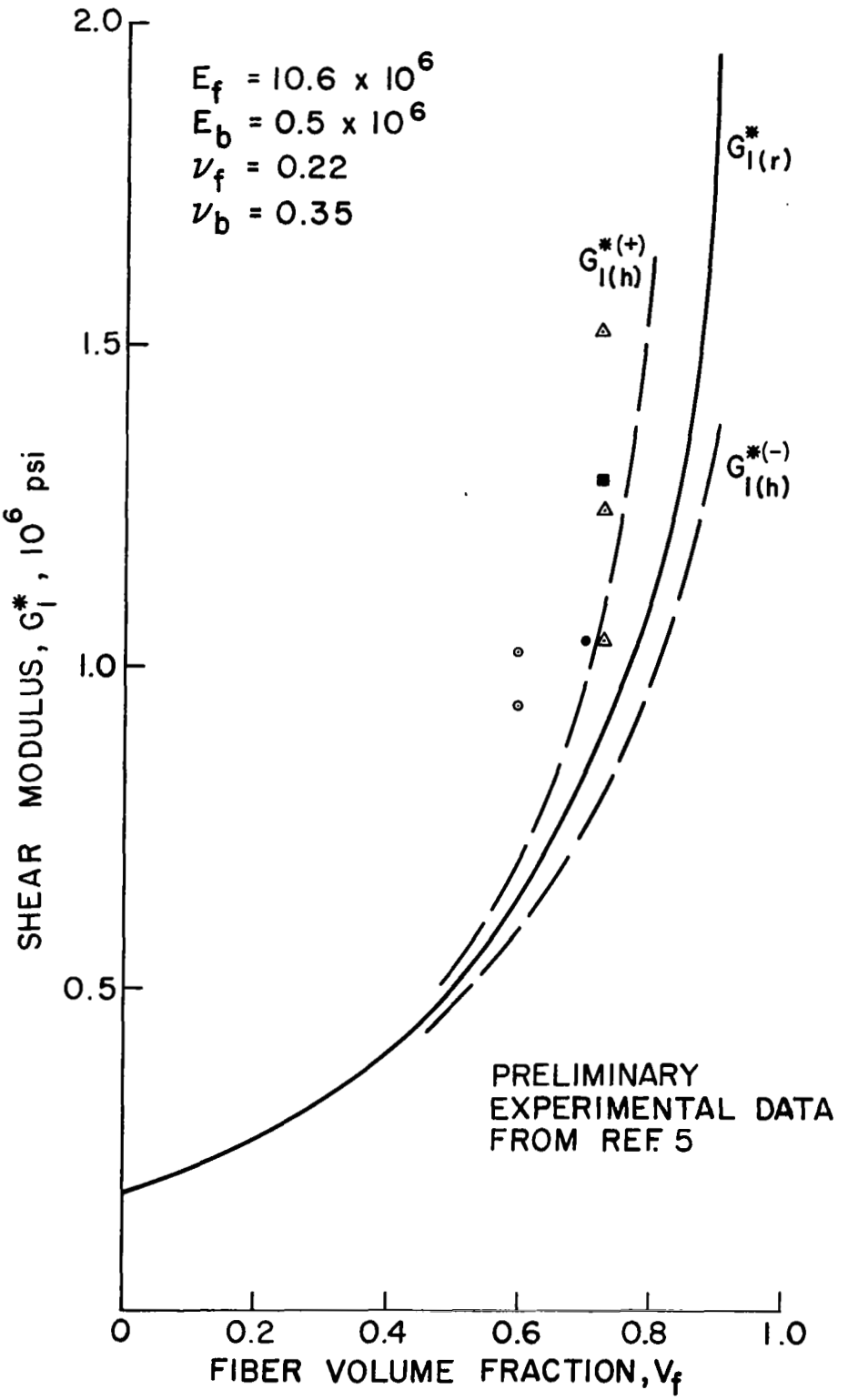


Figure 4. Comparison of Theoretical and Experimental Results For Shear Modulus in the Plane of the Fibers.

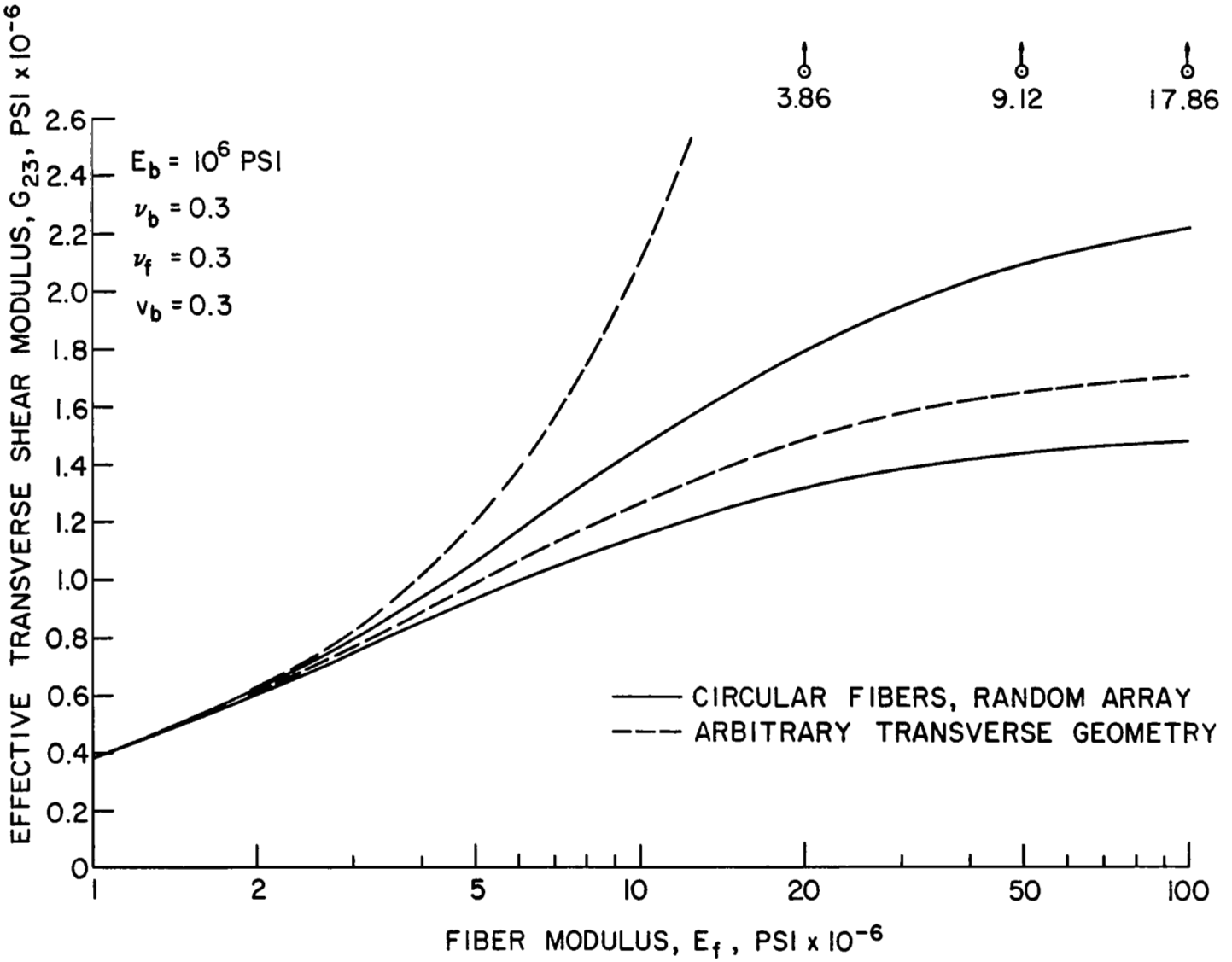


Figure 5. Comparison of Effective Transverse Shear Modulus Bounds Based on Arbitrary Transverse Geometry with the Bounds for a Random Array.

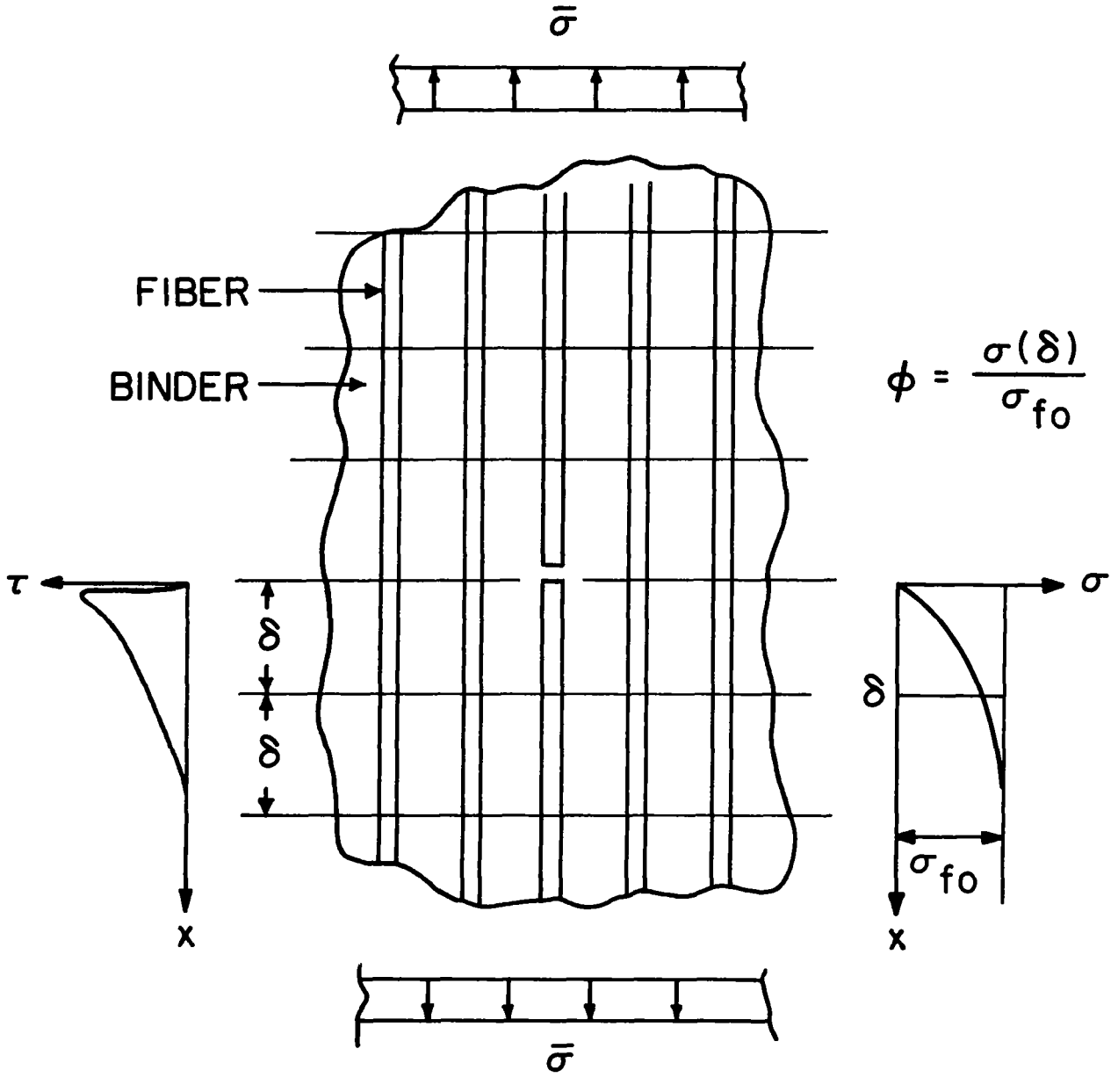


Figure 6. Fiber Reinforced Composite - Tensile Failure Model.

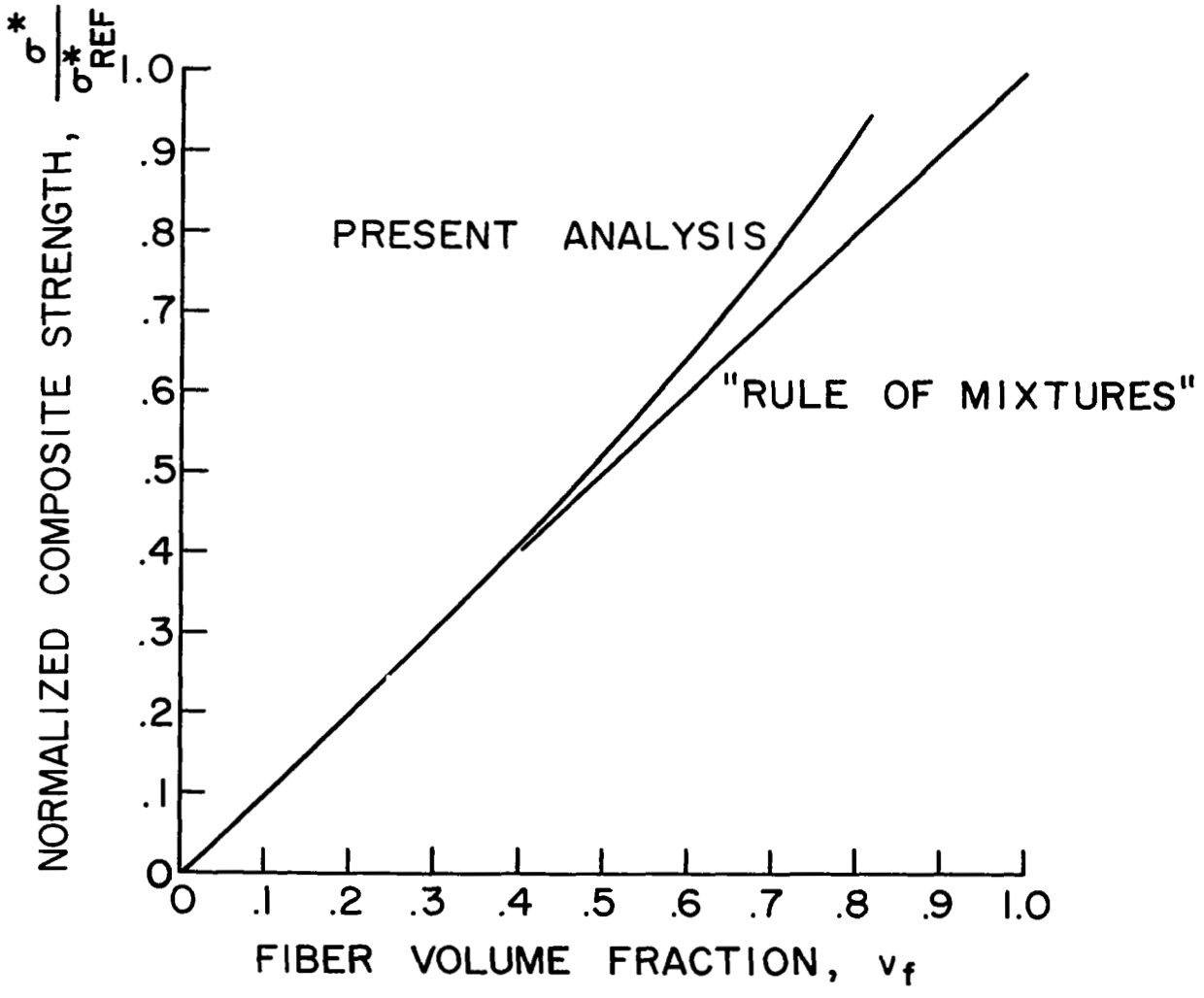


Figure 7. Variation of Composite Tensile Strength with Fiber Volume Fraction for Statistical Failure Model and for "Rule of Mixtures Model.

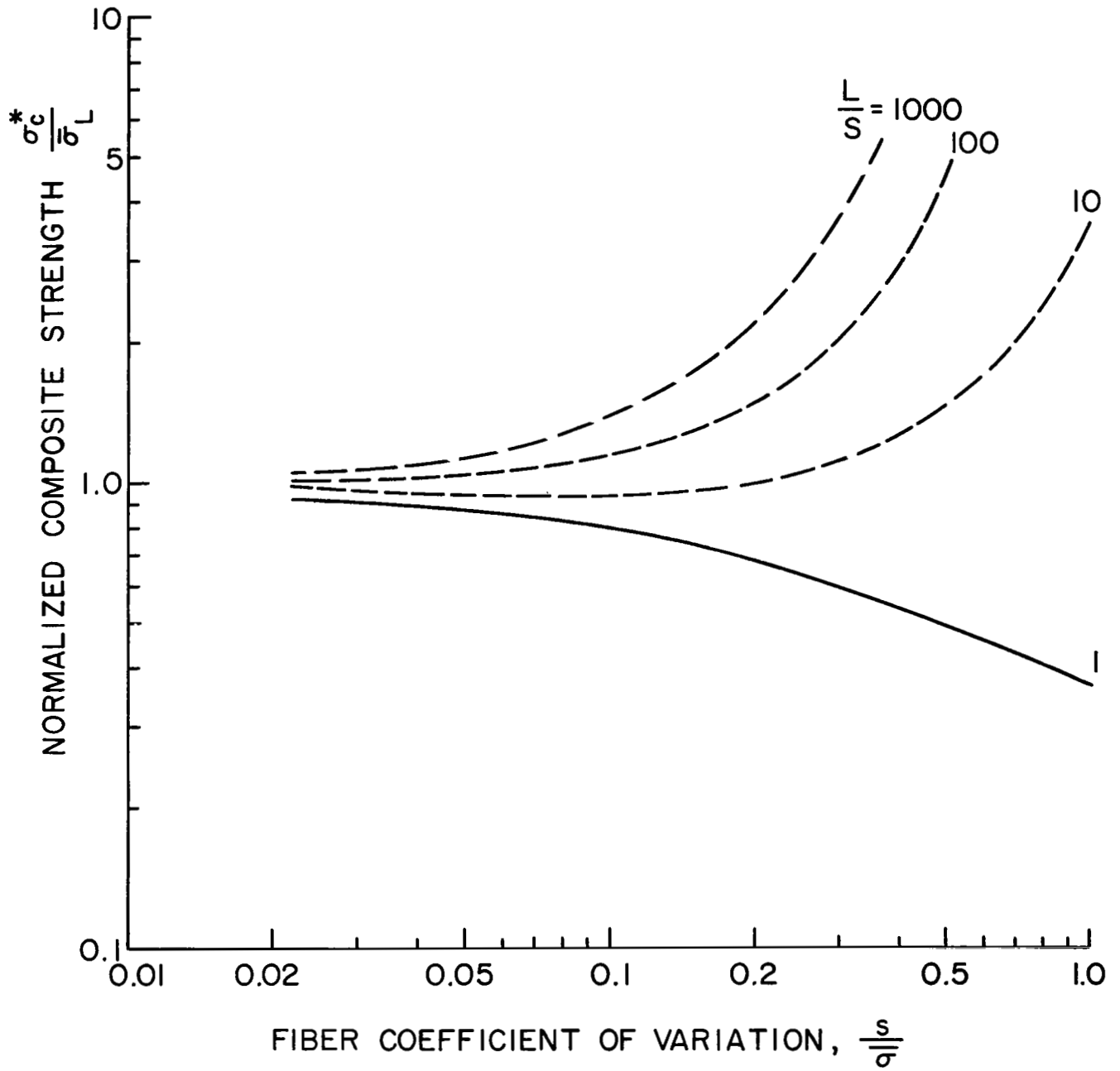


Figure 8. Effect of Fiber Coefficient of Variation and Reference Fiber Strength Upon the Ratio of Composite Tensile Strength (the statistical mode) to Mean Fiber Strength.

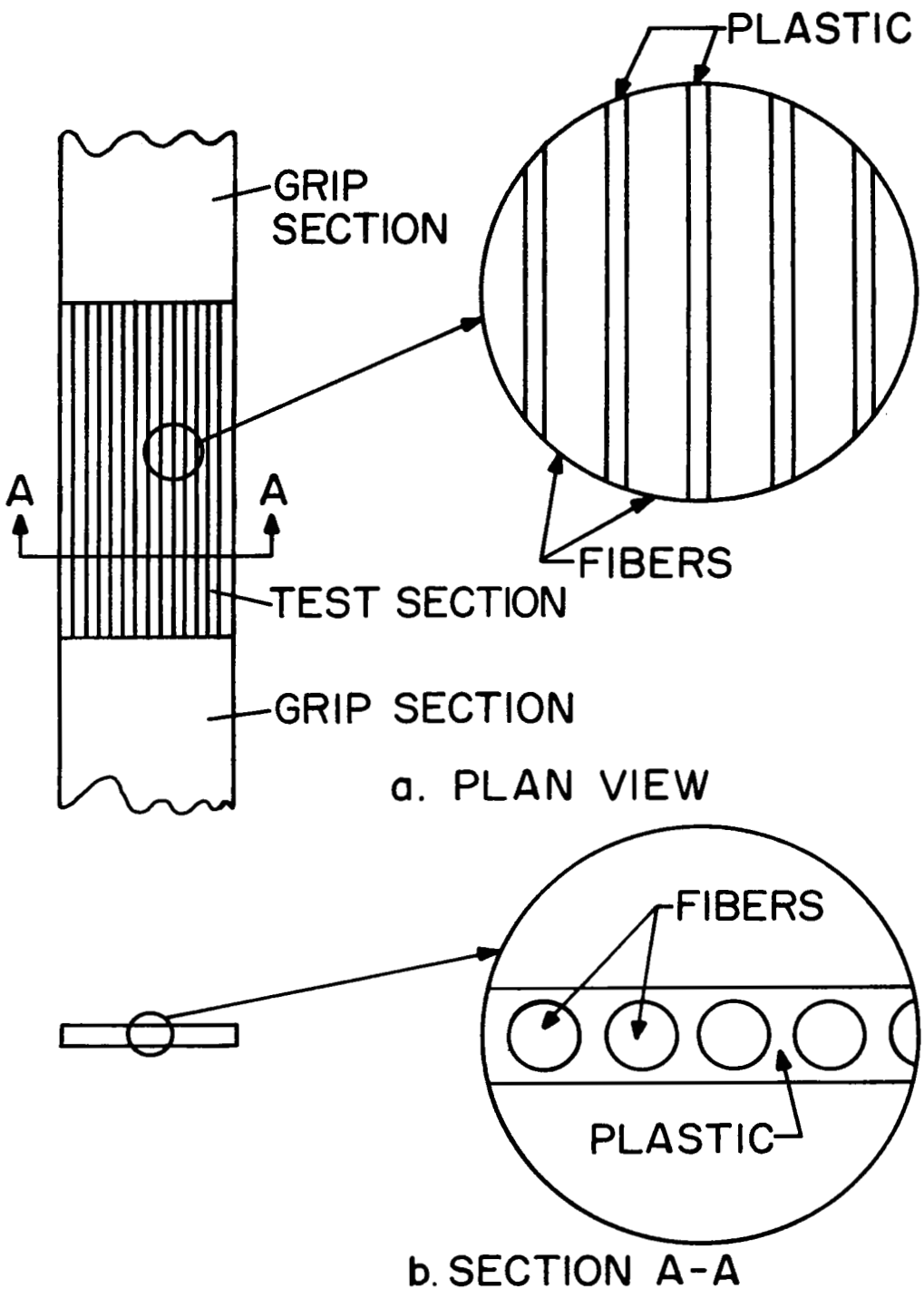


Figure 9. Experimental Tensile Failure Specimen.

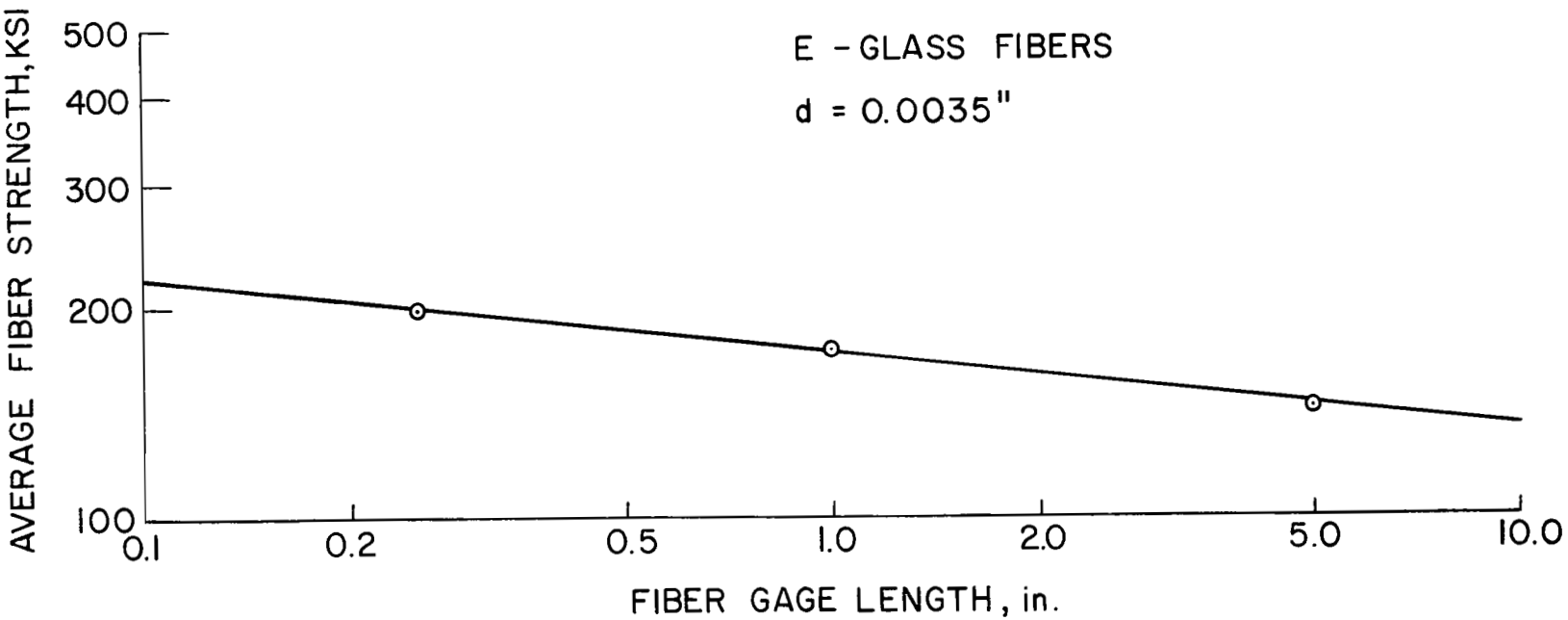


Figure 10. Effect of Length on Mean Fiber Strength.

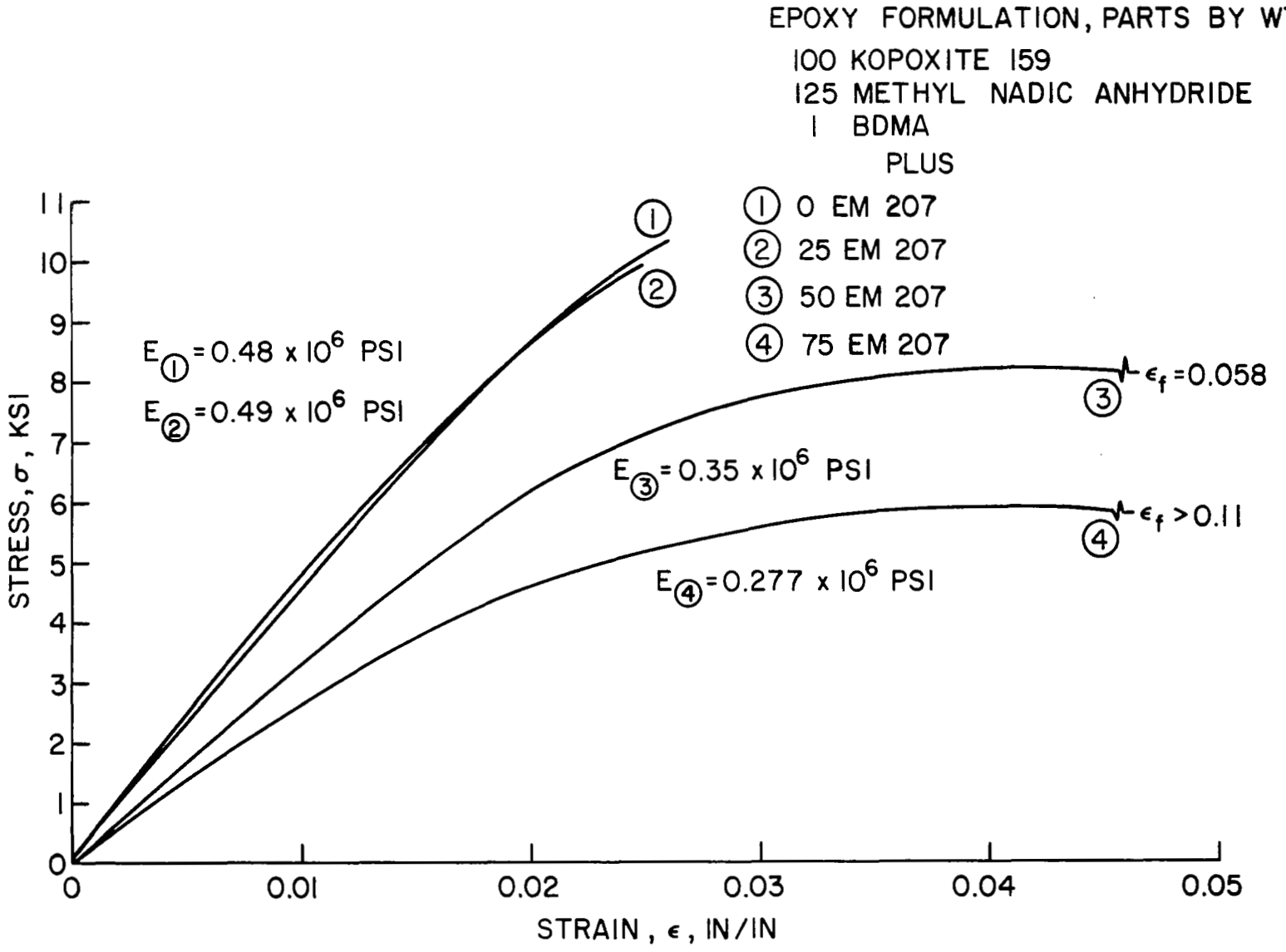


Figure 11. Experimental Stress-Strain Curves for a Series of Epoxy Materials.

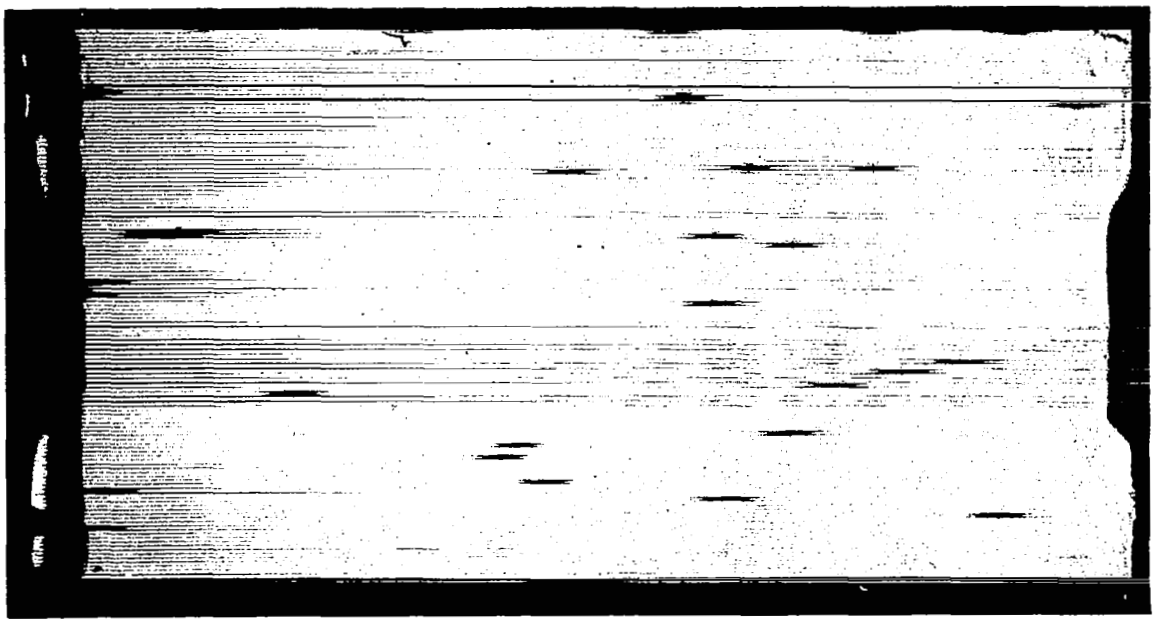

a. Matrix Modulus = $0.48 \times 10^6$ psi

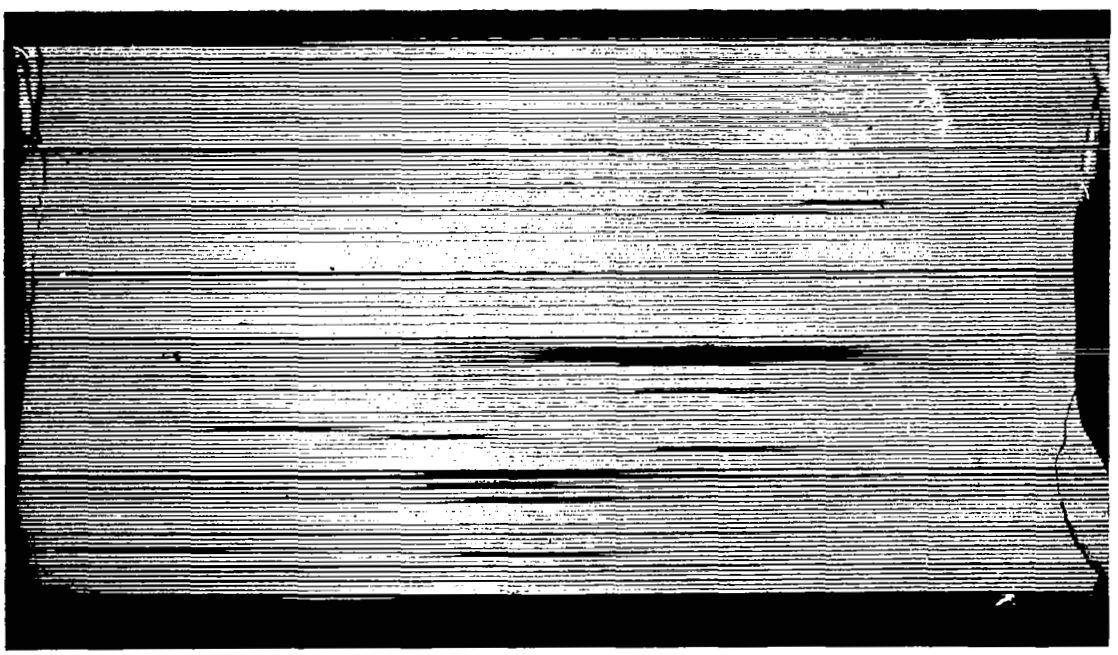

b. Matrix Modulus = $0.28 \times 10^6$ psi

Figure 12. Typical View of Tensile Failure Specimen of 99% of Ultimate Strength. Fibers are 0.0035" Diameter E-glass.

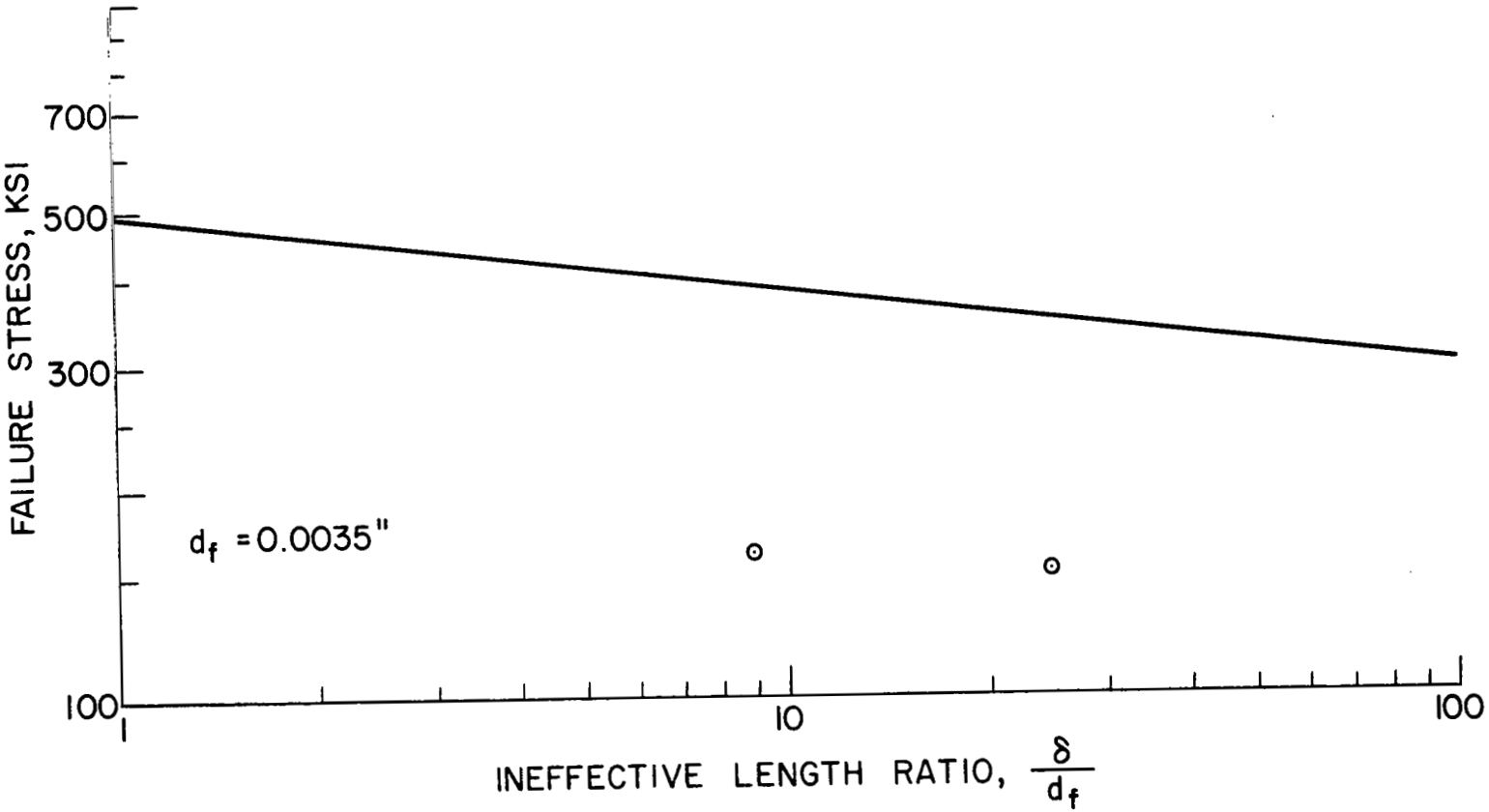


Figure 13. Composite Tensile Strength as a Function of the Fiber Ineffective Length.

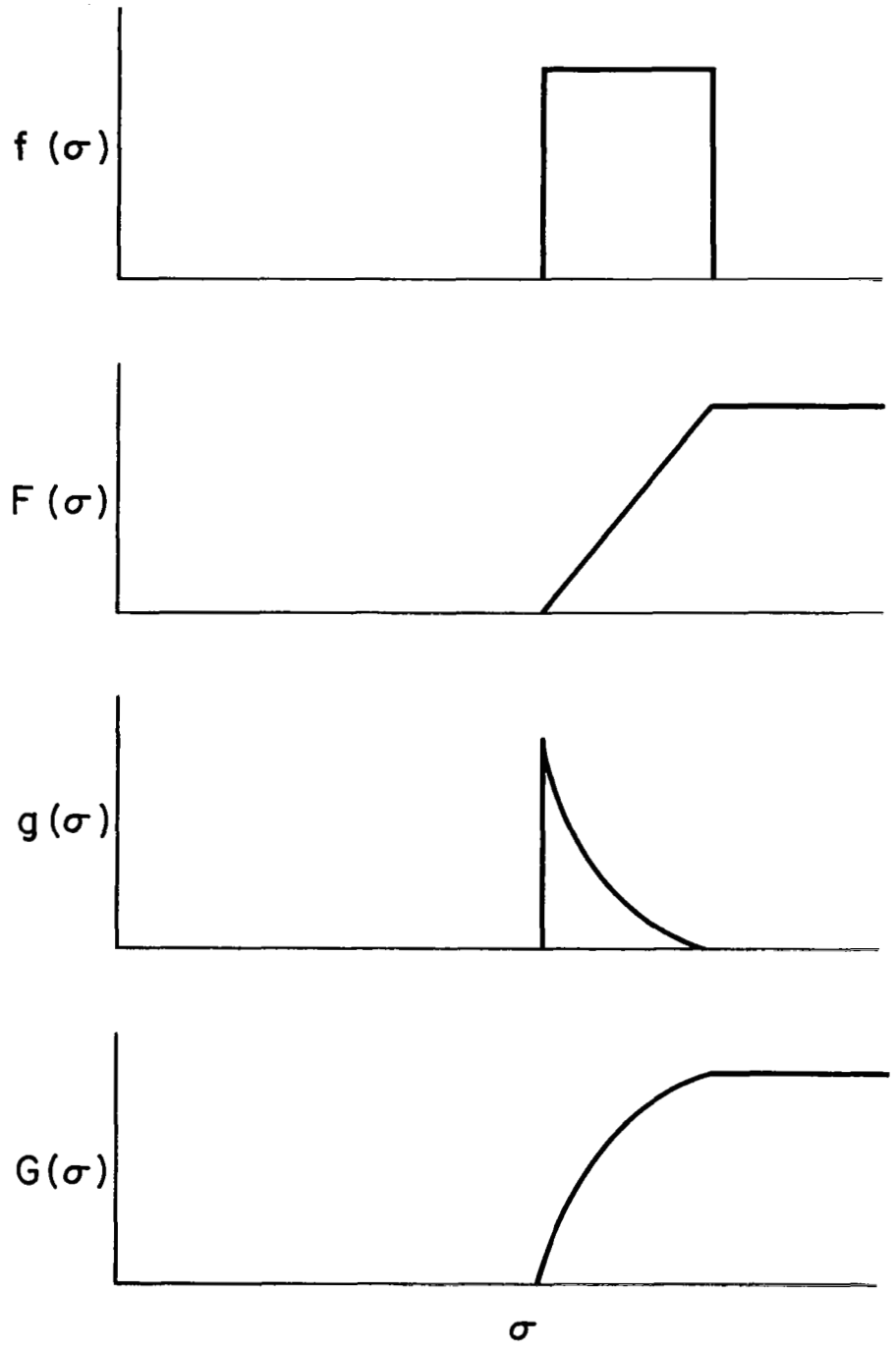


Figure 14. Rectangular Strength Distribution Function for the Links of a Chain.
a. Link Distribution Function
b. Link Cumulative Distribution Function
c. Chain or Fiber Distribution Function
d. Chain or Fiber Cumulative Distribution Function.

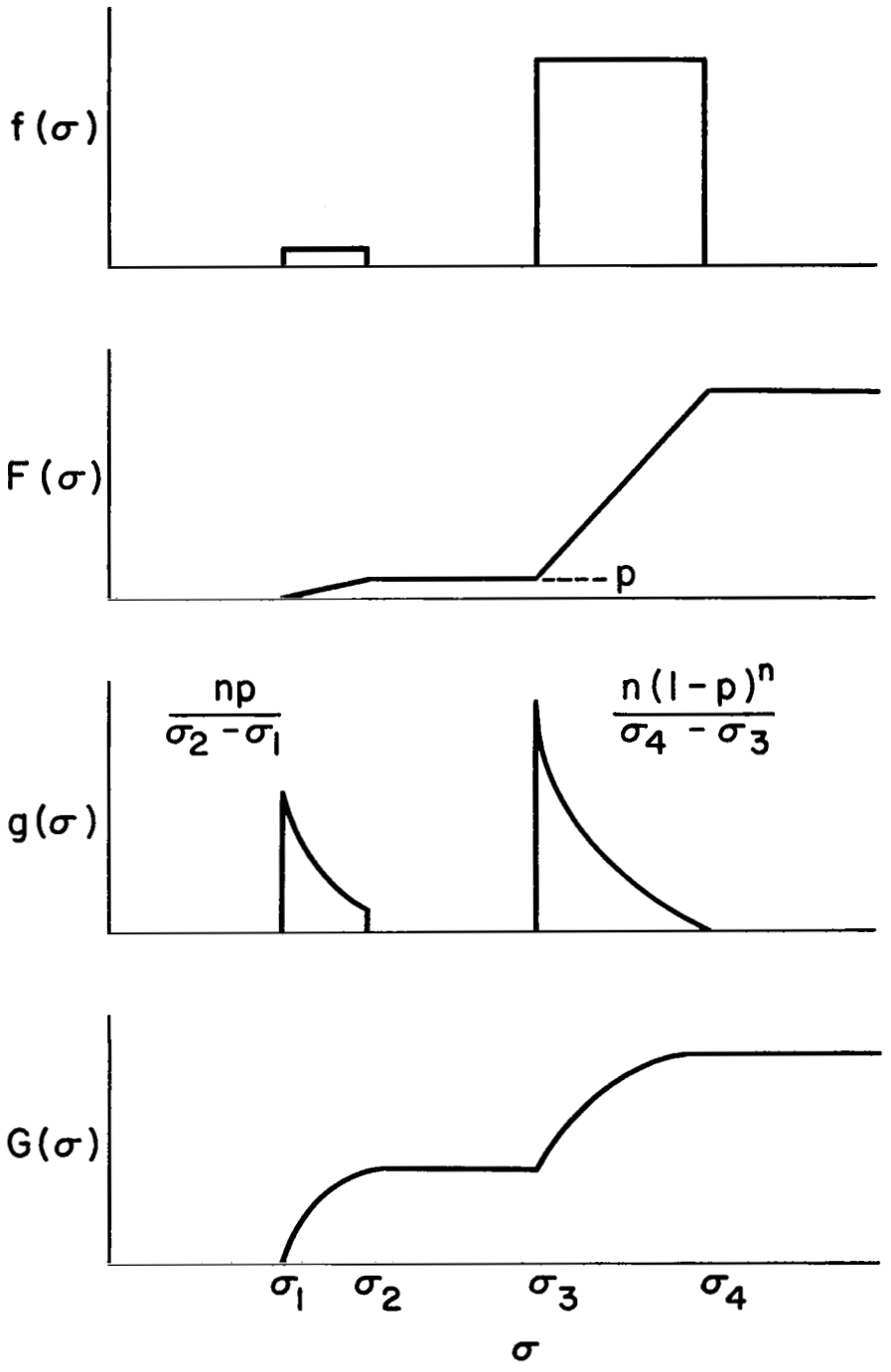


Figure 15. Double Rectangular Strength Distribution Function for the Links of a Chain

a. Link Distribution Function
b. Link Cumulative Distribution Function
c. Chain or Fiber Distribution Function
d. Chain or Fiber Cumulative Distribution Function.

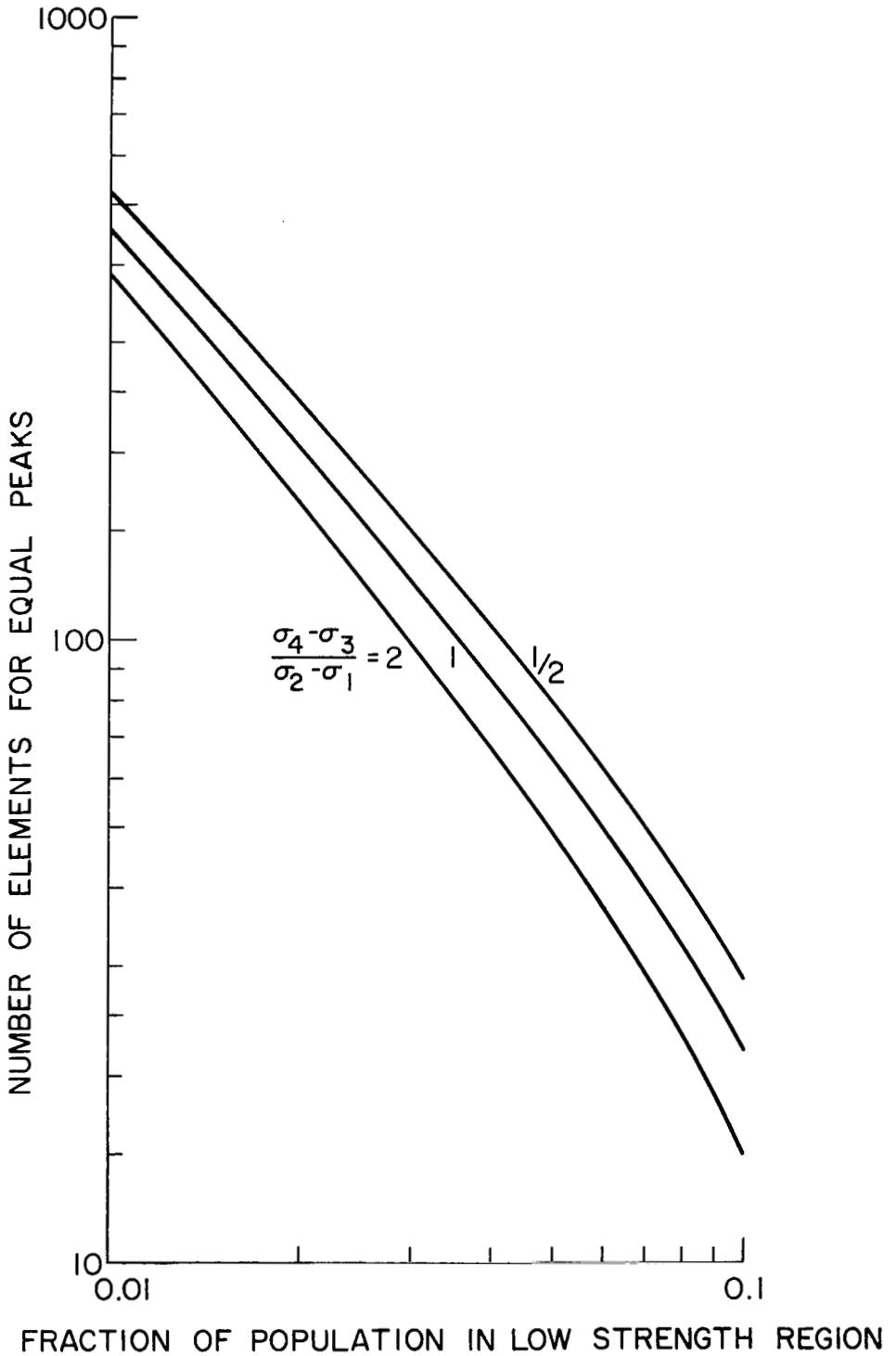


Figure 16. Number of Links in the Chain to Equate the Peaks of the Distribution Function Shown in Figure 15.

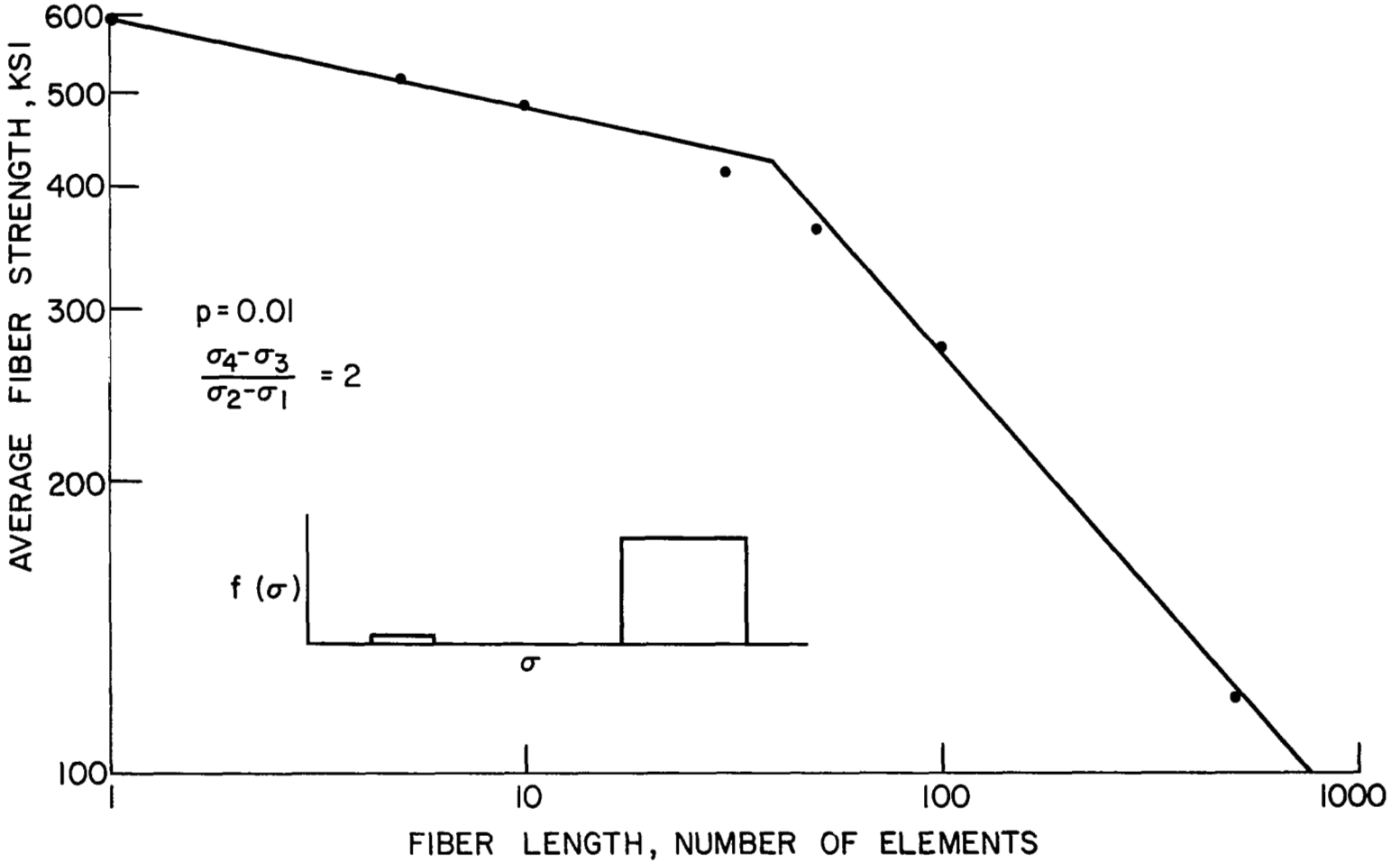


Figure 17. Mean Fiber Strength as a Function of Length for Fiber Links Having a Double Rectangular Strength Distribution Function.

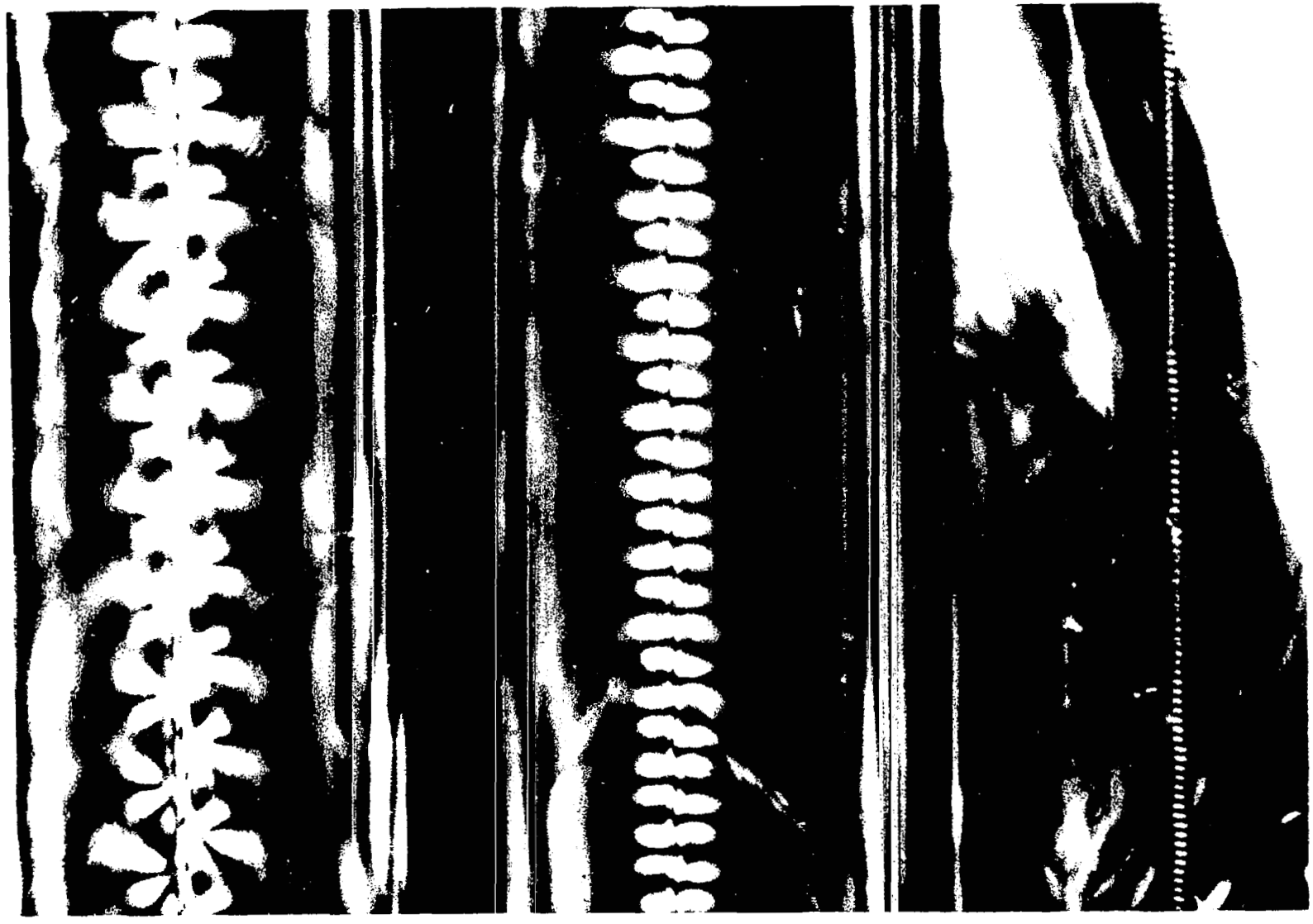

Figure 18. Photoelastic Stress Pattern for Three Individual E-Glass Fibers Imbedded in an Epoxy Matrix Showing Small Wavelength Buckle Patterns.

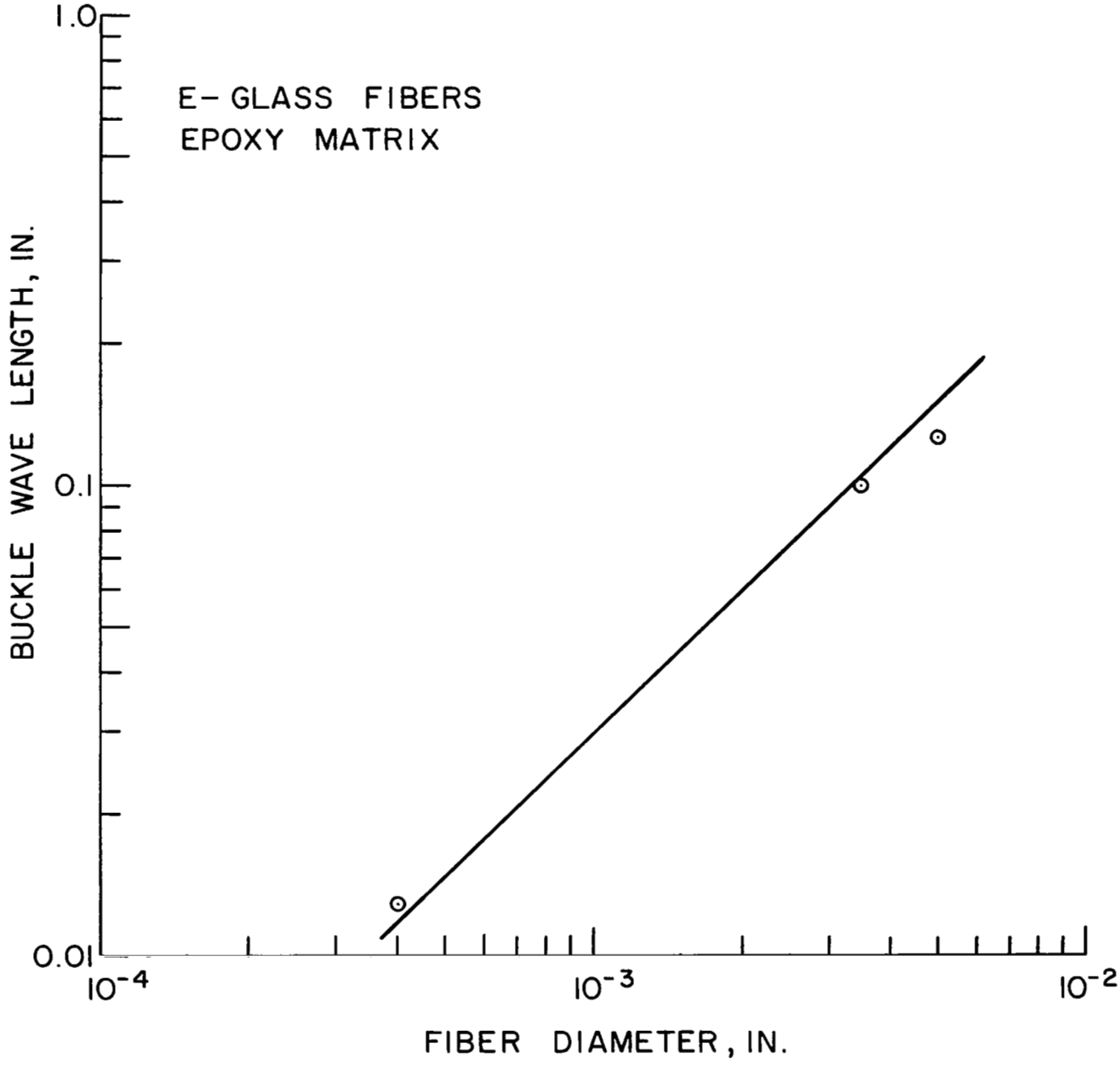


Figure 19. Experimental Results for Fiber Buckling Wavelength as a Function of Fiber Diameter.

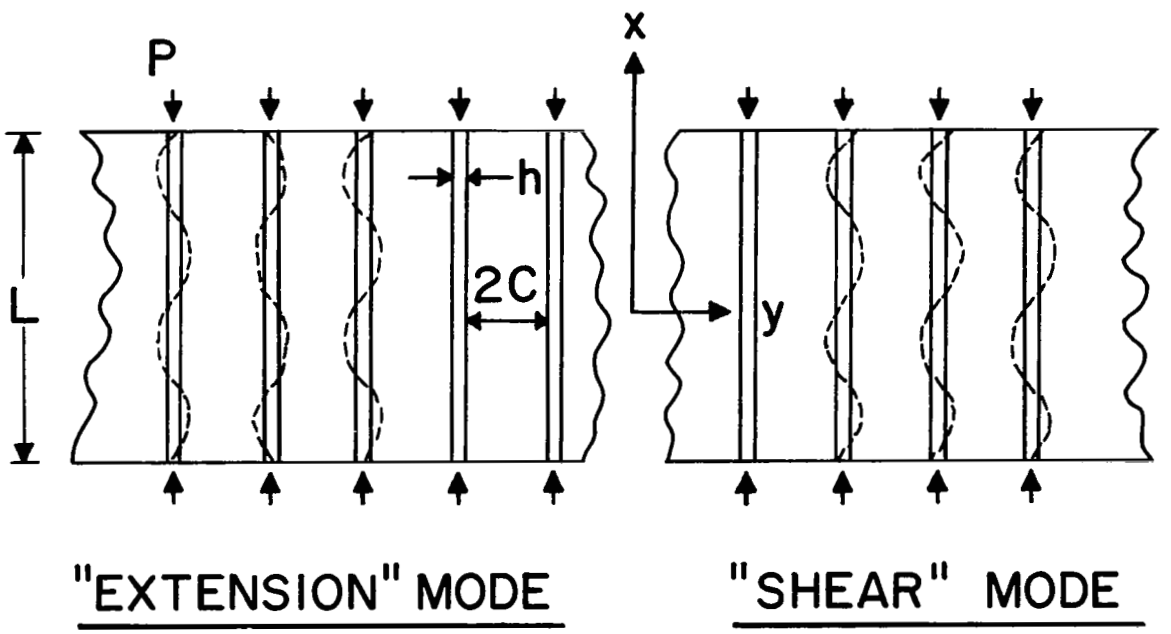


$$\Delta V_f + \Delta V_b - \Delta T = 0$$

$$P = \sigma_f h$$

$$V = \sum_n a_n \sin \frac{n \pi x}{L}$$

Figure 20. Analytical Model for Compressive Strength of Fibrous Composite.

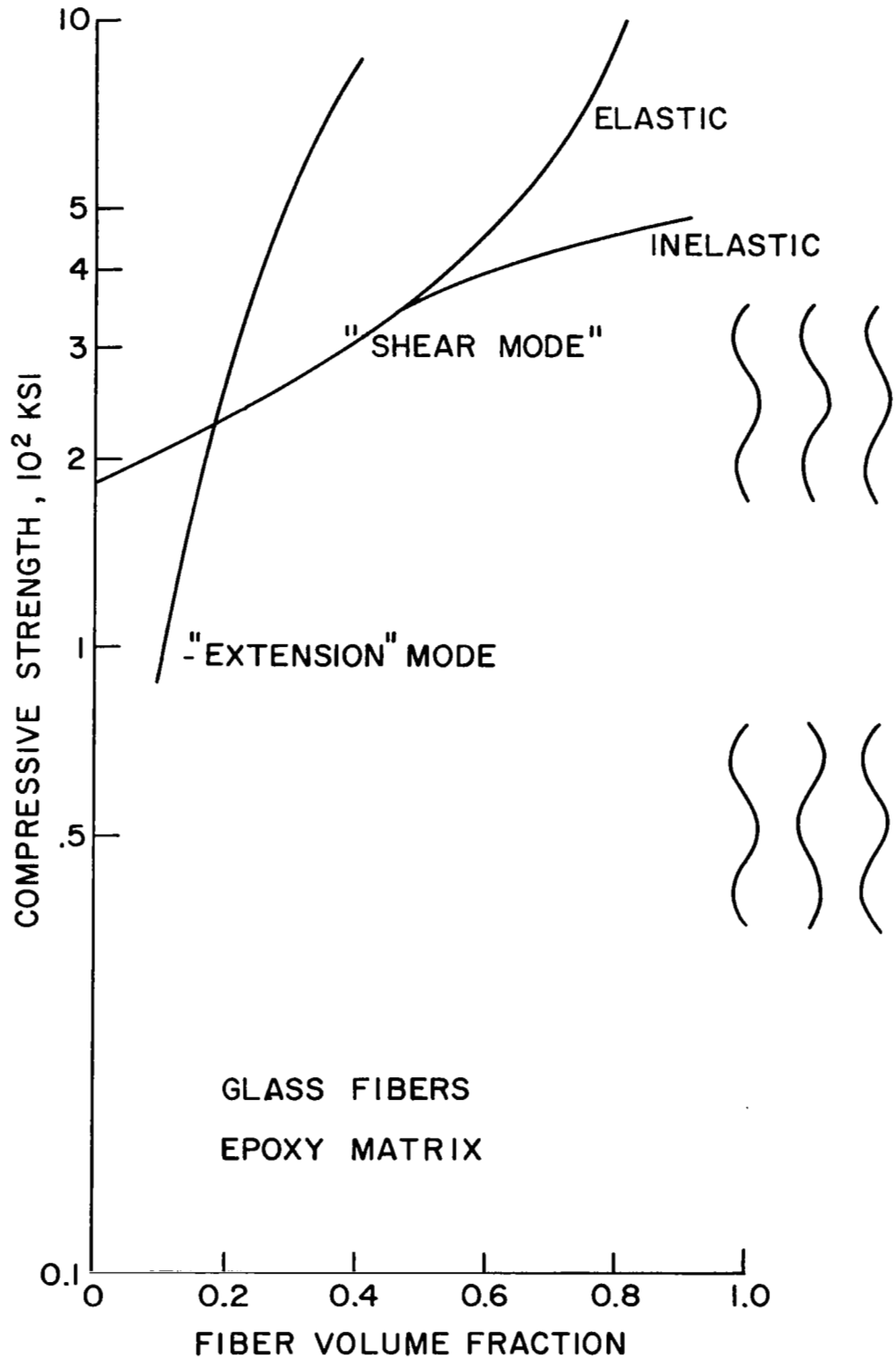


Figure 21. Compressive Strength of Glass Reinforced Epoxy Composites.

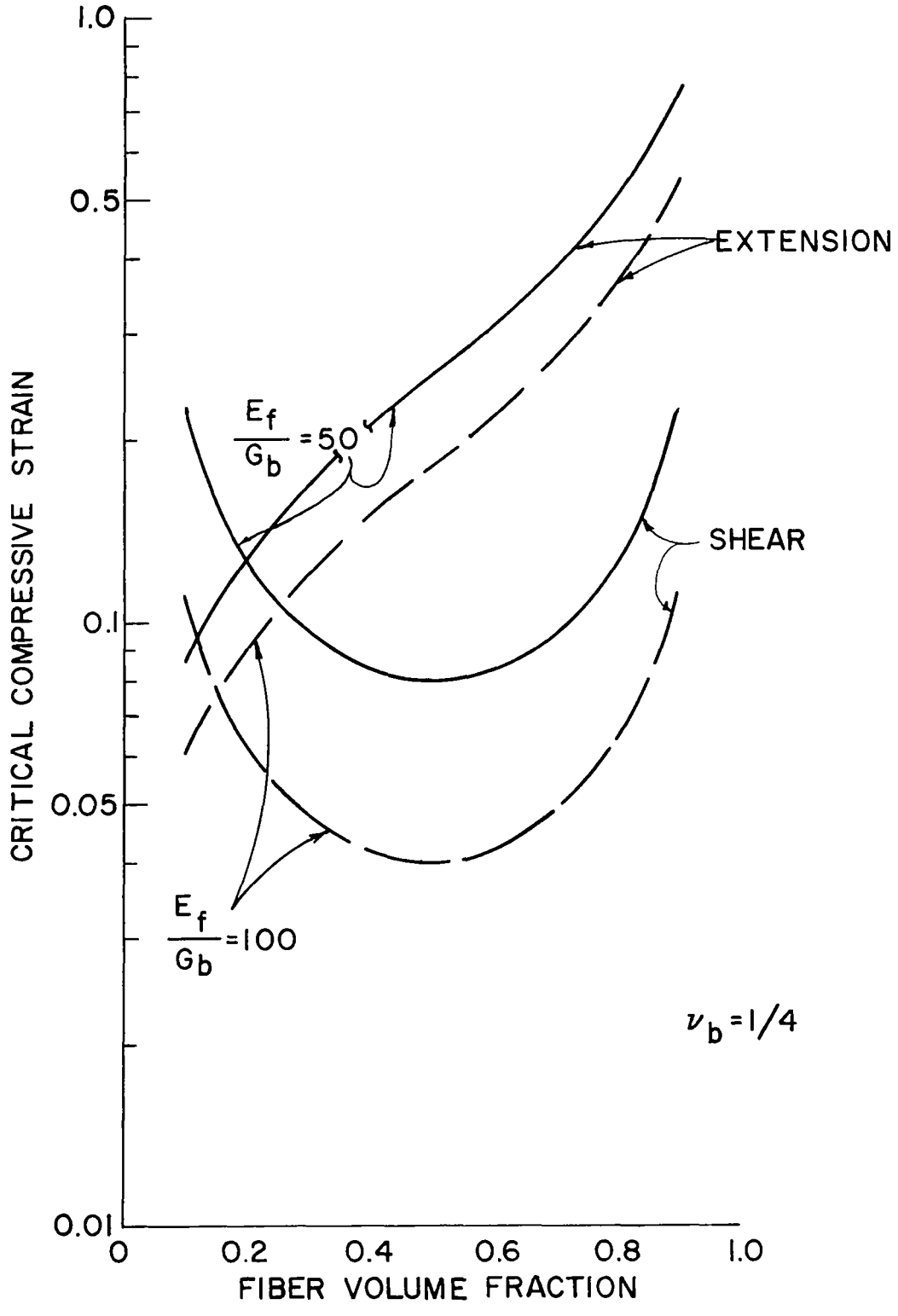


Figure 22. Critical Compressive Strain for Fibrous Composites.

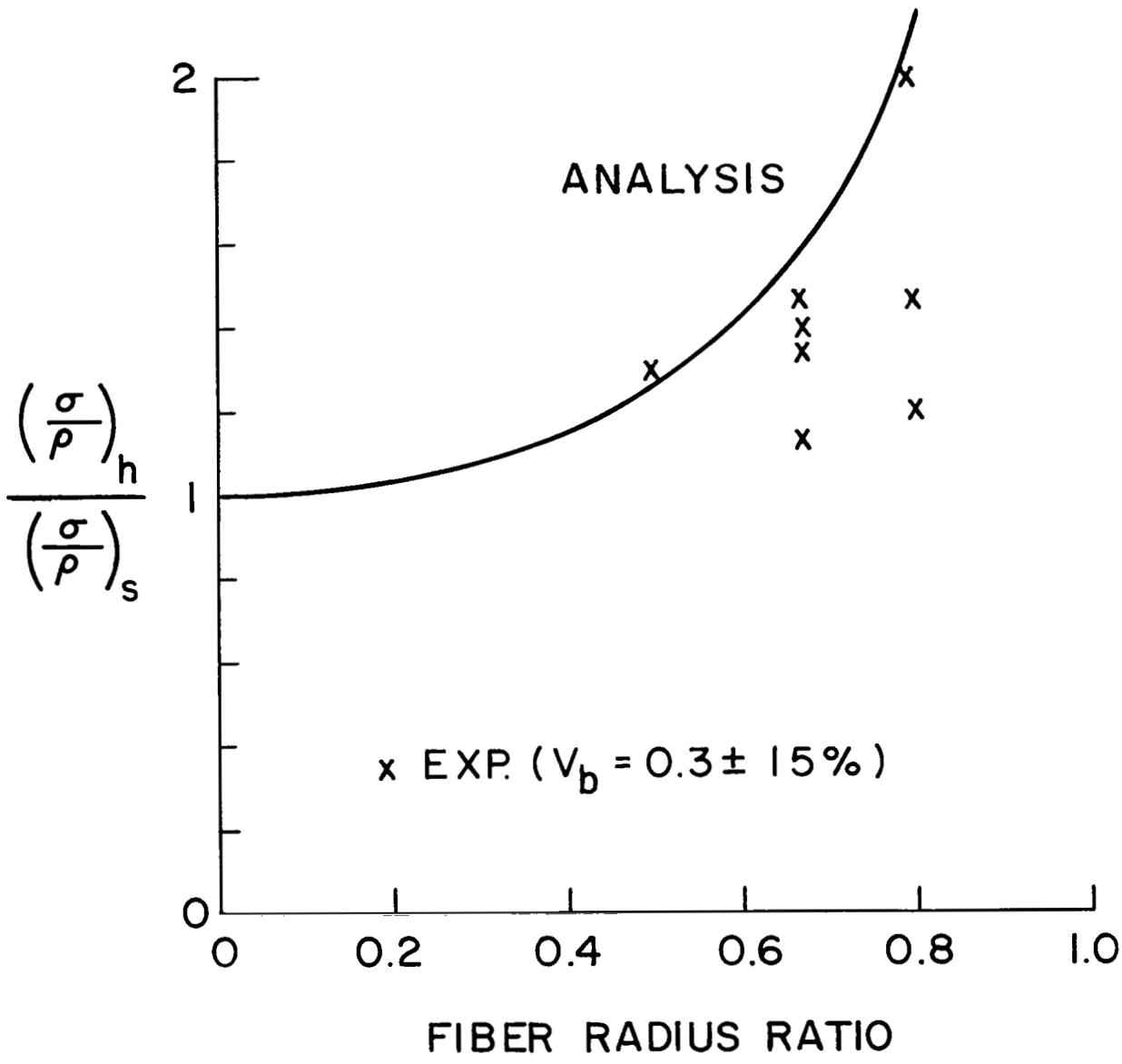


Figure 23. Comparison of Theory and Experiment for Compressive Strength to Density Ratio of Hollow Glass Fiber Composites.

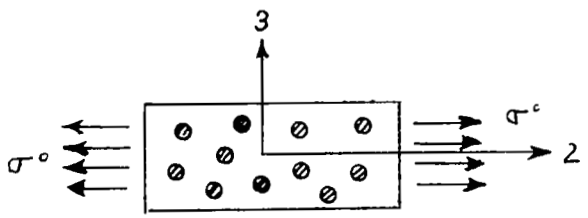


Figure 24a.

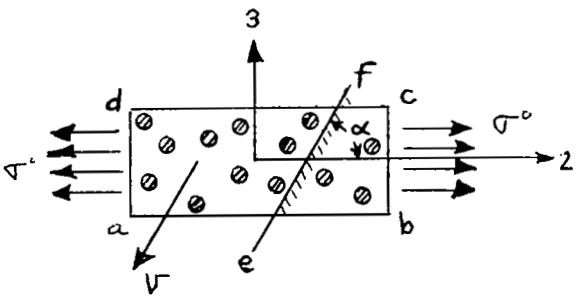


Figure 24b.

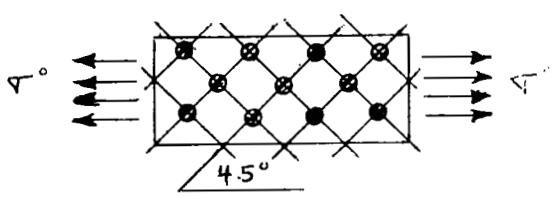


Figure 24c.

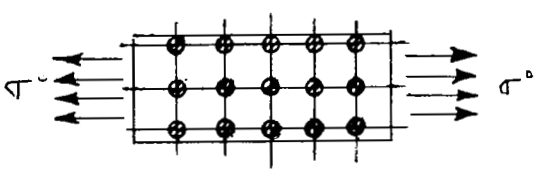

Figure 24d.

Figure 24. Geometries Considered for Limit Analysis of Transverse Strength.

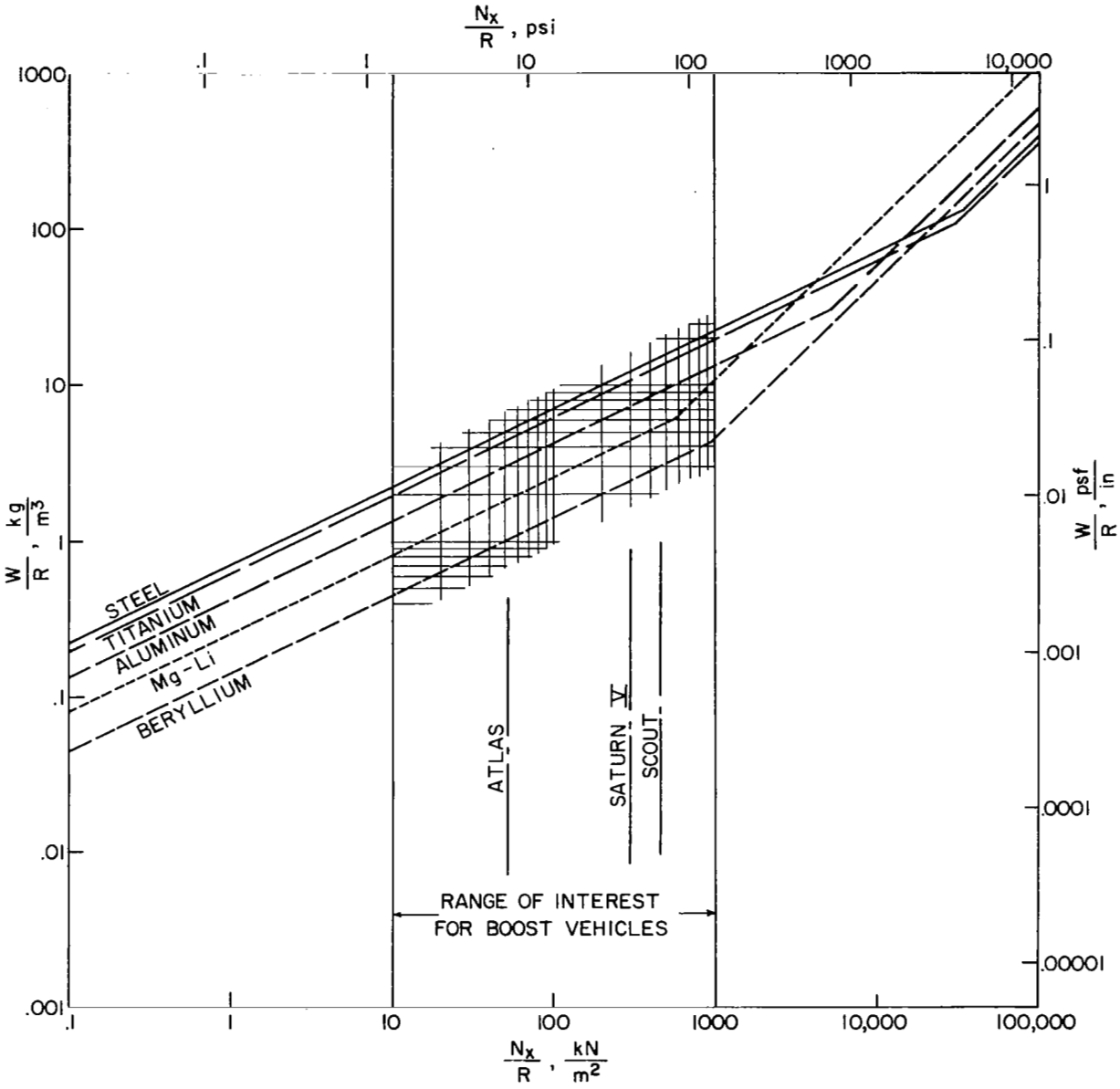


Figure 25. Reference Weight-Efficiencies (weight per unit surface area per unit shell radius) of Idealized, Metal Monocoque Cylindrical Shells for Various Intensities of Axial Compression Loading, and Definition of Loading Range of Interest for Boost Vehicles.

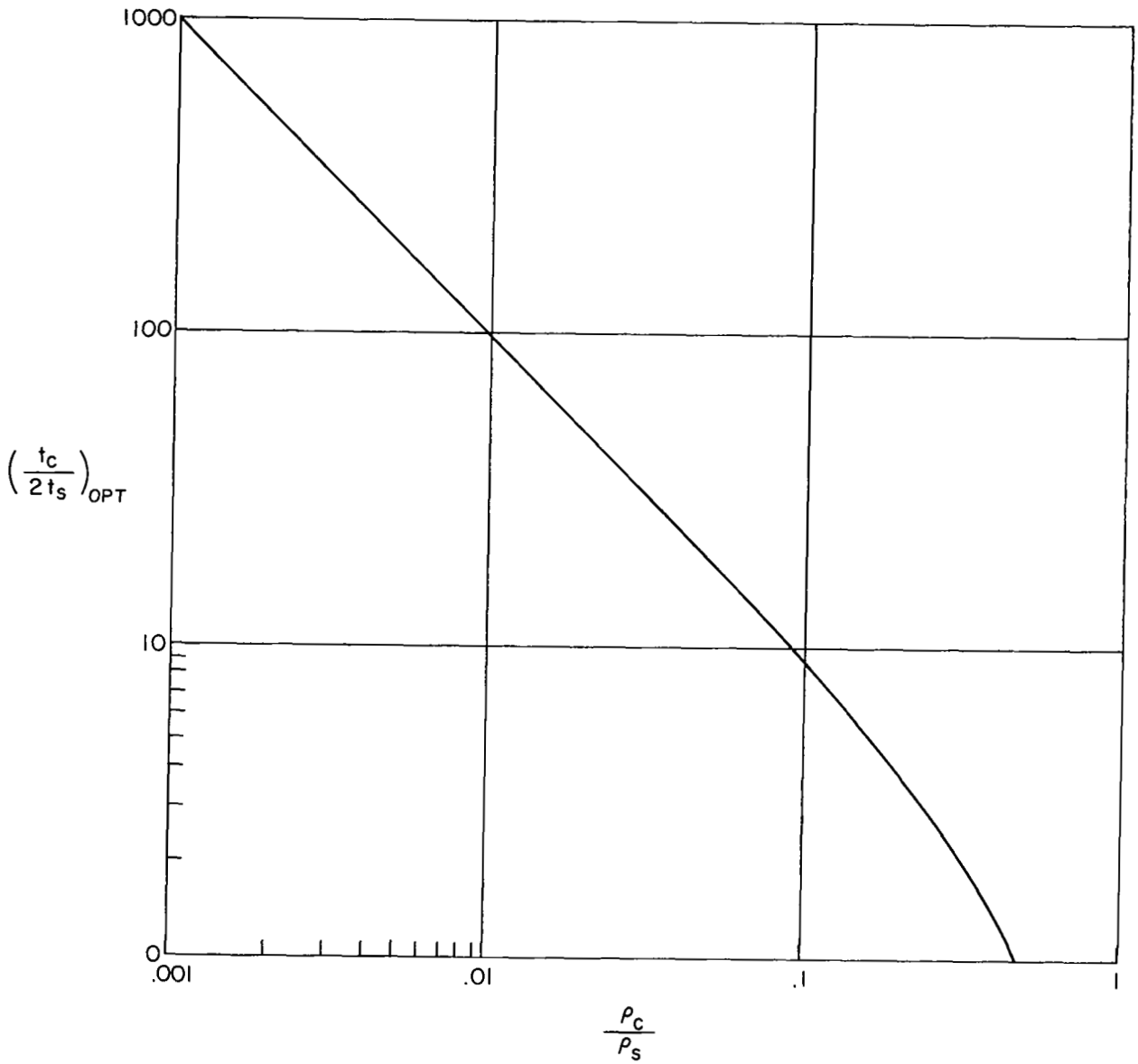


Figure 26. Optimum Ratios of Core Thickness to Face Thickness for Sandwich Shells of Various Core and Face Densities.

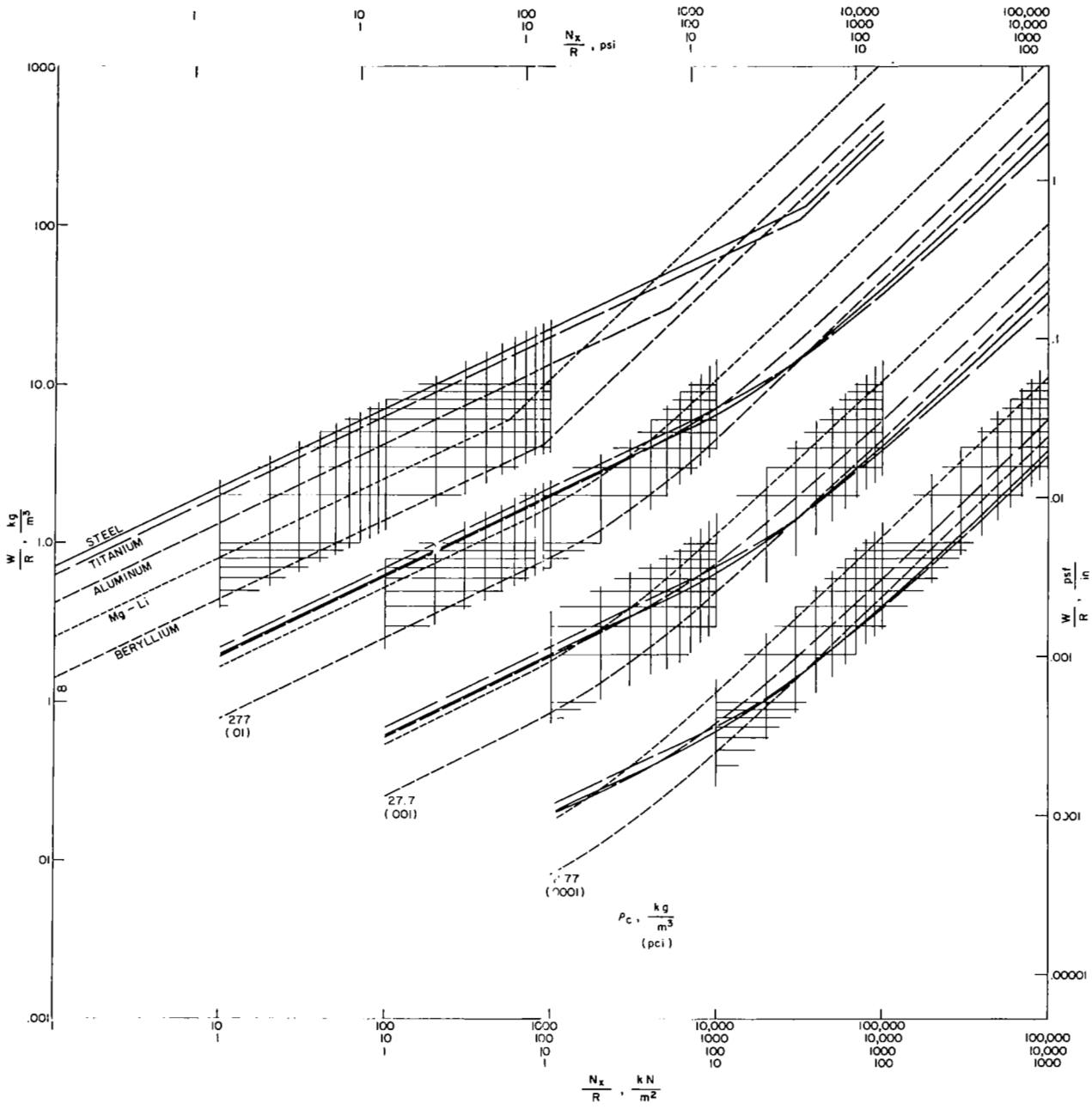


**Figure 27. Reference Weight-Efficiencies of Idealized, Metal-Faced Sandwich, Cylindrical Shells for Various Intensities of Axial Loading and Various Densities of Hypothetical, Ideal Core Material.**

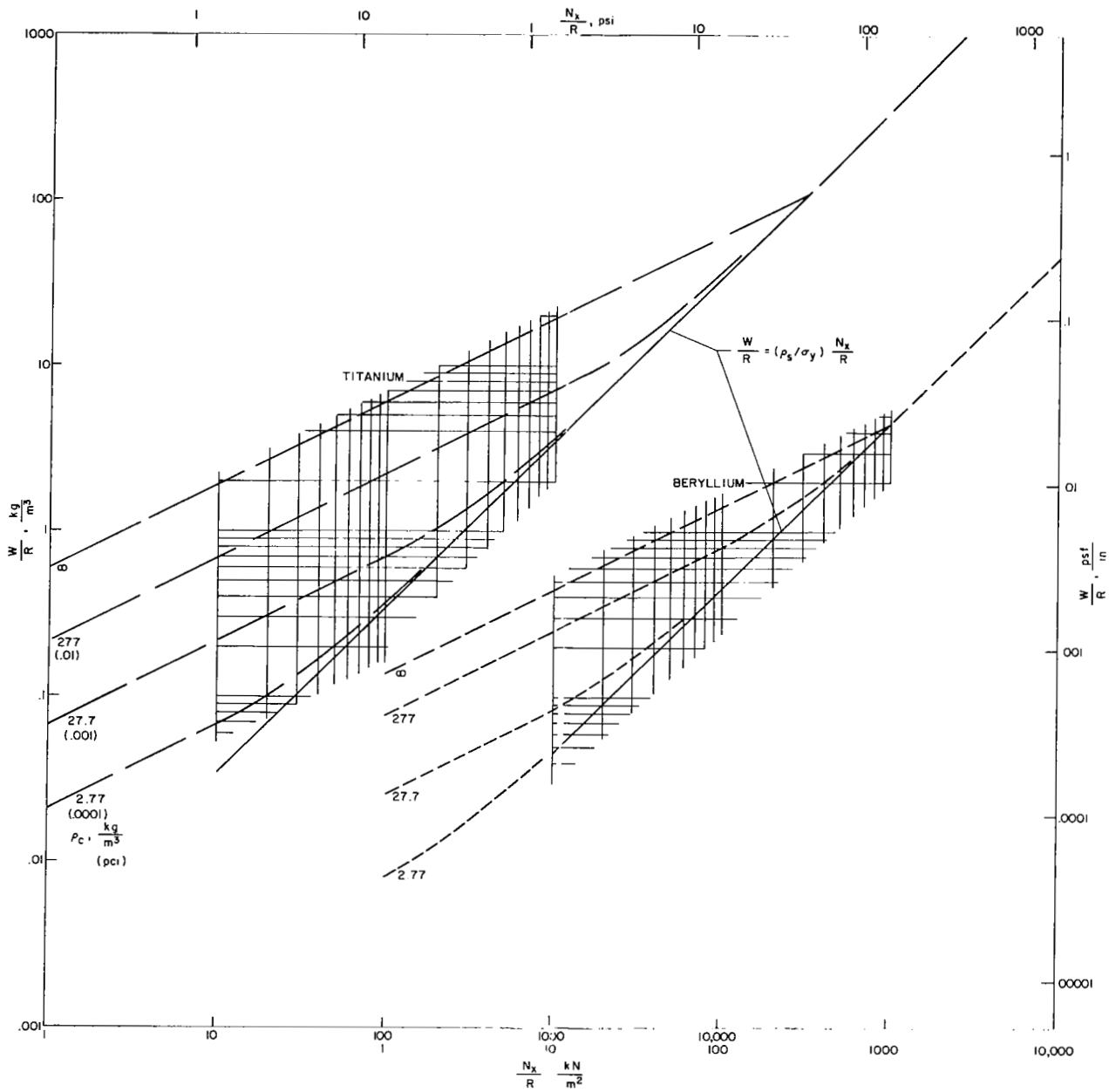


Figure 28. Reference Weight-Efficiencies for Best Metals for Idealized Sandwich Construction of Shells Loaded in Axial Compression in the Range of Interest for Boost-Vehicle Construction.

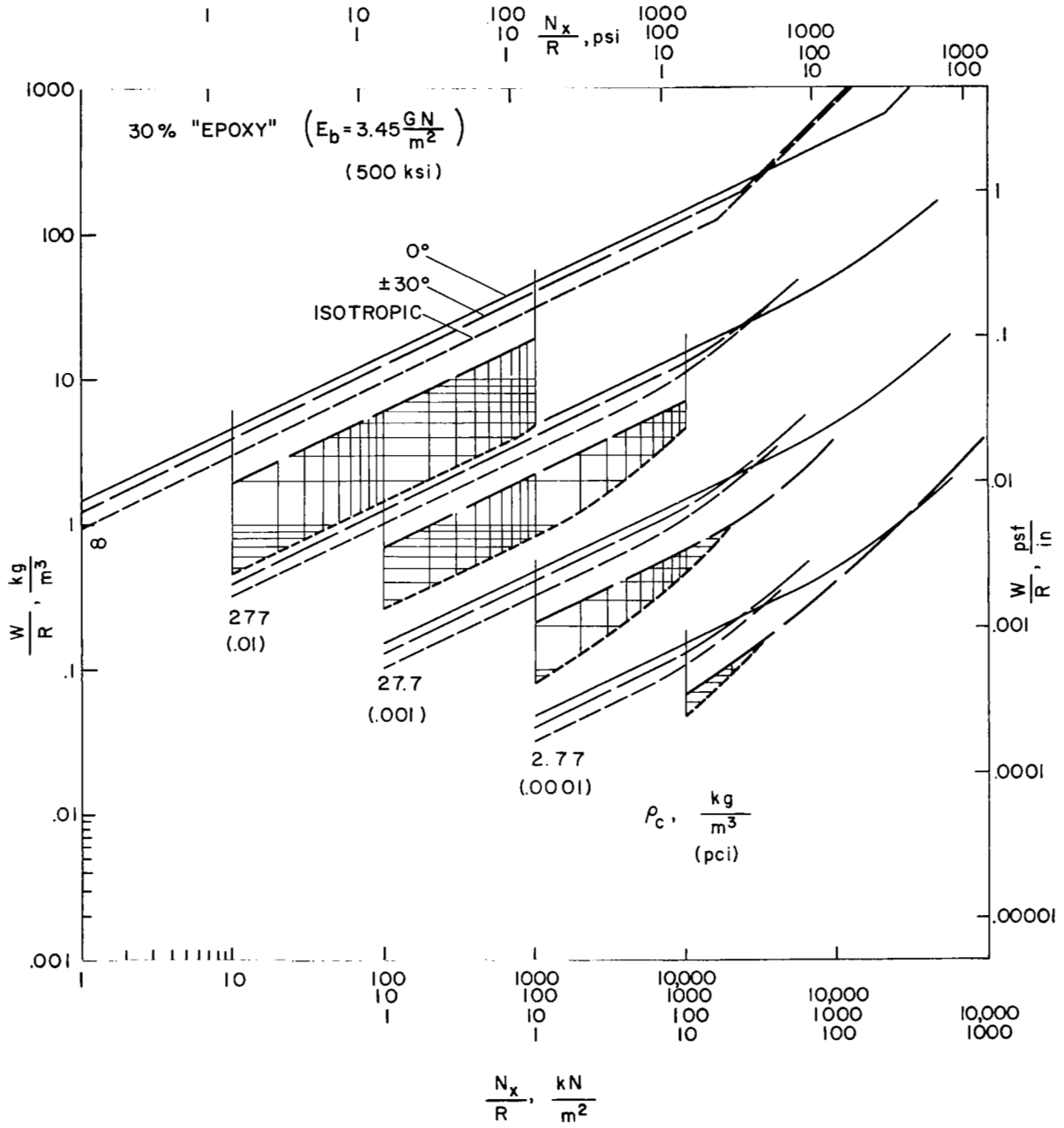


Figure 29. Shell Weight-Efficiencies of Steel Fibers in 30 Volume Percent Epoxy Binder, and Comparison with Metal Efficiencies.

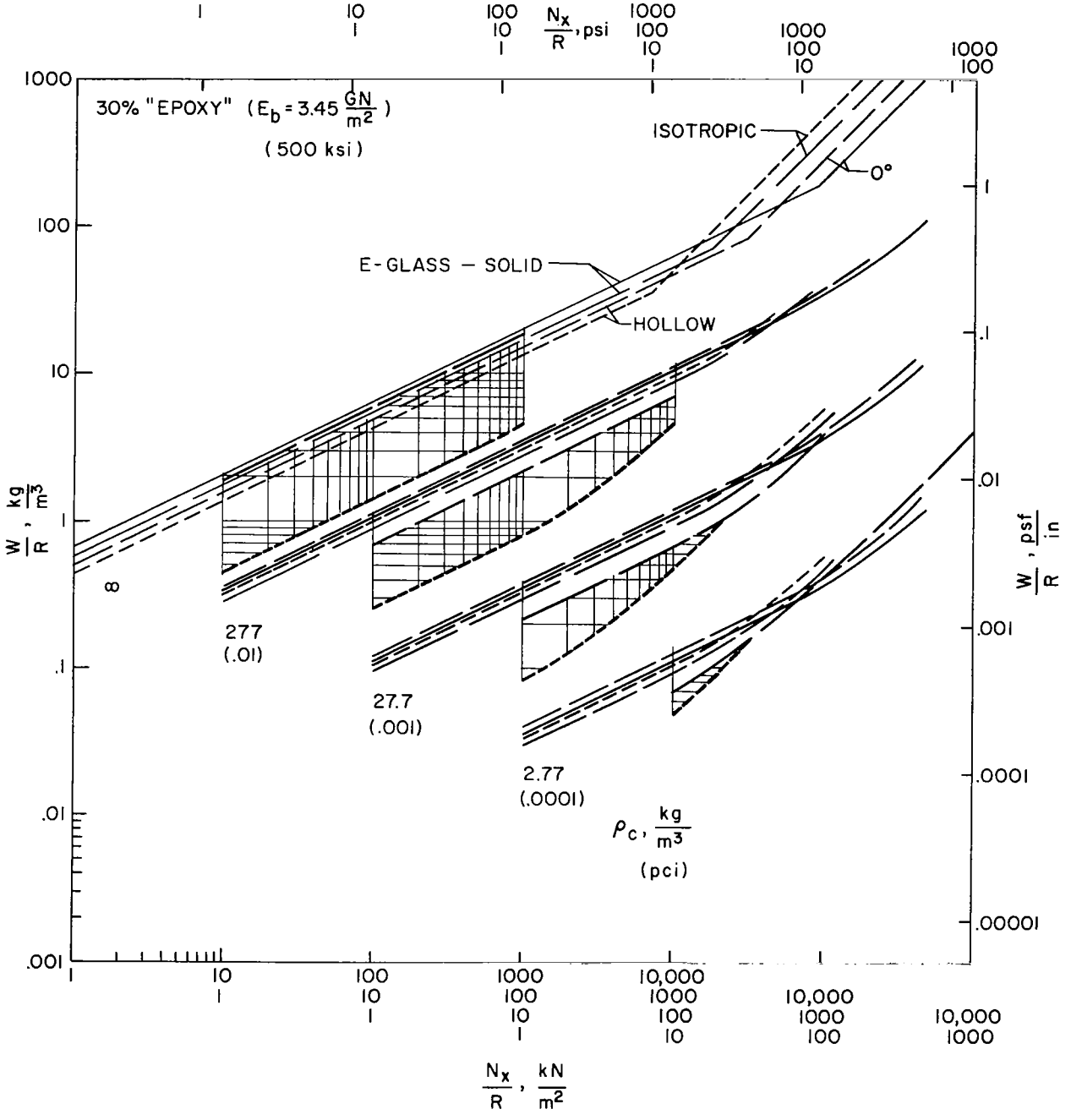


Figure 30. Shell Weight-Efficiencies of Solid and Hollow E-Glass Fibers in 30 Volume Percent Epoxy Binder, and Comparison with Metal Efficiencies.

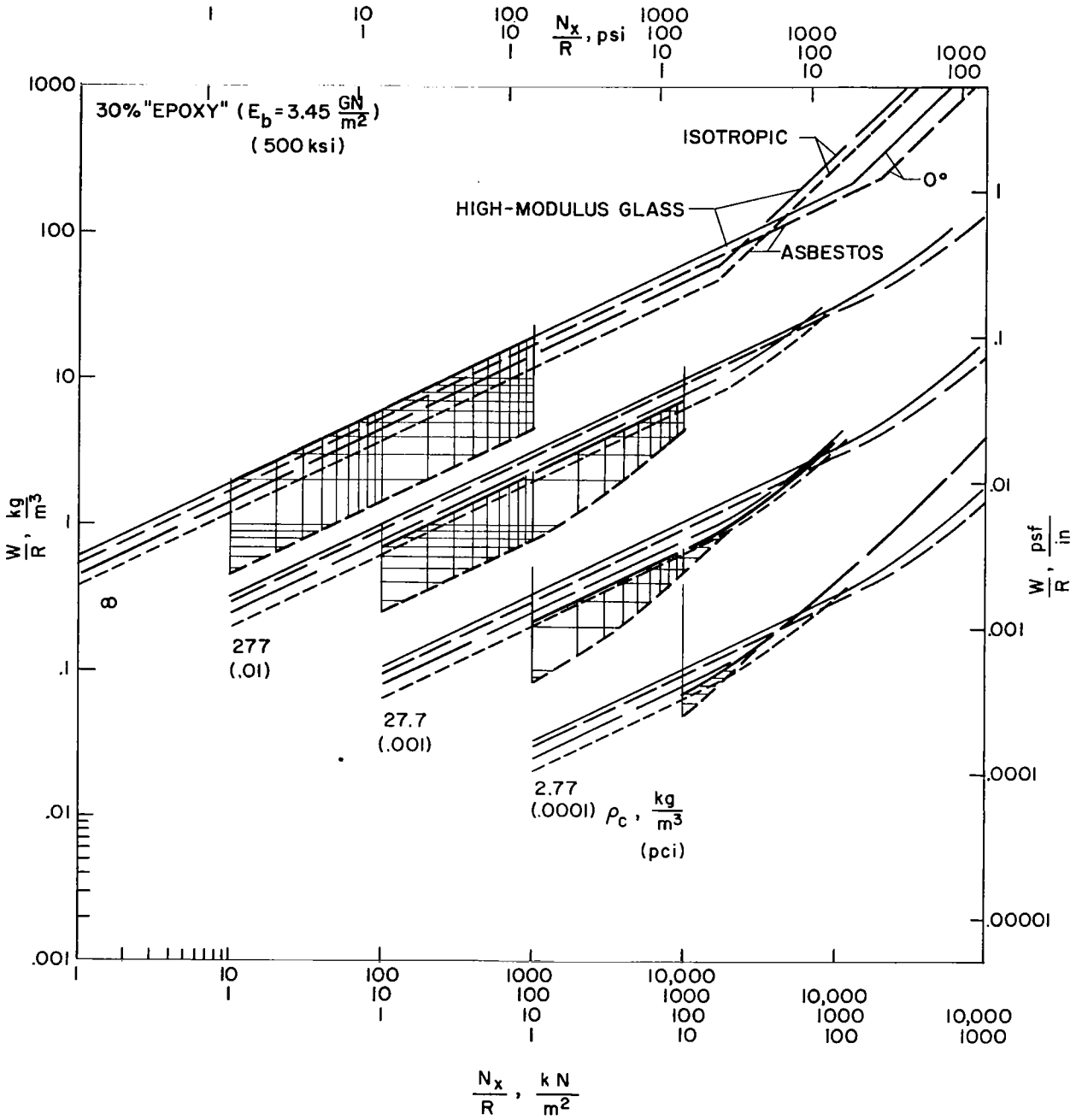


Figure 31. Shell Weight-Efficiencies of High-Modulus Glass and Asbestos Fibers in 30 Volume Percent Epoxy Binder, and Comparison with Metal Efficiencies.

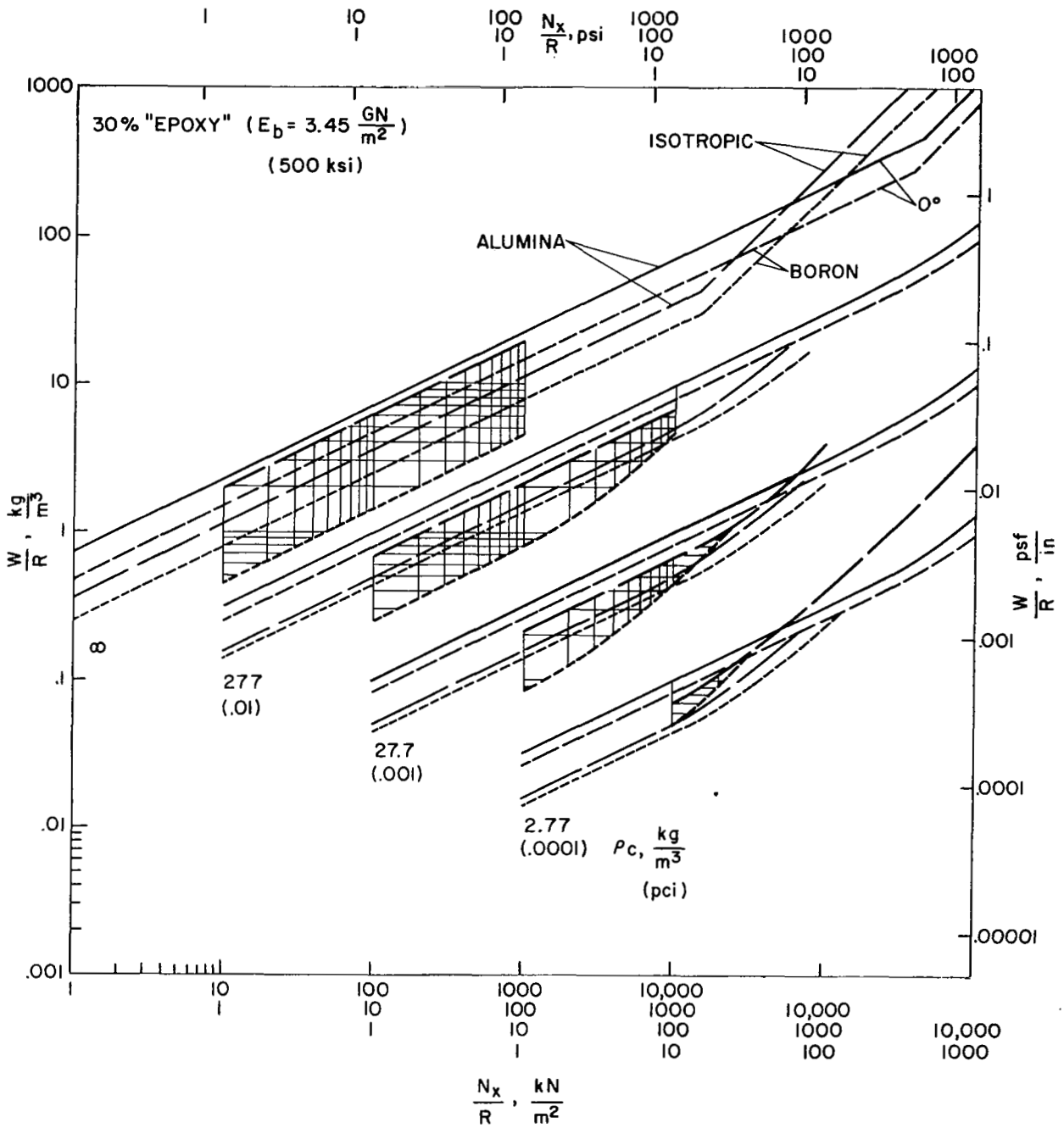


Figure 32. Shell Weight-Efficiencies of Boron and Alumina Fibers in 30 Volume Percent Epoxy Binder, and Comparison with Metal Efficiencies.

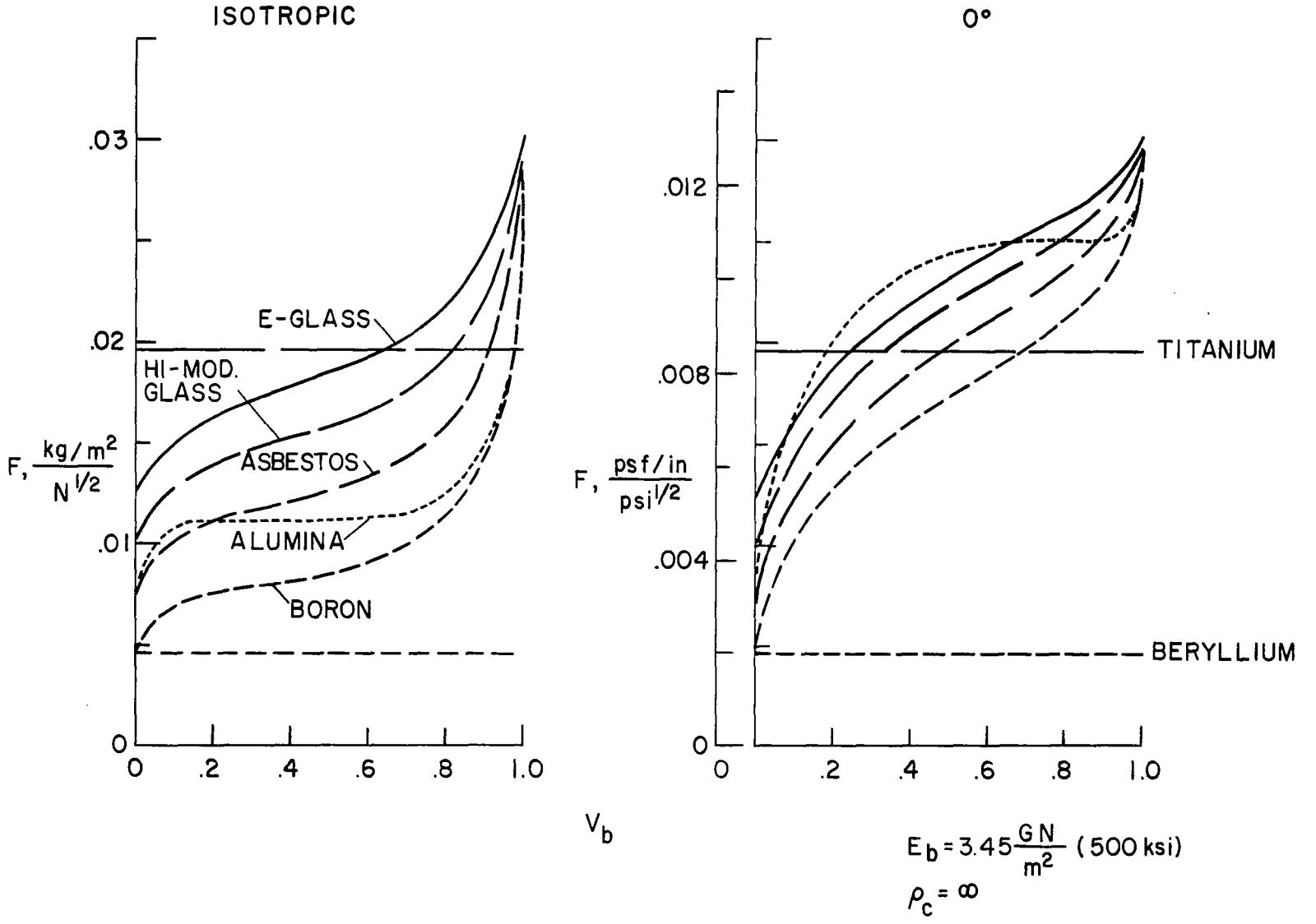


Figure 33. Elastic Buckling Efficiencies of Epoxy-Composite Monocoque Shells, and Comparison with Metal Efficiencies.

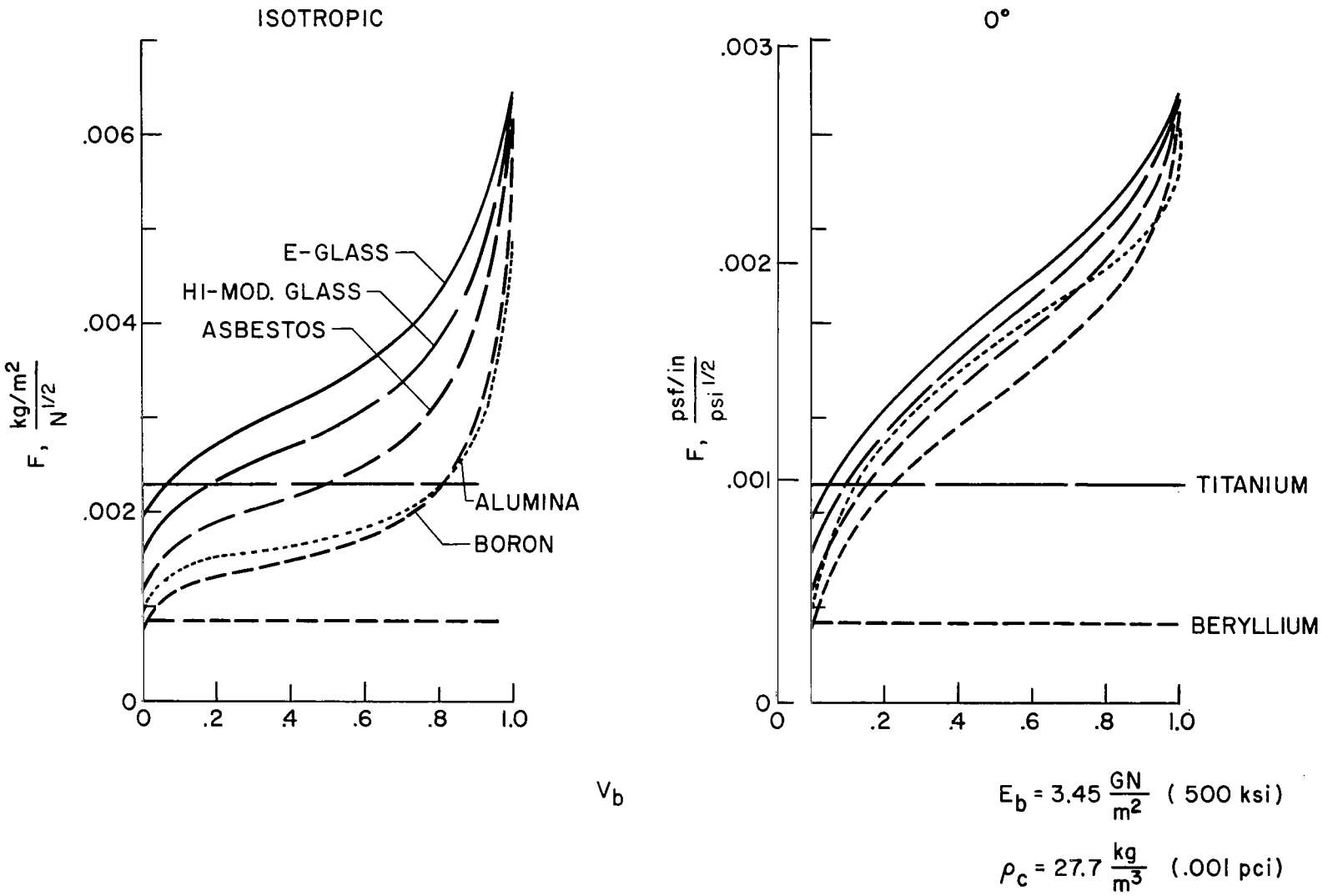


Figure 34. Elastic Buckling Efficiencies of Epoxy-Composite Sandwich Shells, and Comparison with Metal Efficiencies.

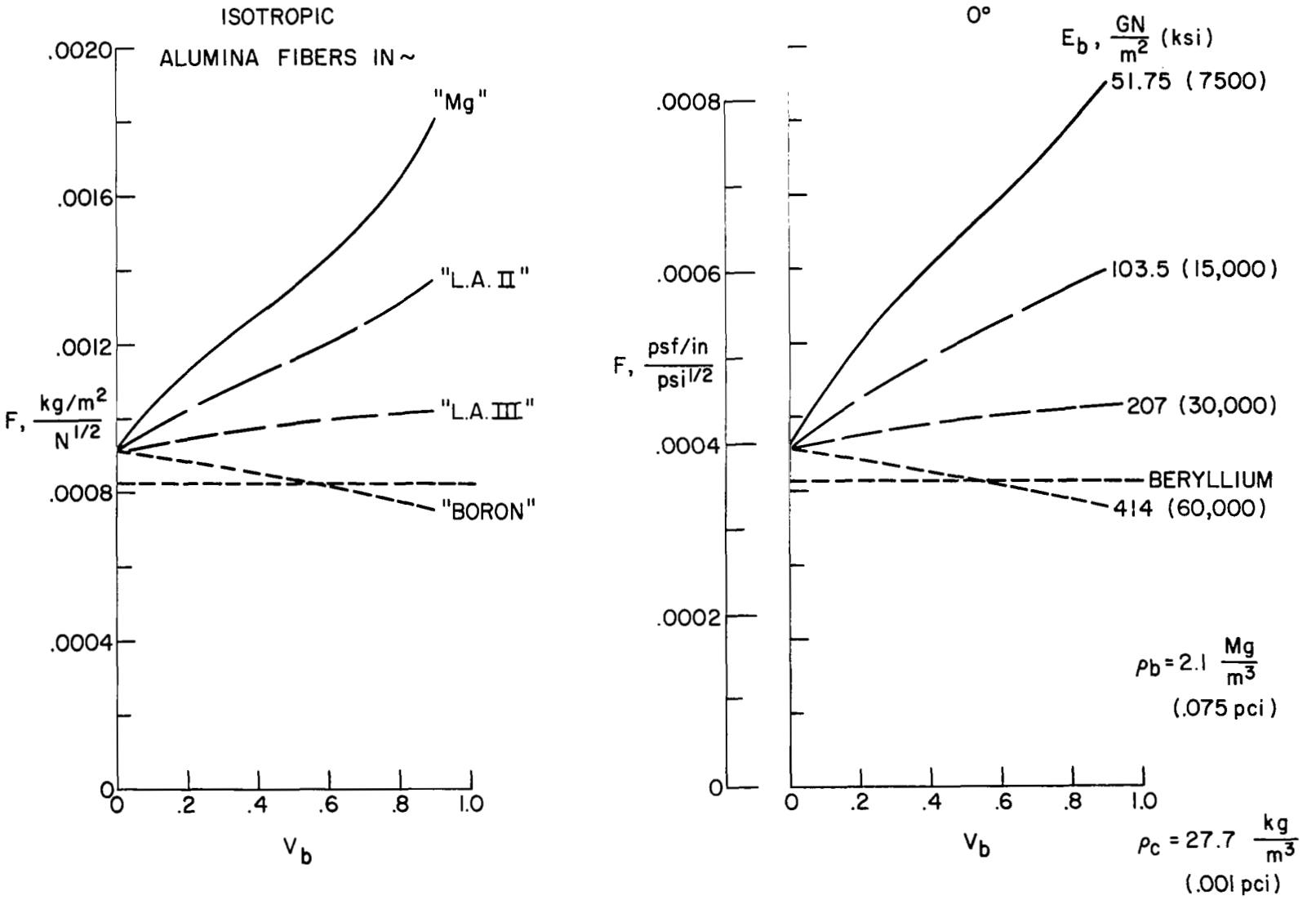


Figure 35. Elastic Buckling Efficiencies of Alumina-Fiber Reinforced Composite Sandwich Shells with Various Binders, and Comparison with Beryllium.

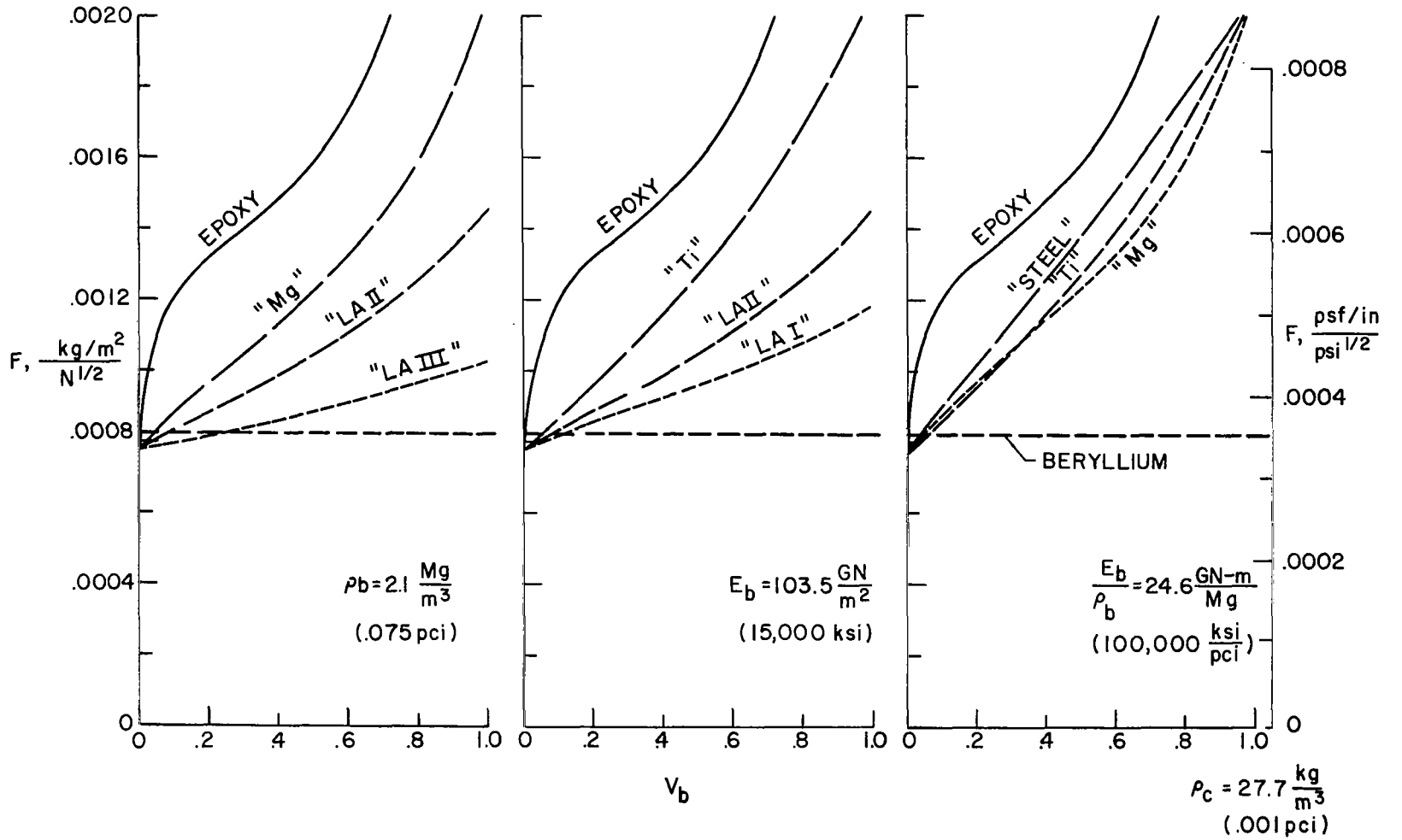


Figure 36. Effects of Variation in Binder Properties on Elastic Buckling Efficiency of $\pm$ 30°, 90° Boron Filament Reinforced Composite Sandwich Shells.

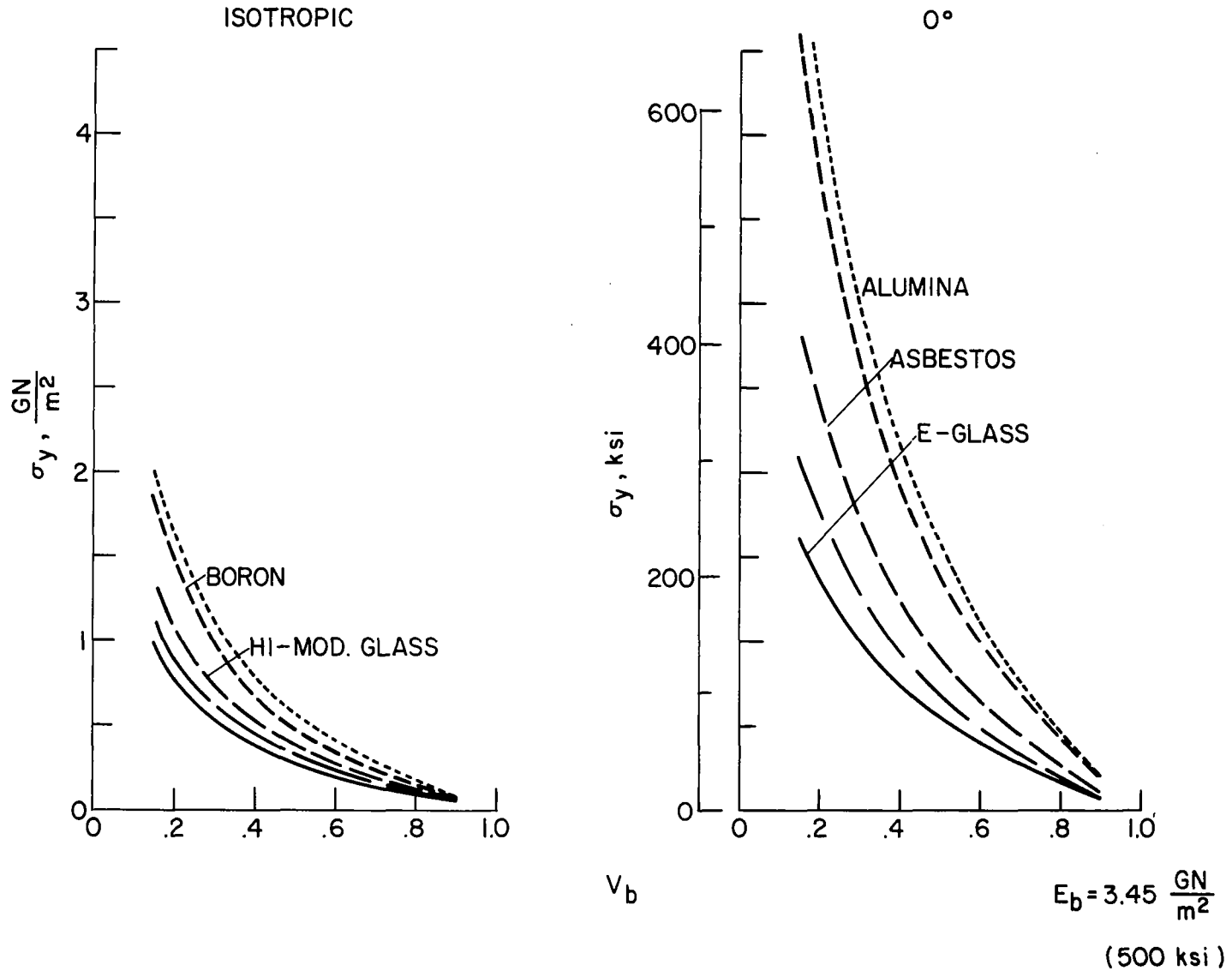


Figure 37. Compressive Failure Stresses Calculated for Various Filamentary Materials in Epoxy Binder.

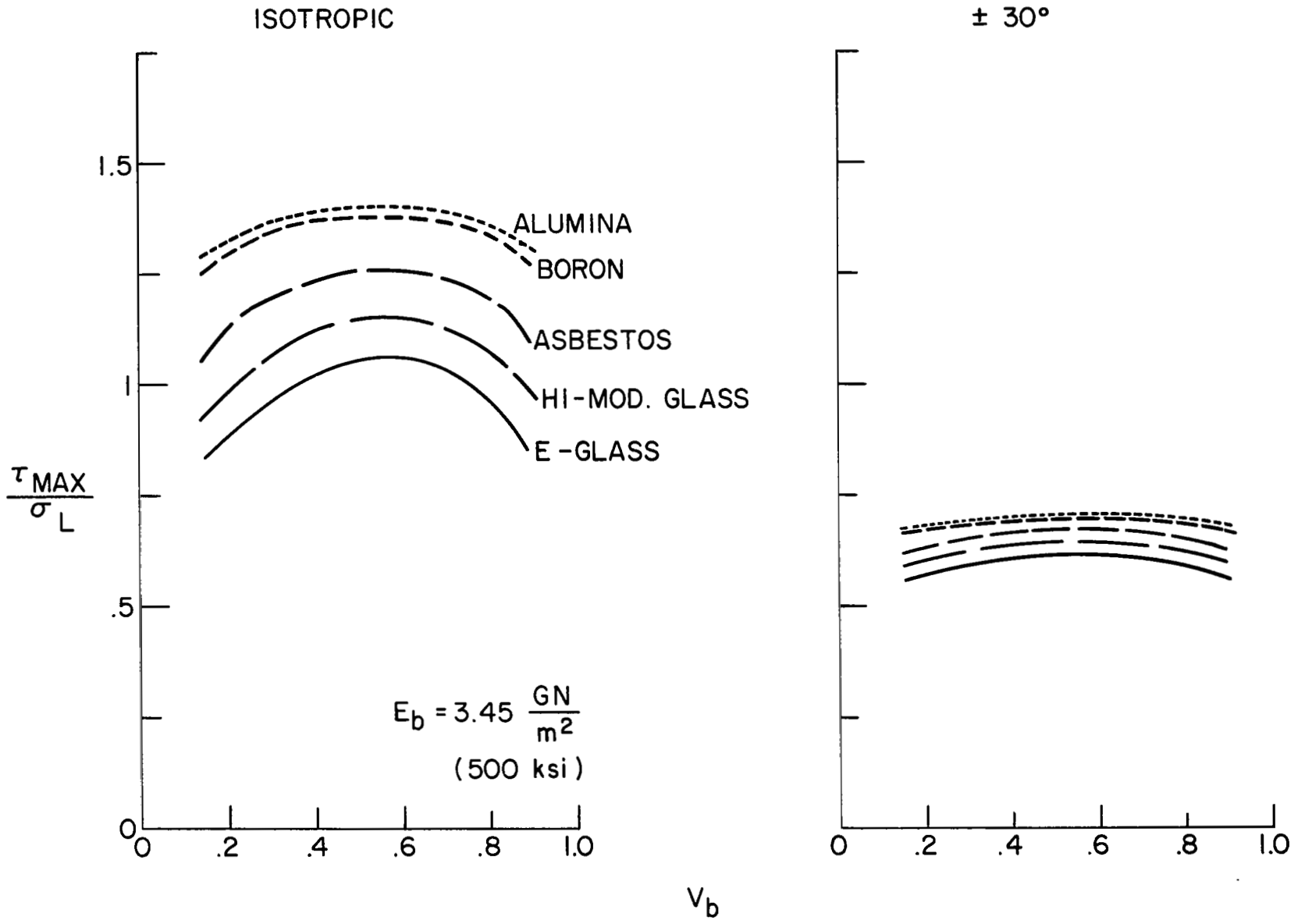


Figure 38. Maximum Shear Stresses Calculated for Various Filaments and for the "Isotropic" and $\pm$ 30° Configuration with Epoxy Binder.

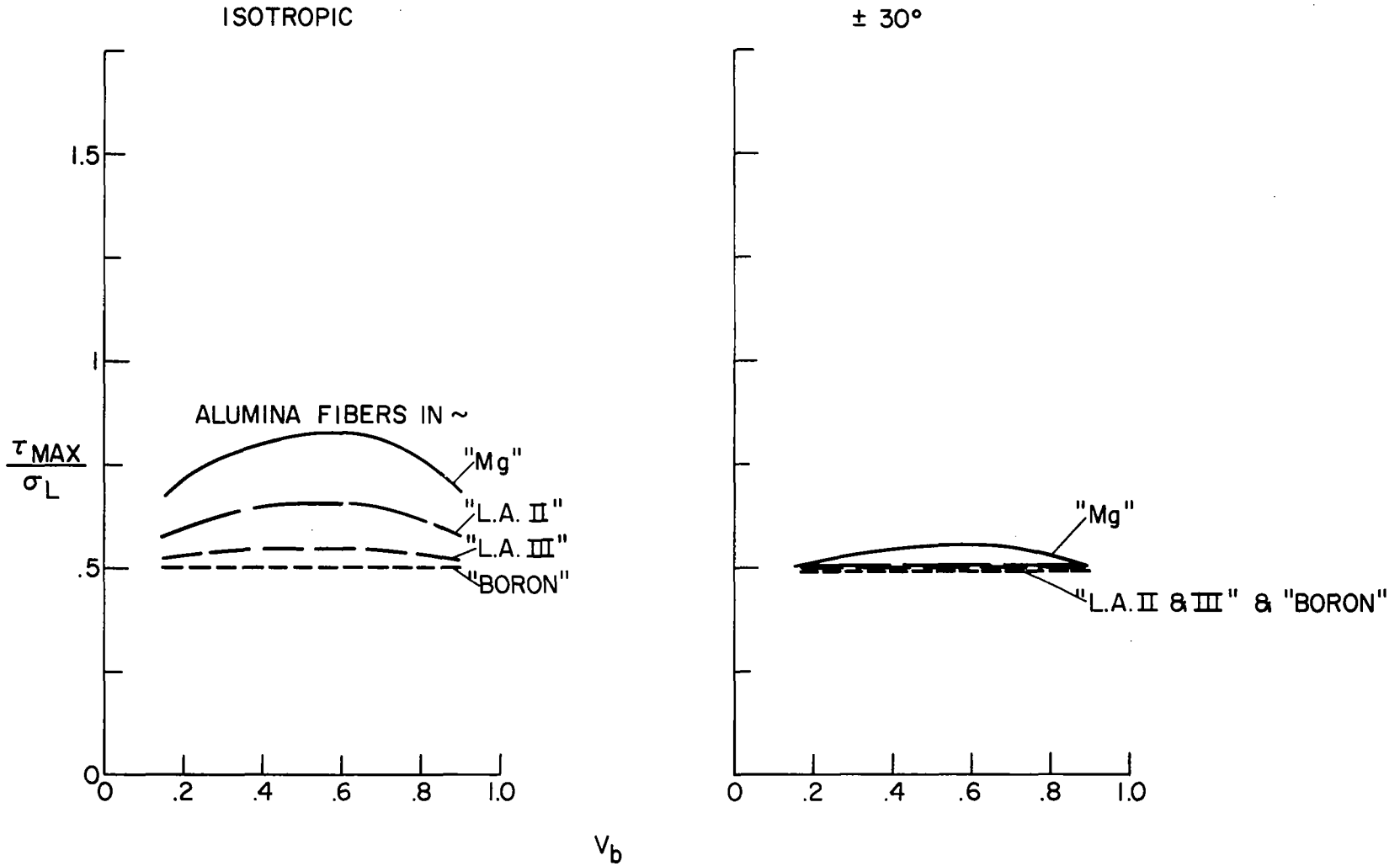


Figure 39. Maximum Shear Stresses Calculated for Alumina Fibers in Various Binders for the "Isotropic" and ± 30° Configuration.

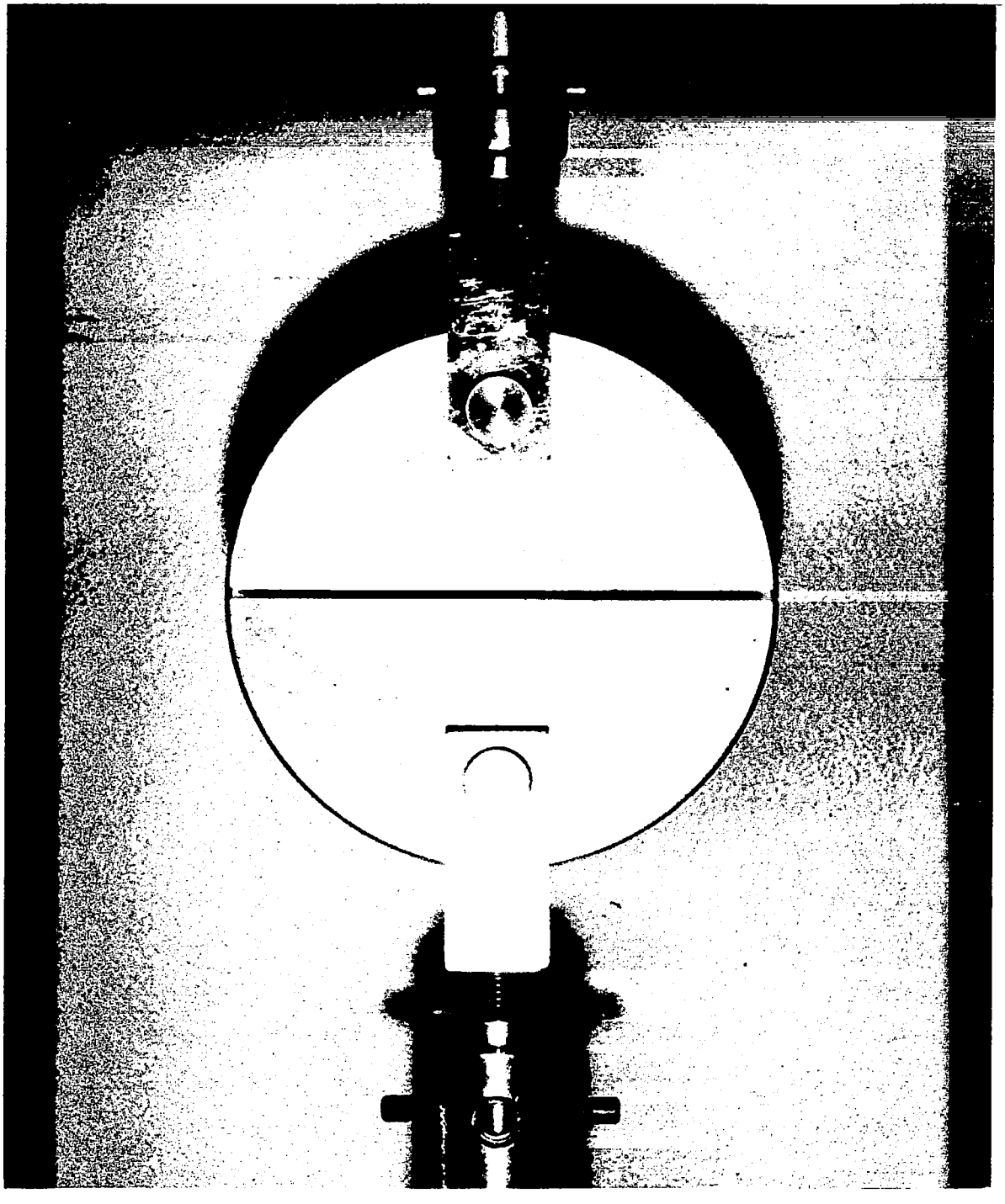

Figure 40. Test Set-Up for Ring Tests